Journal of the
OPTICAL SOCIETY
of AMERICA

VOLUME 36, NUMBER 9 SEPTEMBER, 1946

The Fluorescence of Phosphors in Rare Gases

N. C. BEESE
Research Department, Westinghouse Lamp Division, Bloomfield, New Jersey
(Received June 15, 1946)

Experiments were performed to investigate the fluorescence of phosphors when excited by discharges in rare gases and mixtures of them as a possible substitute for mercury vapor. A special tubular discharge lamp was built that contained a glass strip upon which numerous patches of fluorescent material were painted. Measurements were made on the brightness of the individual patches as the rare gases, mixtures of them, pressures, and tube currents were varied. From a large amount of such data the following conclusions could be drawn: (1) All phosphors showed fluorescence to some degree to all gases or mixtures and operating conditions but the efficiencies were low compared to mercury excitation. Zinc silicate phosphors were always the brightest. The resultant light depended upon the glow from the gas as well as upon the light from the phosphor. (2) Highest efficiencies were obtained with the rare gases at low pressures. The shapes of the curves indicated that resonance radiation was the principal agent in producing fluorescence. In pure gases the optimum pressures were too low to be usable in a commercial lamp. (3) With certain gas mixtures the high light output of low pressures could be carried over to higher pressures. Argon, krypton, or xenon mixed with helium or neon gas showed this desirable characteristic, and is analogous to mercury vapor of a few microns pressure in a gaseous atmosphere of argon at several mm pressure. (4) The highest efficiency is attained with neon gas but the light is predominately the orange-red glow from neon. Neon might become a competitor of mercury only in pink fluorescent lamps. (5) Several interesting relationships associated with the atomic numbers of the rare gases were found.

ABOUT 10 years ago Pirani and Rüttenauer introduced a new type of lighting[1] by describing their experiments on converting ultraviolet radiation from low pressure mercury discharge lamps to visible light by using fluorescent materials inside their tubes. Such lamps had very high efficiencies compared to the best tungsten filament lamps, had long life, and were capable of producing any color including white light, which could be obtained by a suitable blending of phosphors. These early experiments led to the development of our present fluorescent lamps.

USE OF MERCURY VAPOR

Mercury vapor has many inherent chemical and physical properties that make it well suited as an agent to excite phosphors. It is possible to convert approximately half of the wattage supplied to the lamp into useful ultraviolet radiations at 2537A. Since this energy can be utilized by suitable phosphors with nearly 100 percent quantum conversion one can readily see the possibility of high luminous efficiencies for such a device. Our present lamps approach this theoretical value.

The best operating range for a low pressure mercury vapor lamp is near room temperature with the bulb walls between 40° and 50°C. This gives a cool operating lamp of relatively low intrinsic brightness. The pale blue glow of the mercury vapor during normal operation does not

[1] M. Pirani and A. Rüttenauer, Das Licht **5**, 93 (1935).

BOSTON UNIVERSITY
COLLEGE OF LIBERAL ARTS
LIBRARY

seriously affect the color of the resultant light. Phosphors are available to produce any desired color including various shades of "white" by suitable combinations or mixtures of primary colors. While more difficult and expensive to manufacture than incandescent tungsten filament lamps, the tubular fluorescent lamps lend themselves readily to quantity production on semi-automatic machines.

Even with all the desirable qualities associated with mercury vapor lamps, there are several improvements that are desirable. Temperature limitations restrict the use of mercury vapor lamps to moderate ambient temperatures and preclude their use for outdoor illumination in winter. There is also a slight contribution of blue, green, and yellow light from the line spectrum of mercury vapor that distorts some colors. Because of the stroboscopic effect in such devices the light is especially objectionable with low frequency power sources such as the 25-cycle installations in some parts of the country. The elimination of some of these features furnishes the basis for further research on light sources.

USE OF RARE GASES

Many investigations have been carried out in an endeavor to use inert gases such as neon, argon, krypton, and xenon as a substitute for mercury vapor in exciting phosphors within a discharge lamp.[2–4] Most of the fluorescent light given off by phosphors excited by discharges in the rare gases is caused by resonance radiation. This type of radiation can be produced much more efficiently than any other type of radiation. The resonance radiation of the rare gases occurs in the far ultraviolet or Schumann region, which makes for relatively low energy conversion from ultraviolet to visible light and hence low efficiency compared to mercury. The energy relation in converting one quantum of neon 740° radiation to one quantum of visible light at 5180A is 7 to 1, while producing the same visible light from mercury 2537 radiation entails an energy factor of 2 to 1. This assumes a 100 percent quantum conversion for each process which is approximately true. Fonda has estimated that not more than 30 percent of the energy supplied to a neon discharge lamp is converted to the resonance radiation at 740A. This value is considerably below that for mercury vapor which utilizes about 50 percent of the wattage supplied to the lamp. All these considerations indicate a relatively low efficiency of light production by the use of an inert gas and phosphors.

[2] A. Rüttenauer, Zeits. f. tech. Physik **17**, 384 (1936); A. Rüttenauer, Das Licht **7**, (Jan. 1937).
[3] H. G. Jenkins and J. N. Bowtell, Trans. Faraday Soc. **35**, 154 (1939).
[4] G. R. Fonda and H. Huthsteiner, J. Opt. Soc. Am. **32**, 156 (1942).

EXPERIMENTAL WORK-POSITIVE COLUMN DISCHARGES

The response of many phosphors to discharges in various inert gases and mixtures of them was investigated with relatively simple apparatus similar to that of Fonda.[4] A glass plate $\frac{7}{8}$ inch wide and 10 inches long was coated with patches of fluorescent materials, each about $\frac{7}{8}$ inch square. The powders were mixed with a nitrocellulose binder, painted on the glass plate, and baked in air at 500°C to remove the binder. This simulated the phosphor coating in a fluorescent lamp. The discharge tube with the phosphor coated plate within it was exhausted as a normal lamp and then the various rare gases or mixtures of them admitted. The electrodes were heated during all measurements. Most of the time a current of 100 ma a.c. was used. Light measurements were made with a telescope using a hand magnifier to form an image of the fluorescent patches on a Lange photo-voltaic cell fitted with an eye sensitivity filter. The telescope was moved along a horizontal bar parallel to the fluorescent plate so that the various phosphors could be measured. The cell was removable from the telescope so that each spot could be centered with a ground glass screen. One of the patches was aluminum oxide which did not fluoresce. This was used to determine the visible light from the discharge. The photronic cell was connected to a galvanometer shunted with a resistance box so that a great range of intensities could be measured. After completing the work with the rare gases, mercury vapor was distilled into the tube so as to have a direct comparison with mercury resonance excitation.

Figure 1 shows the fluorescent light intensity in arbitrary units obtained from four phosphors

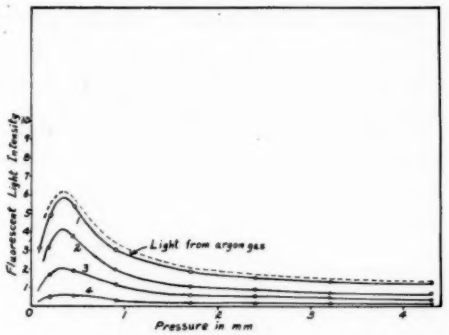

FIG. 1. Fluorescence of various phosphors excited by argon gas. (1) Zinc silicate: (2) zinc beryllium silicate: (3) cadmium borate: (4) calcium tungstate.

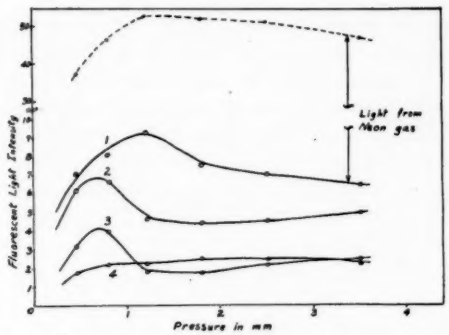

FIG. 2. Fluorescence of various phosphors excited by neon gas. (1) Zinc silicate: (2) zinc beryllium silicate: (3) cadmium borate: (4) calcium tungstate.

similar to those used in fluorescent lamps, using argon gas at various pressures as the exciting agent. The curves show that zinc silicate is the brightest phosphor and the colors are quite pure since the light from the argon gas is but a small portion of the total. The shape of the response curves indicates that the phosphors are excited chiefly by a type of resonance radiation which in this case is at 1066A and 1048A. Maximum response in all cases is obtained at a pressure of 0.3 mm which is too low for use in a commercial lamp.

The results obtained with krypton gas are quite similar to those obtained with argon gas and show that the exciting agent is the resonance radiation at 1236A and 1165A. The silicates are excited better than with argon. The colors are quite pure since the light contributed by the krypton gas is relatively small, but the optimum pressure of 0.25 mm is too low for practical use.

Pure xenon gas with resonance radiation at 1469A gives a response curve similar to that from krypton but even more exaggerated at very low pressures. The maximum response was at or below 0.1 mm pressure. At this low pressure the readings were 50 to 100 percent greater than the highest readings obtained with pure krypton for the same phosphors and for equal tube currents. Since the glow from the xenon gas itself is a pale blue color it contributes an inappreciable amount of light, which results in bright fluorescent colors. For practical applications where highest light intensity is desired, the pure xenon lamps would have to operate at pressures so low that gas clean-up and electrode sputtering would seriously limit the life of such a device.

Neon gas contributes such a large amount of orange-red color to the light from the phosphors that the fluorescent colors are masked and become ineffective. The maximum output is at higher pressures than with argon, krypton, and xenon gases. Figure 2 shows that even at the optimum pressure the maximum fluorescence from zinc silicate accounts for only about one-fifth of the total light from the lamp. In argon, krypton, or xenon gas the fluorescent light from zinc silicate accounts for 85 to 95 percent of the total light.

Helium gas shows characteristics similar to neon gas but the total light as well as the fluorescent light from the various phosphors is less than with neon. Fluorescent light is caused largely by the short wave excitation in the far ultraviolet region at 585A.

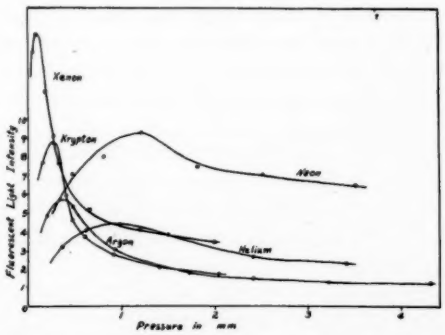

FIG. 3. Fluorescent light from zinc silicate excited by various gases.

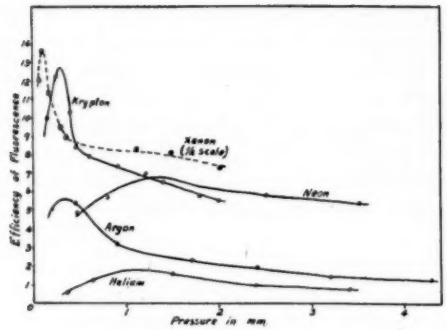

FIG. 4. Relative fluorescent efficiency of zinc silicate in rare gases.

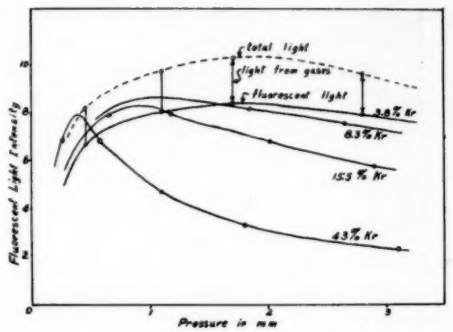

FIG. 5. Fluorescent light from zinc silicate excited by krypton-helium gas mixtures.

The fluorescent light from a zinc silicate phosphor excited by various gases is shown in Fig. 3. The relative efficiencies in these gases are shown in Fig. 4. The data relate to a constant tube current of 100 ma. Xenon is more efficient than the other pure gases and is plotted to half scale. Actually it is about twice as efficient as krypton gas.

MIXTURE OF INERT GASES

Mercury vapor at a pressure of a few microns in a rare gas at several mm pressure has a very high output of resonance radiation at 2537A. By diluting krypton gas with neon or helium it might be possible to maintain the relatively high output of krypton with a total gas pressure of several mm. Such a phenomenon is illustrated in Fig. 5 where a mixture of 3.8 percent krypton in helium produces nearly a constant intensity of fluorescent light from a zinc silicate phosphor over the pressure range of 1 to 3 mm. The fluorescent light is almost as great as the maximum value attained with krypton alone while the contribution of light from the rare gases is much less than that produced by helium alone. The optimum effect is restricted to certain gas ratios or percentage compositions.

The same type of phenomenon is shown with a mixture of about 7 percent argon in helium. The variation of fluorescent light with this and other selected gas compositions over a pressure range of 0 to 3 mm is shown in Fig. 6.

With suitable mixtures of xenon in helium, the high values of fluorescent light attained with pure xenon at very low pressures can be made to extend up to several mm pressure. A mixture

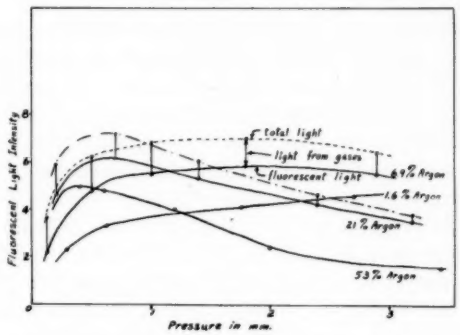

FIG. 6. Fluorescent light from zinc silicate excited by argon-helium gas mixtures.

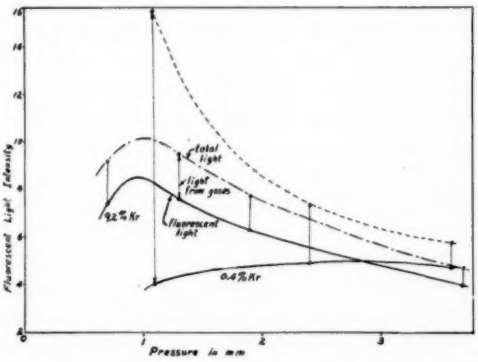

FIG. 7. Fluorescent light from zinc silicate excited by krypton-neon gas mixtures.

of about 2 percent xenon in helium causes the green fluorescence of zinc silicate to appear uniformly bright over a pressure range of 0.5 mm to over 3 mm. The light output is about equal to the highest intensity attained with xenon at

0.1 mm pressure. With these mixtures the efficiency is much less than with xenon alone, but the colors are still bright since the glow from the gas mixture accounts for only 10 or 11 percent of the total light.

Figure 7 shows the fluorescent light from a zinc silicate phosphor excited by two krypton-neon gas mixtures. With the 9.2 percent krypton-90.8 percent neon mixture there is an almost constant ratio of fluorescent light to total light over an extended range of pressures, although the total light is not constant. The neon glow is greatly reduced from that of pure neon at the same pressure. With 0.4 percent krypton-99.6 percent neon gas the fluorescent output is quite constant over a considerable pressure range but the contribution from the neon increases very rapidly with decreasing pressures, so the resultant color is greatly affected by gas pressure.

Mercury was distilled into the lamp after completing the experiments with the rare gases and mixtures of them so that a direct comparison could be obtained on the same phosphors when excited by 2537 radiation. The efficiency and total fluorescent light were always greater with mercury excitation than with rare gas excitation. To obtain a pink fluorescent light it might be desirable to use neon gas to excite the phosphor since its orange-red color could be utilized. The efficiency of such a lamp would be quite comparable to a mercury activated lamp giving a similar color. Table I shows the relationship between various gases at selected pressures used to excite zinc silicate and the resultant estimated luminous efficiencies. The values show what might be approximated in completed lamps, and were obtained by the relative brightness measurements of the various fluorescent materials compared to a 15-watt commercial green fluorescent lamp.

TABLE I. Fluorescence of zinc silicate excited by rare gases (estimated efficiencies).

Gases	Pressure	Phosphor only	Phosphor and gas	Color
Argon	0.35 mm	4.0 lumens/watt	4.1 lumens/watt	Green
Neon	1.2 mm	4.7	25.0	Red
Krypton	0.3 mm	9.0	9.7	Green
Helium	1.0 mm	1.3	5.1	Cream
Xenon	0.1 mm	19.0	20.0	Green
Argon plus mercury	2.8 mm	55.0	60.0	Green

Two lamps were made with a filling of neon gas since this appeared to give the highest efficiency, one coated with zinc silicate that fluoresces green and the other with cadmium borate that fluoresces pink. The lamp with zinc silicate coating gave 21.5 lumens per watt which checks the value in Table I as to order of magnitude. Randall reported the average efficiency of similar commercial lamps to be 22 lumens per watt. The lamp that was coated with cadmium borate gave 19 lumens per watt. In such lamps about $\frac{4}{5}$ of the total light is caused by the neon gas so colors are limited to orange, red, or pink.

Table II indicates the relative values of fluorescent light obtained with several phosphors excited by various gases at selected pressures. All values were obtained in the same experimental lamp. Zinc silicate phosphors always produced greater brightness than any of the other phosphors.

Several interesting relationships associated with the atomic numbers of the rare gases were found. Except for neon there is an increase in the maximum fluorescent light from a zinc silicate phosphor with increasing atomic number of the exciting gas. The wave-lengths of the resonance radiation of the rare gases and mercury vapor also increases with atomic weight from 585A for helium to 2537A for mercury. To produce a flat fluorescent response over a large pressure range the amount of gas added to helium decreases with atomic weight for argon, krypton, xenon, and mercury vapor. The optimum values are 7 percent argon, 4 percent krypton, and 2 percent xenon.

TABLE II. Relative brightness of various phosphors excited by rare gases.

Gas	Pressure	Gas glow	Zr-Be silicate	Cadmium silicate	Cadmium borate	Calcium tungstate	Magnesium tungstate	Zinc silicate
Argon	0.2 mm	0.55	3.5	1.2	1.85	0.55	0.55	4.9
Helium	0.6 mm	13.4	2.55	1.55	1.35	0.5	0.5	4.1
Neon	0.8 mm	38.0	6.4	3.1	4.0	2.2	2.65	8.0
Krypton	0.9 mm	0.55	2.0	0.55	0.6	0.22	0.22	2.75
Argon plus Hg	2.8 mm	8.6	22.3	11.0	15.0	9.8	21.8	50.0

The pressure of pure inert gas for maximum fluorescent response decreases with atomic number. The range of pressure for half-value of the maximum response of pure gases also decreases with increasing atomic numbers, covering a range of several millimeters for helium to less than 50 microns for mercury. The sharp peak of high intensity at low pressure is the best indicator that the activating radiation is of the resonance type. The sharpness of these peaks and their absolute values increase with atomic weight, but the maximum response is attained over progressively smaller pressure ranges. With the heavy gases the fluorescent colors are quite distinct since the glow from these gases gives only a small amount of pale blue light. With neon and helium, however, the gas glow is very intense and noticeably affects the color of the resultant light.

Many measurements on the characteristics of the positive column glow discharges were made in our laboratory by Mr. Harold Hauts while a student in the Westinghouse Training Program during the summer of 1943.

JOURNAL OF THE OPTICAL SOCIETY OF AMERICA VOLUME 36, NUMBER 9 SEPTEMBER, 1946

A Method of Quantitative Spectrochemical Analysis Based on Line Widths

PIERRE COHEUR
University of Liége, Liége, Belgium

(Received June 5, 1946)

A method of quantitative spectrochemical analysis, first suggested by W. Gerlach and W. Rollwagen and making use of line widths, is described and discussed. The method is practical and accurate; it is independent of development conditions or exposure time and it may be applied to cases where customary techniques fail.

REAL progress in the quantitative spectrochemical determination of the concentration of an additional element A in a fundamental element F was made possible only after Gerlach departed from the common practice of basing such a determination on the absolute intensities of the lines of A and introduced instead the relative intensities of properly selected lines of F and A (internal standard principle; homologous pairs of lines). In present spectrochemical work, a plot is prepared of the relative intensities of a line of F and one of A as a function of the concentration of A in F. The relative intensities are usually obtained from measurements of photographic opacities. As a result "for higher concentrations,[1] the error is likely to be increased by the difficulty of finding analytical lines which are not so dense that they lack sensitivity; while for trace concentrations, there is apt to be difficulty in correcting the weak analytical line for plate background."[2]

In 1937, W. Gerlach and W. Rollwagen[3] suggested that the determination of the relative intensities of lines of F and A be replaced by the

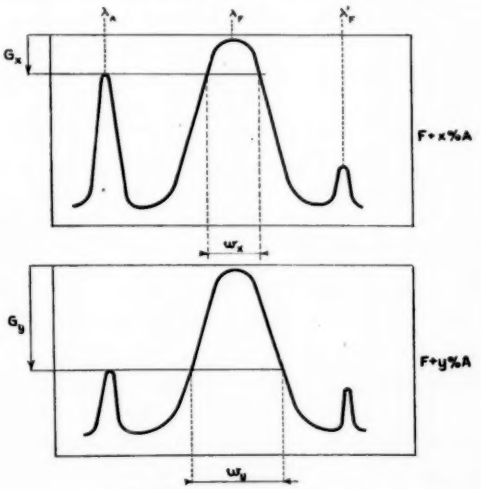

FIG. 1. Principle of the method.

[1] Larger than 5 percent.
[2] Sawyer, *Experimental Spectroscopy* (Prentice Hall, New York, 1944), p. 309.
[3] W. Gerlach and W. Rollwagen, Metallwirtschaft **16**, 1083 (1937).

determination of the width of a line of F at an opacity (or galvanometric deflection) corresponding to the maximum opacity of a line of A. However, no experimental investigation of the validity of this method was carried on until March, 1939, at which time Professor Gerlach suggested that we tackle such a study. A summarized account of our results is given in the present paper.[4]

Any line on a spectrogram possesses an actual width[5] resulting from the combination of physical and instrumental factors. The "physical width" is determined by the natural width and by the broadening due to Doppler-, Stark-, pressure- and reabsorption effects. The "instrumental width" results from the size of the source, the path of the light beam through the spectrograph, the diffraction by the slit, the aberrations of the optical parts and the diffusion of light in the photographic emulsion. If the source is kept constant (i.e., if the excitation conditions as well as the distance and shape of the electrodes remain the same), the physical width of any line will remain constant.

If we use the same light source and the same spectrographic set-up, for taking spectrograms of a series of alloys of different concentrations, the strong lines of the fundamental element F will in general be wider than those of the additional element A. Moreover if we assume that the exposures and development conditions of all plates remain rigorously identical, each line of F will, as a first approximation, retain the same opacity and same width on all spectrograms of the series, while the lines corresponding to A will have intensities depending upon the concentration of A.

TABLE I. Constancy of the photometric width for variable exposure times.

Duration of exposure	Density of λ2933 Mn	Photometric width of λ3082 Al (in μ's)
25 sec.	0.534	205
25 sec.	0.524	204
20 sec.	0.440	206
20 sec.	0.424	203
15 sec.	0.301	205.5
10 sec.	0.238	206.5
5 sec.	0.075	203.5
5 sec.	0.056	204.5

TABLE II. Constancy of the photometric width for variable duration of development.

Duration of development	Al sample with 0.33 percent of Mn		Al sample with 0.80 percent Mn	
	D	w	D	w
4 min.	0.251	175	0.591	116.5
8 min.	0.274	174.5	0.671	117

[4] For additional details, see P. Coheur, Thesis, Mem. Soc. Roy. Sciences, Liége 5, 1–158 (1942).

[5] Physicists generally measure the width corresponding to an intensity in the wings equal to one-half the maximum intensity.

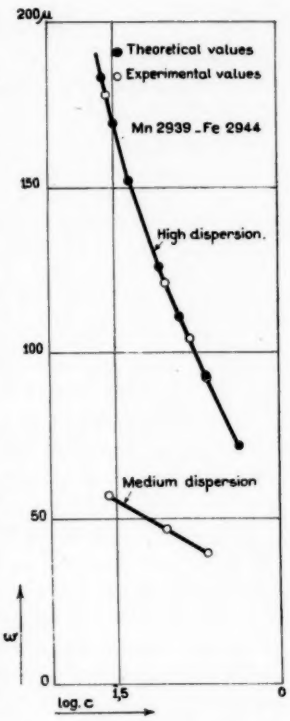

FIG. 2. Calibration curves (w, log c).

This is schematized on Fig. 1 concerned with the spectra of two alloys: one contains $F+x$ percent A, the other $F+y$ percent A; we suppose $x>y$. The wave-lengths are plotted as abscissae and the galvanometric deflections G of a proportional photometer are plotted as ordinates. We measure the width w_x of a line of F at the maximum deflection G_x of λ_A, and propose to call w_x the "photometric width"; the concentration of A in F will be determined on the basis of this width w_x.

Conversely one could measure the width w' of a strong line of the additional element A for the maximum opacity of a weak line of the fundamental element F.

Series of experiments have proved that the photometric width is independent of the duration of exposure and of the conditions of development, not only in the linear part of the HD curve but also in the regions of under- and over-exposure. (Elementary theoretical considerations lead actually to the same result.) As an illustration we give in Table I the observed data for a sample of

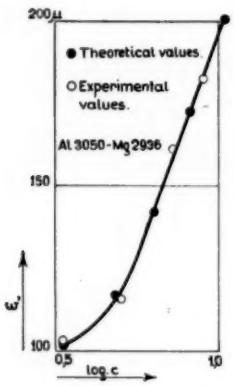

FIG. 3. Calibration curves (w', log c).

aluminium containing 0.33 percent of manganese; the lines used are λ2933 Mn and λ3082 Al.

A variation of the duration of development leads to the results of Table II, relative to two samples of Al containing, respectively, 0.33 and 0.80 percent of Mn; in this table, D is the difference in maximum density of λ3050 Al and λ2949 Mn, while w is the photometric width of λ3082 Al for the maximum deflection of λ2939 Mn.

In the course of a quantitative analysis, it is necessary to keep as constant as possible the following instrumental factors: effective aperture of the optical system (diaphragms), slit width, and size of the source.

The results of the complete experimental discussion may be summarized as follows.

1. Emission spectra.—For quantitative analysis calibration curves similar to those of Fig. 2 are prepared on the basis of standard samples. The logarithm of the concentration c is given in abscissa and the photometric width w in ordinate. Such calibration curves may actually be obtained from the profile of the selected line of F, when two samples of known concentration are available. In order to obtain the highest precision, a line of F should be selected which does not present a steep profile, and a sufficiently high dispersion should be utilized.

As an illustration of this point, we may mention that when determining manganese in steel, standard deviations of 6 and 1.9 percent, respectively, were obtained with dispersions of 16 A/mm and 4 A/mm, respectively, the line pair being λ2944 Fe−λ2939 Mn. When utilizing intensity ratios, we obtained in these same cases errors of 2.5 percent.

In determinations of Si in steel, the standard deviation by the method of photometric widths was 2.70 percent as against 3.85 percent by the intensity ratios (line pair λ2880 Fe−λ2881 Si). In determining Mn and Si in Al (λλ3082 Al, 2933 Mn, and 2881 Si), the error was smaller than 1.50 percent by the method of photometric width (using fine grain emulsions and a medium dispersion of 16 A/mm at λ3000), while the error was of the order of 3 percent by the intensity ratios in optimum conditions.

In all the preceding applications the width w of a line of F was measured for the maximum opacity of a line of A. As mentioned above we may also prepare calibration curves giving the width w' of a line of A for the maximum opacity of a weak line of F. Obviously in this latter method the calibration curve is no longer a representation of the profile of a specific spectral line, since the measures of w' are made for a definite galvanometer deflection on lines of different profiles, corresponding to different concentrations.

Yet excellent calibration curves may still be obtained, even on the basis of two samples of known composition only, by proper consideration of spectral variations due to changes in exposure time, account being taken of the Schwarzschild coefficient.

This method is advantageous in the case of fairly high concentrations (for example, higher than 5 percent) of A in F.

We have applied it to the determination of Mg in Al at concentrations from 5 to 9 percent of Mg (see Fig. 3); the error of a determination based on the measurement of w' was only 1.3 percent as against 3.1 percent by intensity ratios.

2. Raman Spectra.—The technique described here may be applied to any spectroscopic type of analysis in which the intensities of two emission lines are compared. Hence it is readily applicable to Raman spectroscopy. Dr. G. Duyckaerts[6] has determined in this way cyclohexane in carbon tetrachloride with a standard deviation from 1 to 2 percent, while the method of J. Goubeau-L. Thaler gave a mean error of 5 percent[7]; the range of concentration was from 5 to 20 percent.

[6] Dr. G. Duyckaerts of the University of Liége; private communication.

[7] J. Goubeau and L. Thaler, *Physikalische Methoden der analytischen Chemie*, edited by W. Böttger, (1939), p. 315.

JOURNAL OF THE OPTICAL SOCIETY OF AMERICA VOLUME 36, NUMBER 9 SEPTEMBER, 1946

Light Storage in Infra-Red Sensitive Phosphors*

R. T. ELLICKSON†
The Polytechnic Institute of Brooklyn, Brooklyn, New York
(Received June 19, 1946)

From experiments on samples of different thickness the amount of stored light in a particular sample of the infra-red sensitive phosphor made by activating strontium sulfide with cerium and samarium is calculated to be 2.6×10^{16} quanta per cubic cm. This corresponds, for this sample, to one quantum of light for every 8 samarium atoms or every 60 cerium atoms.

THERE have been developed recently[1] a number of phosphors that show a remarkable increase in brightness upon illumination with infra-red radiation. By taking into account the absorption of the stimulating infra-red light and the emitted visible light an equation has been derived[2] that fits the decay or exhaustion curves of these phosphors very well. The equation is

$$B(t)=B_0\frac{p+1}{(\alpha t)^{p+1}}\int_0^{\alpha t}\frac{y^p}{(1+y)^2}dy, \qquad (1)$$

where $B(t)$ is the brightness at time t, B_0 is the brightness at $t=0$, α is a constant proportional to the infra-red intensity, and p is the ratio of the absorption coefficient for visible light, μ_2, to that for infra-red light, μ_1. B_0 is proportional to the product αN, where N is the number of active centers per unit volume in the phosphor.

The remarkable agreement with the experimental data makes it possible to use Eq. (1) to determine the light sum, or total amount of light stored in the phosphor. Integrating Eq. (1) with respect to the time it is found that the light sum, L, is given by $L=(B_0/\alpha)(1+1/p)$. This is the observed light sum, which must be multiplied by μ_2, the absorption coefficient for visible light, to give the light sum per unit volume. This absorption coefficient is not readily measurable directly. However, the following procedure can be used. The shape of the decay curve depends on the ratio of the absorption coefficients; the brightness of samples of different thickness can be shown to depend on the sum of the absorption coefficients. The two experiments together then serve to determine the absorption coefficients.

Figure 1 is a typical exhaustion curve for the phosphor dealt with here, strontium sulfide activated with cerium and samarium.[3] The circles are experimental points and the solid line is from Eq. (1) with $p=0.2$. A value of p different from this by more than twenty percent would give a curve that would differ very markedly from the experimental points.

Figure 2 shows the results of measurements on two sets of samples of this phosphor of different thickness. The phosphorescent powder was sprayed on graphite from a suspension and then

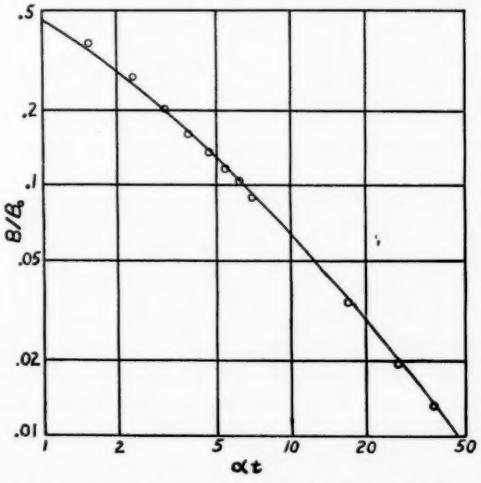

FIG. 1. Decay of brightness under constant infra-red intensity. Circles are experimental points; solid line is from Eq. (1) with $p=0.2$.

* The work described in this paper was carried out under contracts between the Office of Scientific Research and Development, the Bureau of Ships, and the Polytechnic Institute of Brooklyn.
† Present address, Reed College, Portland, Oregon.
[1] See the reports of F. Urbach, R. Ward, G. R. Fonda, and others in the proceedings of the March, 1946 meeting of the Optical Society of America.
[2] R. T. Ellickson and W. L. Parker, Phys. Rev. **68**, 534 (1946).
[3] The marked response of this phosphor to infra-red radiation was discovered by F. Urbach, reference 1.

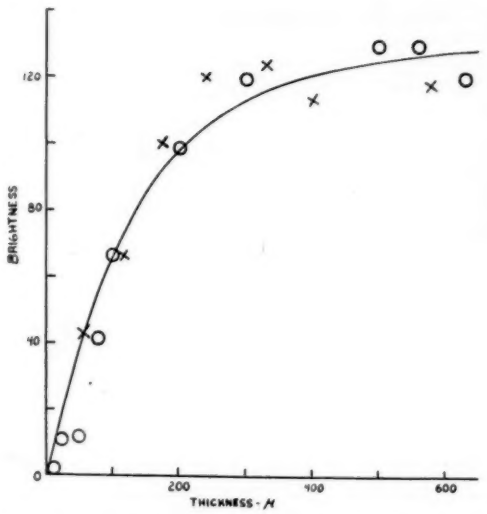

FIG. 2. Variation of initial brightness in arbitrary units with thickness of phosphor sample in microns.

refired. The thickness was determined by breaking the samples in several pieces and measuring the thickness of the layer with a comparator. The variations in thickness over the surface were less than ten percent. The solid line in Eq. (2) is from the equation $B=B_{\max}(1-e^{-.007x})$ where x is the thickness of the phosphor layer in microns. As can readily be verified from Eq. (1), the data would be expected to fit an equation of this form, where the number multiplying the thickness is equal to the sum of the absorption coefficients for visible and for infra-red light. Therefore, from the form of the decay curve μ_2/μ_1 is about 0.2; from the dependence of the brightness on thickness $\mu_1+\mu_2$ is about 70 cm^{-1}, from which $\mu_2 \approx 12$ cm^{-1} and $\mu_1 \approx 58$ cm^{-1}.

From these data it is possible to calculate the number of light quanta released per cubic cm of the phosphor. The light sum for a sample of the same composition as that used for the data in Fig. 2 was found to be 1700 micro-lambert minutes, which is equivalent to 0.1 lumen-sec. per cm^2. This should be multiplied by 12 cm^{-1}, the absorption coefficient for visible light, and by 2 because the light is emitted in both directions, giving 2.5 lumen-sec. per cm^3 as the actual light sum.

The visual efficiency of this phosphor[4] is known to be about 40 percent. Since 621 lumens is equivalent to one watt at 100 percent visual efficiency, this means that 250 lumens is equivalent to one watt for this phosphor. The energy stored is then $2.5 \div 250 = 0.01$ joule per cm^3. The average energy of the emitted quanta is about 2.5 electron-volts, from which one can calculate the number of stored quanta to be 2.6×10^{16} per cm^3.

The density of the phosphor layer has been determined to be 2.0 g per cm^3, about half that of the crystalline material. For these samples the activator concentration was 25 parts per million by weight of samarium and 200 parts per million cerium. The number of activator atoms present per cm^3 is then 2×10^{17} samarium and 16×10^{17} cerium. The number of light quanta stored per cm^3 was just calculated to be 0.26×10^{17}. This is one quantum for every 8 samarium atoms or one for every 60 cerium atoms. An earlier estimate[5] gave something more than one quantum per atom of samarium. This estimate, however, did not take into account the absorption of the infra-red and was too high on that account.

It is perhaps not significant that the number of stored quanta is only twelve percent of the number of samarium atoms present instead of being equal to it, since it is not known what the actual concentration of activator atoms in the base material is. The activator atoms are added to the flux and in the course of the subsequent firing it is not known in what proportion they distribute themselves between the flux and the base material. Experiments to determine this proportion would indeed be valuable but they are not easy to devise.

I am indebted to Professor Roland Ward, the director of the laboratory, under whose supervision the phosphors were made, to Mr. John Gentile who prepared the samples, and to Dr. W. L. Parker who built the electron multiplier apparatus with which the decay curves were determined.

[4] R. T. Ellickson, J. Opt. Soc. Am. **36**, 261 (1946).
[5] R. T. Ellickson, Phys. Rev. **70**, 685A (1946).

JOURNAL OF THE OPTICAL SOCIETY OF AMERICA VOLUME 36, NUMBER 9 SEPTEMBER, 1946

The Use of Heterochromous Lines in Spectrographic Photometry

S. LEVY AND O. W. CHRISTINE
Carnegie-Illinois Steel Corporation, Gary Works, Gary, Indiana
(Received May 23, 1946)

1.

THE spectral lines used as "working pairs" in spectrographic analysis are as a rule of a small wave-length difference. The main reason for this is that the characteristic curves of the photographic plate usually vary with the wavelength. The inconvenience of this restriction in the choice of lines is obvious, particularly in the analysis of non-ferrous metals when the number of suitable lines is limited. It might be desirable therefore to know just how much a large $\Delta\lambda$ could affect the reliability of the analysis in a given case. For this purpose, the relationship between the transparencies caused by spectral lines of a large $\Delta\lambda$ must be investigated as a function of exposure and plate contrast.

The results of such an investigation for a particular case made with Eastman Kodak Spectrum Analysis No. 1 plates are given here. A procedure based upon this relationship is described, permitting the use of lines of a large $\Delta\lambda$ when no other suitable lines are available.

2.

A typical example of erroneous analyses with lines of large $\Delta\lambda$ made with various exposures is given in Table I.

The first and the second columns represent the transparencies of the lines 3683.5 Pb and 3223.6 Sn, respectively. The third column gives the "analyses" of lead in tin in a sample containing 0.041 percent Pb, calculated with a calibration made with spectrograms of nearly uniform exposures, with transparencies of the Sn line between 0.6 and 0.7. Two tin pins were sparked and the variation in exposures achieved by introducing neutral screens of different transparencies. The range of variations of exposure are exaggerated purposely. In practical work the variation will usually be smaller. However, variations in the light source, in the optical arrangement, in plate sensitivity, and in developing procedure, particularly when accumulated, may produce noticeable deviations from standard exposure. In the above example, heavier exposures produce larger intensity ratios than the light ones, when calculated in the usual way, using plate calibration for one spectral region.

3.

If the relationship (obtained with a certain sample) between the transparencies such as the one shown in the Table I, column 1 and 2, were known for each plate, it could be used in the following way for calculation of the relative intensities (concentrations) in unknown samples. By measuring the transparency of the available reference line (in our example the tin line), with the aid of the mentioned relationship, the transparency of a line (not on the spectrogram) is determined of the same wave-length as that of the admixture line which can be used as an "internal standard line." Hence a characteristic curve of the plate can be applied to the transparency of the two lines, one of which is directly measured and the other deduced from a chart or diagram after measuring the line of the matrix. Thus, the intensity of the admixture line in a sample of unknown concentration is expressed in terms of the intensity of the same line corresponding to another sample of known concentration.

4.

It is unnecessary for this purpose to make a series of different exposures with a standard sample on each plate. It can be shown that changes in the relationship between the transparencies caused by lines of a considerable $\Delta\lambda$, such as that given in Table I, are small on plates

TABLE I.

T_{Pb}	T_{Sn}	Percent of Pb in Sn
0.12	0.19	0.068
0.22	0.27	0.055
0.27	0.30	0.053
0.63	0.54	0.040
0.92	0.85	0.038

of the same emulsion type but of varying contrast. Moreover, these changes can be accounted for on each plate if the characteristic curve of the plate for one wave-length region is known.

This can be demonstrated experimentally and also can be deduced by recalling the features of the characteristic curves of the photographic emulsions. They were discussed in a previous paper[1] in so far as the application to spectrographic analysis is concerned and have been since extensively tested in this laboratory. Their validity within the limits necessary for our present purpose can be considered established.

According to the previous findings the transparency of the emulsion in question can be considered (in a limited transparency range) as a function of $p \log E$ only, where p is a constant, characteristic of the plate contrast, and E is the light intensity (or exposure). In other words, the characteristic curve of a plate with a particular constant p_1 is obtained from that of a plate with different constant p_2 by expanding or compressing the $\log E$ abscissa in the ratio p_1/p_2. For the purposes of the present estimation we will consider the analytical approximation for the transparency as a function of exposure

$$T=\exp\left[-(k \log E)^2\right]$$

which, as was shown previously, correctly represents the characteristic curves for Spectrum Analysis No. 1 emulsion in the range of transparencies between 0.20 and 0.80. For lower and higher transparencies the same expression with a smaller k is suitable. For plates of different contrast, with k_s for the shorter wave-length and k_l for the longer, the following relationship (at least approximatively) exists: $k_s/k_l=\text{const.}$

TABLE II.

Plate	T_1	T_2	R	k
1	0.70	0.40	0.50	0.79
	0.50	0.24	0.50	0.79
	0.30	0.13_5	0.50	0.72
	0.20	0.09	0.50	0.64
2	0.70	0.35_5	0.44	0.96
	0.50	0.20_5	0.44	0.95
3	0.70	0.28	0.36	1.15
	0.50	0.17	0.36	1.13

[1] J. Opt. Soc. Am. **34**, 447 (1944).

This makes possible the use of characteristic curves prepared with light of one wave-length for working pairs of another wave-length, as pointed out previously.[1]

5.

Having in mind the features of characteristic curves mentioned in Section 4, the following estimation can be made of the influence of the plate contrast on the relationship between the transparencies of two lines of a considerable $\Delta\lambda$, at different exposures. The expression

$$T=\exp\left[-(k \log E)^2\right] \qquad (1)$$

will be used as a basis for the estimation.

(a) Let us first evaluate the k for plates of different contrast and consider T_1 and T_2, the transparencies of two lines of a small $\Delta\lambda$ denoted in the previous paper as the "gamma-pair." From (1) it follows $(-\log T_1)^{\frac{1}{2}}-(-\log T_2)^{\frac{1}{2}} = -k \log (E_1/E_2)$. With $E_1/E_2=0.5$ for the chosen lines, and transparencies measured on different plates, we obtain the values of k (Table II).

In the third column, R is the "intensity ratio" of the gamma-pair as determined with a certain characteristic curve accepted as the "basic" one. Its purpose is the determination of the characteristic curves for the individual plates (for details see reference 1). It can be seen that k is practically a constant in the range of transparencies, important for photometric measurements, in which the slope of H and D curve changes rapidly. Incidentally, a fair linear approximation for this part of the characteristic curve is obtained by plotting transparencies against $\log E$.

(b) Let us assume now that T_1 and T_2 belong to lines of a large $\Delta\lambda$. Suppose that for a certain plate the characteristic curves for the two wave-lengths correspond to k_1 and k_2, respectively. Then we have, using (1),

$$(-\log T_1)^{\frac{1}{2}}-(-\log T_2)^{\frac{1}{2}} = -k_1 \log E_1-k_2 \log E_2. \qquad (2)$$

Substituting $k_2=ak_1$, and $E_2=E_1m$, where m is the true intensity ratio of the two lines, (2) becomes

$$(-\log T_1)^{\frac{1}{2}}-(-\log T_2)^{\frac{1}{2}} = -k_1[\log E_1(1+a)+a \log m]=k_1 f(E). \qquad (3)$$

The Eq. (3) shows that $(-\log T_1)^{\frac{1}{2}}-(-\log T_2)^{\frac{1}{2}}/k$ is for the two lines a function of exposure only, that is, of the density level only, which is characterized, for instance, by T_1. For each k, T_2 can then be calculated, that corresponds to a given T_1, if the relationship is known for a certain k. That is to say, the relationship of transparencies of these two lines of different wave-lengths for plate of any contrast can be calculated if it has been found empirically for a certain contrast.

6.

This relationship can be found by making a series of spectrograms with a sample of known concentration of the impurity, preferably with one in the middle of the desired concentration range, using various neutral filters (wire screens, for instance). By averaging the results obtained with plates of varying contrast, a curve is obtained (the full curve of Fig. 1), which represents the relationship in question. In our case the average value for k was 0.96. The dotted and the broken curves are calculated with $k_1=0.79$ and 1.13, respectively, using (3). The calculated curves for different contrast were found to be consistent with the experimental results. The deviations of the calculated curves from each other are small. They are only slightly larger than the experimental scatter even for extreme variation of contrast.

7.

The relationship between the transparencies permits the use of lines of a large $\Delta\lambda$ for analytical purpose as indicated in Section 3. Since the changes in the relationship with varying contrast are small, three curves might be sufficient, as in Fig. 1, for the average and for the highest and the lowest contrast that can be anticipated. For intermediate values an interpolation can be applied. The use of these curves or of the corresponding tabulations is simple. It will be illustrated by means of Table III. It reproduces the measurements on plate with $k=0.96$ ($R=0.44$). With the help of the Fig. 1, for each T_{Sn}, a T_{ref}, the transparency of the reference line is found which has the same wave-length as the Pb line. Next, the intensity ratios or concentrations are determined, as usual, with the corresponding characteristic curve from T_{Pb} and T_{ref}. In the fourth column the resulting concentrations are given and in the fifth, for comparison, are the results obtained with T_{Pb} and T_{Sn} directly.

TABLE III.

T_{Pb}	T_{Sn}	T_{ref}	Percent Pb from T_{Pb} and T_{ref}	Percent Pb from T_{Pb} and T_{Sn}
0.11	0.18	0.13	0.043	0.068
0.16	0.21	0.16	0.039	0.058
0.23	0.27	0.24	0.041	0.053
0.32	0.33	0.33	0.041	0.050
0.52	0.45	0.52	0.040	0.043
0.51	0.46	0.53	0.041	0.044
0.57	0.50	0.58	0.040	0.041
0.61	0.53	0.63	0.041	0.041
0.68	0.56	0.66	0.038	0.038
0.69	0.57	0.67	0.038	0.038
0.73	0.61	0.70	0.038	0.038
0.83	0.72	0.81	0.039	0.037
0.85	0.77	0.84	0.041	0.039
0.95	0.90	0.94	0.040	0.038

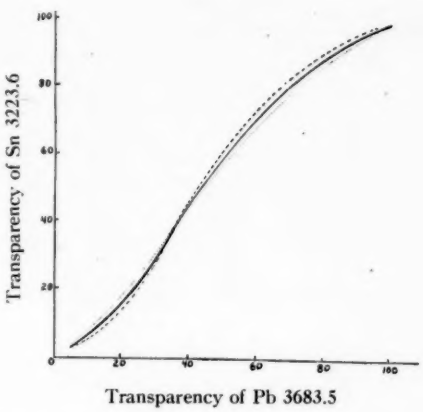

FIG. 1. The relationship between the transparencies of Sn and Pb lines at a certain Pb concentration. The full curve is the relationship for the average contrast ($k=0.96$), the broken curve is for high contrast ($k=1.13$), the dotted curve is for low contrast ($k=0.79$).

The same curve is applicable, of course, to other combinations of lines in the vicinity of those used for establishing the curve. Table IV gives the intensity ratios of two lines of iron spectrum, 3217 and 3650, obtained with the same curve. As it can be seen, the procedure eliminates the dependence of the ratios on the exposure.

Hence, this simplified method of heterochro-

TABLE IV.

T_{3217}	T_{3650}	T_{ref}	Intensity ratios from T_{3650} and T_{ref}	Intensity ratios from T_{3650} and T_{3217}
0.13	0.05	0.07	0.78	0.51
0.22	0.12	0.17	0.78	0.65
0.31	0.20	0.30	0.76	0.75
0.42	0.35	0.48	0.78	0.87
0.47	0.40	0.54	0.77	0.88
0.50	0.46	0.57	0.81	0.93
0.66	0.65	0.75	0.82	0.98
0.67	0.66	0.76	0.78	0.98
0.81	0.83	0.89	0.83	1.06

mous photometry can be used also in other cases where the true values of intensity ratios are of no importance and where, therefore, a calibrated light source is unnecessary; for instance, in the quantitative analysis by means of the Raman effect which is in principle similar to the spectrographic analysis by emission.

It must be pointed out, however, that the results of the heterochromous photometry can be expected, in general, to have a somewhat larger scatter in comparison to those in the usual monochromous photometry. The non-uniformity of the developed photographic emulsion might increase with the distance of the lines from each other. A smaller dispersion is therefore preferable.

JOURNAL OF THE OPTICAL SOCIETY OF AMERICA VOLUME 36, NUMBER 9 SEPTEMBER, 1946

A Theory of the Stiles and Crawford Effect

BRIAN O'BRIEN
Institute of Optics, University of Rochester, Rochester, New York
(Received June 22, 1946)

SOME thirteen years ago Stiles and Crawford[1] reported that light entering the human eye at the center of the pupil was several times more effective in producing the sensation of vision than light entering near the margin of the pupil. This is usually known as the Stiles and Crawford effect, and has been amply confirmed by several other investigators.[2–4] Subsequent work by the discoverers of the effect[5,6] has shown that it occurs for the light adapted but not for the dark adapted eye. Stiles[7] has shown that the effect is definitely related to cone vision, since it is found at all levels of adaptation when measurements are confined to the fovea. The effect is also found in any part of the retina when deep red light is used for illumination. In other words the effect is found to exist in all cases where the visual response is owing primarily to the cone cells, while under conditions where pure rod vision is assured there appears to be no Stiles and Crawford effect at all.

In Fig. 1 is shown a plot of the logarithm of the physical light flux necessary to produce a constant visual sensation as a function of position in the pupil through which the flux enters the eye. The abscissae are given in millimeters from the center of the pupil across a horizontal diameter. Negative values are used to denote distances nasalword, while positive values denote distances templeword from the center of the pupil. The points plotted are taken directly from published values of Stiles[7] and both sets of points are for wave-length 5000A. The upper set marked *PL* is for the light adapted parafovea while the lower set marked *FD* is for the dark adapted fovea. The smooth curves in Fig. 1 were not drawn by Stiles nor are they the curves best fitting the experimental points. These smooth curves will be discussed below.

It will be seen from Fig. 1 that the Stiles and Crawford effect is quite pronounced, since an area of the pupil some 3 mm from the center is only about one-third as effective as an equal area in the center of the pupil. A moment's consideration will show that the light loss along a marginal

[1] W. S. Stiles and B. H. Crawford, Proc. Roy. Soc. **B112**, 428 (1933), **B116**, 55 (1934).
[2] W. D. Wright and J. H. Nelson, Proc. Phys. Soc. **48**, 401 (1936).
[3] W. Dziobek, Licht **4**, 150 (1934).
[4] C. F. Goodeve, Proc. Roy. Soc. **A155**, 664 (1936).
[5] W. S. Stiles, Proc. Roy. Soc. **B123**, 90 (1937).
[6] B. H. Crawford, Proc. Roy. Soc. **B124**, 81 (1937).
[7] W. S. Stiles, Proc. Roy. Soc. **B127**, 64 (1939).

ray is actually less than that along the central ray because of the lesser thickness at the edge of the crystalline lens which is the principal absorber in the ocular media. For this reason it has been generally assumed that the Stiles and Crawford effect is caused in some manner by the obliquity of the marginal ray striking the retina. Since the distance from the second principal point of the eye to the retina is about 22.5 mm, we can convert displacements in millimeters across the pupil into angle of incidence on the retina. This has been done and the angle θ in degrees is also included in the scale of abscissa in Fig. 1.

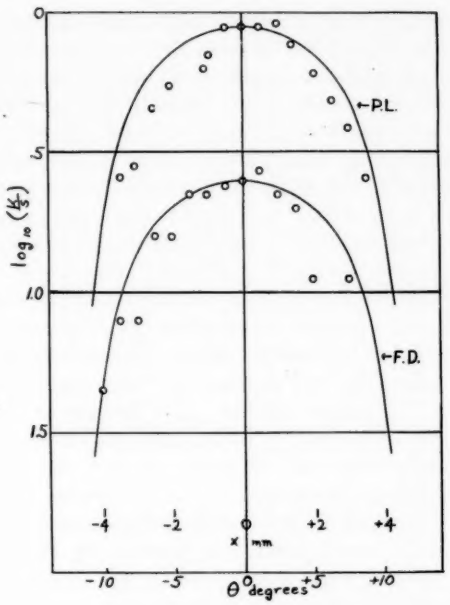

FIG. 1.

If the retinal cones were separated from each other by absorbing septa, one would expect precisely the effect observed, since light entering the retina obliquely would undergo greater absorption in the septa, so that less light would be available for absorption in the light receptor portions of the cone. However, with the exception of the very tips of the cones and rods, which under certain conditions are separated by pigment granules of the pigmented epithelium, no such absorbing septa or boundary layers for the rods or cones have been observed. The portion of the cone tips covered by these pigment granules is so small in any case that it seems very improbable that absorption by the pigmented epithelium can be of importance in causing the reduction in efficiency of the marginal rays.

It seems possible that the explanation of the Stiles and Crawford effect is to be found in the structure of the individual cone cell. The posterior termination of such a cell is shown schematically in Fig. 2. The cylindrical portion of the diagram from *A* to *B* represents the cone body from the external limiting membrane to the beginning of the so-called cone ellipsoid. The latter is represented by the conical region from *B* to *C*, while the outer segment of the cone is represented by the cylindrical region of smaller diameter from *C* to *D*. The proportions represented are roughly those to be found in cones at or just beyond the margin of the fovea, with the diameter of the outer segment about one-third the diameter of the cone body.

It has been observed for many years that the refractive index of the cones is higher than that of the surrounding medium. As early as 1843 Brücke[8] described the high refractive index of the retinal elements, and pointed out that because of their roughly cylindrical shape light should be

FIG. 2.

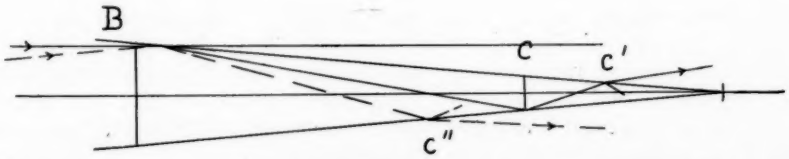

FIG. 3.

[8] E. Brücke, Archiv für Anatomie u. Physiologie **11**, 444 (1843), **14**, 387 (1847), **14**, 225 and 479 (1847).

multiply reflected down each element. Brücke further stated that such multiple reflection within the cylindrical portion of a rod or cone cell would prevent spreading of the image in the retina and thus improve visual acuity. We may go farther and examine the behavior of light in the conical portion of the cone cell from B to C. This is shown on a large scale in Fig. 3. It is evident that light entering parallel to the axis of the cone will be internally reflected at B, and will reach the surface of the cone again at C. If α be the half-angle of the cone it is evident that the angle of incidence at B will be $90-\alpha$, while the angle of incidence at C will be $90-3\alpha$. If the difference in refractive index between cone and surrounding medium is sufficient the light will again be totally reflected at C and will strike the surface of the cone a third time at C' at an angle of incidence $90-5\alpha$, etc., in the well-known manner of reflection of light within a polished cone. Let us suppose that the ratio of refractive index of the cone material to that of the surrounding medium, and the angle of the cone, are such that $90-3\alpha$ is the critical angle, the total reflection just occurring at C. Referring now to Fig. 2, it will be evident that all light entering at A parallel to the axis of the cell will be totally reflected within the conical portion BC, and will continue to be totally reflected down the cylindrical portion CD. This will result in a very marked concentration of light flux within the outer segment of the cone CD.

Numerical values for the refractive index of the various portions of cone cells are not available, but the effect of concentrating all the light into the outer segment of the cone can be accomplished with very reasonable values of the refractive index. Thus if the half-angle of the conical portion be taken as 4° then the ratio of the refractive index of the cone to that of the surrounding medium need be only 1.022 in order to provide the total reflection shown, with a reduction of diameter from cone body to outer segment in the ratio of three to one, or a concentration of light flux in the ratio of nine to one. Since the cone and rod bodies or inner segments are packed tightly together, it follows that substantially all light incident upon the rod and cone layer may be concentrated in the outer segments of the retinal elements.

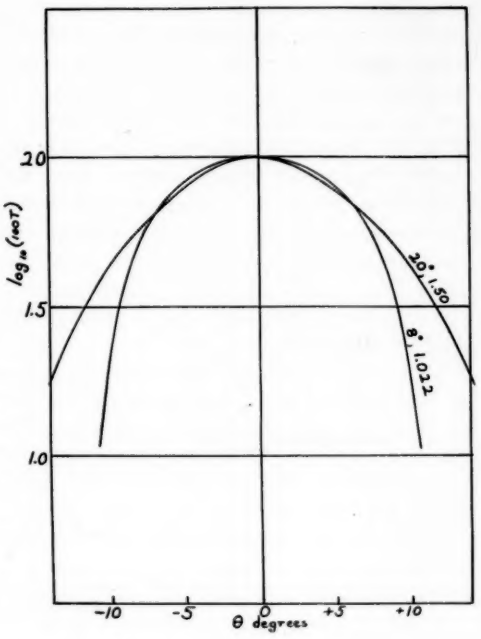

FIG. 4.

Let us now consider an oblique ray entering the conical portion as shown by the dotted line of Fig. 3. Total reflection may still occur at B, but under the conditions described above total reflection will no longer take place on the second incidence of the ray upon the cone surface at C'', and much of the light will escape into the surrounding medium. Thus for the particular example cited there will be a marked reduction in the light flux passing down the outer segment of the cone CD when the incident bundle makes a small angle with the axis of the cell. The fraction of the light entering the cylindrical outer segment at C for the particular numerical example mentioned above is shown by the full curves of Fig. 1 as a function of the angle between the axis of the bundle and the axis of the cell. The condition for all the light entering the cylindrical outer segment at C is represented by the highest point of the smooth curves. As with the plotted points, the absolute values of the smooth curves are of no significance, the curves like the experimental points of Stiles being plotted on a relative logarithmic scale.

The smooth curves of Fig. 1 are certainly not

the best fit to the experimental points which might be made, but when one considers the simplified optical system used to represent a cone, the agreement is quite striking. The form of the curves is not very sensitive to the angle of the cone or refractive index ratio selected. This is shown by Fig. 4 where a very different case, that of a cone of full angle 20° with refractive index 1.5 times its surroundings, is plotted on the same scale with the previously cited case of a cone of 8° full angle with refractive index 1.022 times that of its surroundings. In the case of the 20° cone the frustrum was terminated at the point C' in Fig. 3 where the third reflection occurs, rather than at the point C (second reflection) as used in the first example. In spite of the large difference in angle and refractive index, it will be noted that the general form of the two curves in Fig. 3 is the same. By properly selecting cone angle, length of frustrum, and refractive index ratio, it is probable that a very much better fit to the experimental points could be obtained, but this does not appear useful at present. The cone ellipsoid is not a simple conical member, and we do not know either the value of the refractive index or whether this index is constant throughout the outer portions of the cone cell. Thus a better fit to the experimental points would add little in substantiating the present hypothesis. It is necessary to make more careful measurements of cone sections from various portions of the retina and to attempt fair quantitative determinations of refractive index before much dependance can be placed on further numerical results. These measurements are being undertaken.

For the present it appears that total internal reflection within the conical portion of the retinal cones may be responsible for very substantial concentration of light in the outer segments, and also responsible for the Stiles and Crawford effect, providing that the principal absorption resulting in cone vision occurs in the outer segment of the cone cells. If the photo-receptor pigment of the cones is concentrated largely in the outer segments, and if the cones have a higher refractive index than their surroundings, a Stiles and Crawford effect would necessarily follow, although not necessarily in quantitative agreement with the observed results. Conversely, the existence of the Stiles and Crawford effect would seem to be evidence that the principal photo-reception does occur in the outer segment or at least in the smaller diameter end portions of the cones.

It may well be asked why, according to the present hypothesis, there is no Stiles and Crawford effect observed for pure rod vision. This may be accounted for by differences between the rods and cones in geometry, refractive index, and distribution of the respective photo-receptor pigments. The inner and outer segments of the rods are nearly the same diameter, and geometry alone might be sufficient to explain the absence of the effect were it not for the morphological similarity between the rods and the foveal cones. If the refractive index of the rods is found to be substantially lower than that of the cones, this may account for the observed difference in behavior. Of equal or perhaps greater importance may be the difference in pigment distribution. In addition to the factors of shape and index, it would be necessary that the rhodopsin be concentrated largely in the outer segment of the rods if a Stiles and Crawford effect for rod and vision were to be predicted on the present hypothesis.

In conclusion it must be emphasized that the theory of the Stiles and Crawford effect here proposed does appear to fit the observed facts in a roughly quantitative manner. More quantitative data on the retinal elements are required, however, to provide a critical test of its validity.

Announcement

The new officers of the Optical Society of America, Rochester Section, for the coming year are as follows:

President: ROBERT E. HOPKINS
Vice President: ARTHUR F. TURNER
Secretary: ROBERT N. WOLFE
Treasurer: ERNEST H. GREPPIN
Councillors: BRIAN O'BRIEN, ALAN A. COOK, MRS. H. G. KINGSLAKE, GORDON L. WALLS
Program Committee: MAX HERZBERGER, WAYNE G. NORTON, HARRY D. POLSTER.

A Reflectance Measuring Attachment for the Beckman Spectrophotometer*

G. E. PRIDE
Research Division, American Optical Company, Scientific Instrument Division, Buffalo, New York

THIS paper describes an attachment for the Beckman spectrophotometer[1] which extends the use of this instrument to include the measurement of regular spectral reflectance at 45° or normal incidence of thin glass plates, up to 2″×2″ in size. This unit is conveniently mounted on the spectrophotometer in place of the photo-tube compartment. The latter is attached to the unit at its exit aperture.

The essential components are shown in Figs. 1 and 2. Figure 1 shows: *A*—sliding carrier for the sample and standard plates; *B*—the 45° beam splitter; *C*—the collector lens; *D*—the autocollimating telescope with Gaussian eyepiece; *E*—the inclined shielding mirror for the telescope objective. Figure 2 shows: *F*—the externally-manipulated screwdrivers for turning the adjusting screws in the plate carrier *A*; *G*—the clamp bearings for the beam splitter and plate carrier posts; and *H*—the light trap. Figure 1 also shows some of these parts in their respective places in the apparatus as it is used in the measurement of reflectance at normal incidence. The path traversed by the light beam through the unit is indicated. Since measurements are made of the sample's reflectance in terms of the known reflectance of a standard plate, the sample and the standard are alternately exposed to light from the beam splitter by moving the plate carrier along its slide. Light is reflected normally from the plates' surfaces and passes through the beam splitter to the collector lens, which focuses the light into a definite area on the photo-tube.

The plate carrier holds the standard and sample plates side by side with their surfaces parallel. Each plate is held in the carrier by three screw-opposed springs. The screws have slotted heads and are engaged by the three externally-manipulated screwdrivers during the autocollimation of the standard and sample plates. The carrier is mounted on a carefully fitted, lapped dovetail slide. The quality of the fit in the slide is important since the standard and the sample must move and remain in parallel planes during alternate exposure to the incident light beam. The preservation of parallelism after autocollimation insures that the surfaces of both plates shall remain normal to the incident beam. External means for moving the carrier along its slide is afforded by a removable handle which is inserted through a sliding light-shield in the closed cover of the unit, Figs. 1 and 2. This handle fits into a socket in the top of the carrier. The whole carrier assembly is mounted on a cylindrical post which projects

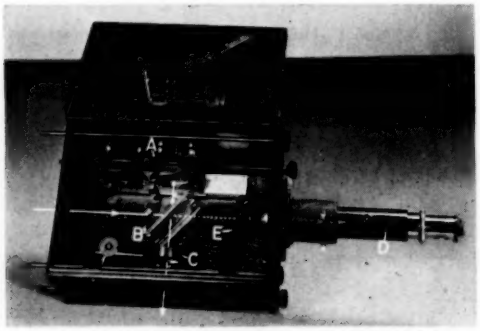

FIG. 1. Top view, showing components of attachment as used in measurement of reflectance at normal incidence; *A*—plate-carrier; *B*—beam splitter; *C*—collector lens; *D*—autocollimating telescope; *E*—inclined shielding mirror for telescope objective.

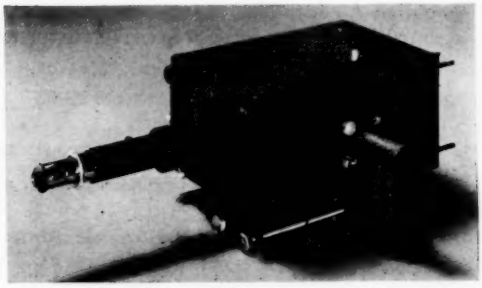

FIG. 2. Rear view of attachment, showing: *F*, externally-manipulated screwdrivers; *G*, clamp bearings for plate-carrier and beam splitter; *H*, light trap.

* Paper presented at the Winter meeting of the Optical Society of America at Cleveland, Ohio, March 7–9, 1946.

[1] H. H. Cary and Arnold O. Beckman, J. Opt. Soc. Am. **31**, 682 (1941).

through the bottom of the case into an external clamp bearing, Fig. 2.

The beam splitter, *B*, Fig. 1, has a three-point spring contact mounting, with a screw opposing the upper of the springs. This screw provides a tilt adjustment which is used in autocollimation. The whole beam splitter unit is mounted on a cylindrical post which fits, just as for the plate carrier, into an external clamp-bearing. This similarity in mounting of the plate carrier and beam splitter permits substitution of the former for the latter in measurements of reflectance at 45° incidence as in Fig. 3.

The autocollimating telescope is mounted in a ball-and-socket joint in the end of the case opposite to the entrance aperture, Fig. 1. It is used to autocollimate the beam splitter, the standard and the sample plates. Autocollimation assures that the light reflected from the surfaces of the plates shall always strike the same area on the surface of the photo-tube and that the angle between the incident light and the plates' surfaces shall be 90°.

When measurements are being made, the light which would be incident upon and reflected normally by the objective lens of the telescope and back into the system is deflected upward by the inclined shielding mirror *E*, Fig. 1, and is absorbed by the blackened top and sides of the case.

Another precaution against the re-entrance of unwanted light into the system is the light-trap *H*, Fig. 2. This consists of an L-shaped tube (Fig. 4) mounted in the side of the case directly

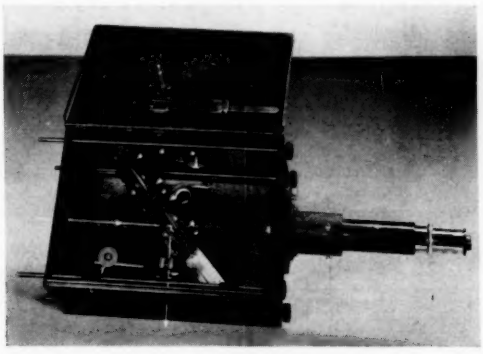

FIG. 3. Attachment as used in measurement of reflectance at 45° incidence.

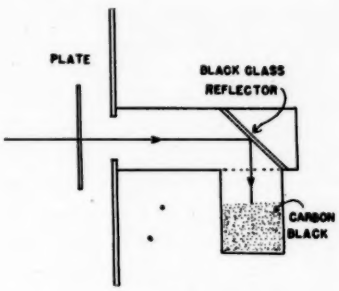

FIG. 4. Schematic diagram of light trap.

behind the plate carrier (Fig. 2). Light which is not reflected from the sample and the standard plates is transmitted and passes down the long portion of the *L*, where it is partially absorbed by a black glass reflector set at 45°. The remainder is reflected downward through 90° into the short arm of the *L* where it is further absorbed in a deep, loosely packed bed of carbon black. Thus, the large quantity of light which is transmitted through highly transparent plates cannot re-enter the system and subsequently be picked up by the photo-tube along with the reflected light.

Additional measures have been taken to exclude errors in measurement. These include the treatment, where feasible, of the air-glass surfaces in the spectrophotometer itself with reflection-reducing coatings. In the optical system of the attachment, the second surface of the beam splitter and the surfaces of the collector lens have been similarly treated. Coating was also applied to the entrance windows of the photo-tubes. This treatment reduces injurious effects of light scattered and inter-reflected from air-glass surfaces, and a portion of the light energy which might thus be lost is now utilized. Apertures have been modified in the exit arm of the spectrophotometer and in the photo-tube compartment. This results in further elimination of scattered light.

The housing of the unit is made from an aluminum casting. This accomplishes two purposes. The weight of the unit is held to a minimum, thereby lessening mounting strain, while enough wall thickness is provided to allow drilling and tapping of holes of sufficient depth for the attaching of the photo-tube box, the telescope

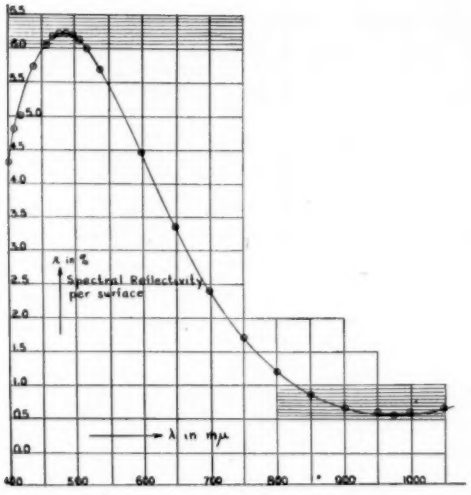

FIG. 5. Spectral reflectivity of MgF_2-coated glass surface.

r_{max} (theoretical) = 6.287 percent;
r_{max} (from curve) = 6.230 percent;
difference = 0.057 percent;

$$\text{percent error} = \frac{0.057}{6.287} \times 100 = 0.91.$$

mount and the external clamp bearings. The top of the housing has a tightly fitted cover which is hinged from the outside and which, when closed, drops into a milled-out ledge around the top of the housing.

Following autocollimation of the sample and the standard plates, the measurement of reflectance of the sample in terms of that of the standard are made by the same operations one uses in measuring the spectral transmission of a sample with respect to the known transmission of a standard.

Only one step need be taken to convert the attachment for the measurement of spectral transmission. The beam splitter is removed, and in its place is installed a full-silvered mirror. This mirror receives light from the transmission sample at the exit of the monochromator and reflects it through 90° to the photo-tube. When desired, for this purpose, the unit is easily converted to the conventional spectrophotometer arrangement except for the altered apertures.

The experimental error encountered in reflectance measurements is within ±0.5 percent of the measured values at high reflectances, that is, of high reflecting surfaces such as silver or aluminum. This error increases slowly with decreasing values of reflectance.

The attachment has been successfully used, for example, in the investigation of the optical properties of magnesium fluoride-coated glass surfaces. Figure 5 shows a sample curve taken from the above work. This graph represents reflectance per surface of a magnesium fluoride-coated glass plate measured at normal incidence in terms of the known reflectance of an uncoated spectacle crown glass standard. The sample plate was coated on both sides with identical thicknesses of material in order to reduce error and uncertainty in interpreting the measurements. It can be shown that the experimental error is minimized when the front and back surfaces are thus coated. This curve affords a numerical check on the corresponding error in measurement of surface reflectance in the vicinity of 6 percent. Since the theoretical value of the maximum reflectance of the coated glass surface (occurring here at 487 millimicrons) should be equal to that of the same glass surface uncoated, we may see what error is present. The theoretical value of the reflectance for the uncoated surface is 6.287 percent while the measured value is 6.230 percent. The difference is 0.057 percent and hence the error in measurement is 0.91 percent.

Table I shows other checks made on the accuracy of measurement. Reflectances of two

TABLE I. Reflectances of two dense flint glasses, *A* and *B*, measured at normal incidence, in terms of a spectacle crown standard.

R (%) \ λ (mμ)	450	500	550	600	650	700	750	800
Theoretical	13.2683	12.9507	12.7433	12.5937	12.4685	12.3491	12.2792	12.2094
Measured *A*	13.17	12.95	12.74	12.59	12.47	12.39	12.33	12.36
% Error *A*	−0.72	−0.030	−0.20	−0.44	+0.15	+0.35	−0.38	+1.24
Measured *B*	13.13	12.97	12.79	12.64	12.55	12.45	12.34	12.36
% Error *B*	−1.03	+0.20	+0.35	+0.35	+0.61	+0.80	+0.53	+1.24

dense flint glasses of the same and accurately known index were measured at normal incidence in terms of the calculated reflectance of a spectacle crown standard. The theoretical values for reflectances of the flint glass were also calculated from the index of refraction and tabulated over the range of wave-lengths of the measurements. A comparison between theoretical and measured values shows that the experimental error varied between −1.03 percent and +1.24 percent of theoretical values. Absorptions of all the glasses were measured and properly taken into account.

Systematic errors of about 1 percent of the reflectance itself may be expected in measuring reflectances in the neighborhood of 6 percent per surface. This error is sufficiently small so that the apparatus can be used to confirm the conclusions drawn from the electromagnetic theory with regard to thin films on glass.

JOURNAL OF THE OPTICAL SOCIETY OF AMERICA VOLUME 36, NUMBER 9 SEPTEMBER, 1946

Experimental and Theoretical Results in Two-Layer Low Reflecting Coatings for Glass

PETER KING AND LUTHER B. LOCKHART
Naval Research Laboratory, Washington, D. C.
(Received June 8, 1946)

INTRODUCTION

ALTHOUGH much material is to be found in the literature[1–3] on low reflecting coatings for optical surfaces, few experimental results obtained with a two-layer coating have come to our attention. Until Mooney[4] published his results of the exact treatment of the one- and two-layer case, there was not available any easy means of calculating the results to be expected with this system. A method, valid for the general case of absorbing layers and all angles of incidence, has been in use for some time at the Naval Research Laboratory for calculating the case of n layers with very little difficulty and will be published at a later date.[5]

This general method has been applied to the present case of two transparent layers with the light at normal incidence. The relationship between the indices of the two layers and the glass for quarter wave films is presented here to show the tolerance allowable in the thicknesses of the two layers used for coating the optical surfaces. Also, curves are presented to show the agreement with theory of actual spectral curves of coatings with different thickness layers and different indices.

The general equation[5] for reflection of light, considering no absorption, from a transparent surface coated with two superimposed films is given in the following relation:

$$R=|[n_2n_3(1-n_1)-(n_2^2-n_1n_3^2)\tan w_2\tan w_3]+i[n_3(n_1-n_2^2)\tan w_2\cdots +n_2(n_1-n_3^2)\tan w_3]/[n_2n_3(1+n_1)-(n_2^2+n_1n_3^2)\tan w_2\tan w_3]\cdots +i[n_3(n_1+n_2^2)\tan w_2+n_2(n_1+n_3^2)\tan w_3]|^2, \quad (1)$$

where

n_1 = index of refraction of the material coated,
n_2 = index of first or bottom layer, d_2 its thickness,
n_3 = index of second or top layer, d_3 its thickness,
$w_2=2\pi n_2d_2/\lambda$,
$w_3=2\pi n_3d_3/\lambda$,
λ = wave-length, and
$i=(-1)^{\frac{1}{2}}$.

For two superimposed quarter-wave films (optical thickness is meant in all cases) it is seen, dividing the right-hand side of Eq. (1) by $\tan w_2 \tan w_3$, that the reflection is given by the expression

$$R=[(n_2^2-n_1n_3^2)/(n_2^2+n_1n_3^2)]^2. \quad (2)$$

[1] C. H. Cartwright and A. F. Turner, U. S. Patent 2,281,474, April 28, 1942.
[2] A. Smakula, Physik. Zeits. **43**, 217 (1942).
[3] British Sci. Inst. Research Assn., British Patent 538,273, July 28, 1941.
[4] R. L. Mooney, J. Opt. Soc. Am. **35**, 574 (1945).
[5] B. Salzberg, private communication, to be published soon.

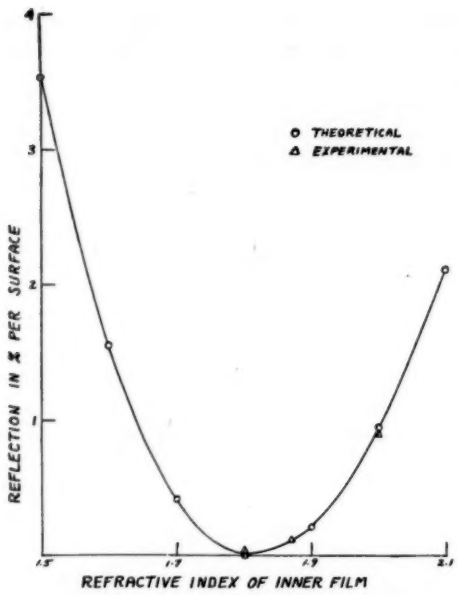

FIG. 1. Effect of changes in the refractive index of the high index film on the minimum reflection obtainable with two quarter-wave films. Index of top film, 1.47; index of glass, 1.525.

The reflection becomes zero when

$$n_2=(n_1n_3^2)^{\frac{1}{2}}, \tag{3}$$

which is the same as that given by Mooney.[4]

Comparing this with the expression for zero reflection in the case of a one-layer quarter wave film, $n_2=(n_1)^{\frac{1}{2}}$, where n_1 is the index of coated material and n_2 the index of the film, it is seen that in order to achieve low reflection there are more variables involved and a wider choice of materials possible. As all practical substances available at present have an index of refraction much higher than $(1.5)^{\frac{1}{2}}$ or $(1.6)^{\frac{1}{2}}$, there is little hope of obtaining really low reflection from a single layer which is both durable and non-scattering. With the greater choice of materials in the two-layer case it should be possible to produce coatings which, for a particular wave-length, will give nearly zero reflection.

Also it is readily seen that quarter-wave films are not necessary in order to obtain zero reflection at a particular wave-length. This requirement has been implied in previous reports on this subject.[4]

Considering Eq. (1), we see that it is of the form

$$R=|(a+ib)/(c+id)|^2.$$

If $a=0$, and $b=0$, while c or d does not equal zero, the reflection is equal to zero. From Eq. (1)

$$\tan w_3=-n_3(n_1-n_2^2)\tan w_2/n_2(n_1-n_3^2), \tag{4}$$

$$\tan w_2=[n_2^2(n_1-1)(n_1-n_3^2)/(n_2^2-n_1n_3^2)(n_1-n_2^2)]^{\frac{1}{2}}. \tag{5}$$

If the quantity in the brackets of Eq. (5) is positive, there is a solution and thicknesses other than a quarter-wave will result in zero reflection. For the films considered here

$$n_2^2>n_1,$$
$$n_3^2>n_1.$$

The term in the brackets will be positive for those values of n_1, and n_2 and n_3 where $n_2^2>n_1n_3^2$ and thus there will be a number of combinations of n_1, n_2, n_3 that will give zero reflection. Holding n_1, the index of the glass constant, there still exist many combinations of n_2, n_3, which give zero reflection. If we assume the following practical values for the indices, $n_2=2.0$, $n_1=1.75$, we find n_3 must be less than 1.51, which is possible to attain. When $n_2^2=n_1n_3^2$ we return to the quarter-wave case.

EXPERIMENTAL

All experimental coatings produced for this work were made by deposition of the coating material from solution.[6] Using this process it is possible to vary the index of the coating material from about 1.47 to 2.0 with ease.

The index of the particular material used was determined by coating glass of known index with a quarter-wave film of the material, obtaining the spectral curve with a General Electric recording spectrophotometer and calculating the index from the maximum or minimum reflection value, using the relation[2]

$$R=[(n_1-n_2^2)/(n_1+n_2^2)]^2,$$

where n_1=index of glass and n_2=index of coating.

This procedure also permitted the determina-

[6] This process was originated by the American Optical Company, Southbridge, Massachusetts.

tion of the experimental conditions necessary for depositing a film of known thickness.

For ease of identification the high index material next to the glass will be called the first layer and the low index material the second layer. Knowing the relationship between the indices (Eq. (3)), and also that the lowest index easily available without evaporation which is both durable and non-scattering is of the order of 1.47, one obtains 1.81 for the index of the material to be used next to glass of index 1.525. What happens to the minimum reflection with changes in the index of the first coating is shown in Fig. 1. It is apparent that considerable variation in its index is permissible without the loss of much efficiency in reflection reduction, provided true quarter wave films are used. The points marked with small triangles are experimental values obtained with three different indices and show what can be expected in comparison with theory. These cases are for quarter-wave films and the question arises, "What happens to the amount of light reflected if the thicknesses are not exactly a quarter-wave?" Holding the thickness of the first layer at a quarter-wave-length and allowing the second layer to vary in thickness, one obtains Fig. 2. Figure 3 is obtained when the thickness of the second layer is held constant at a quarter-wave and the first layer varied. It appears that small changes in the thickness of the second layer have a greater effect on the reduction at the minimum point than the same changes in the first.

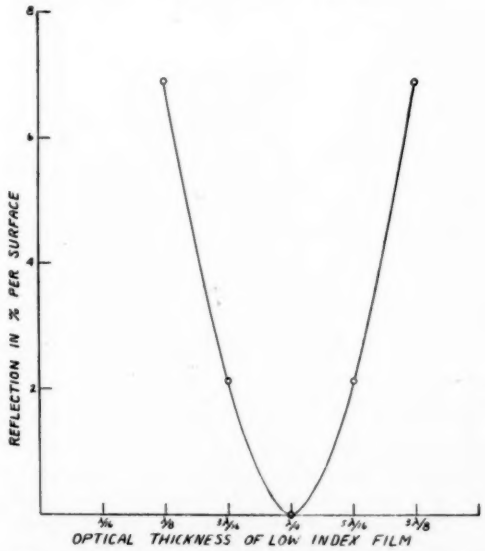

FIG. 2. Variation of the reflection minima of a two-layer system with changes in thickness of the low index film over a quarter-wave film of high index material. Index of top film, 1.47; index of inner film, 1.80; index of glass, 1.525. (Theoretical)

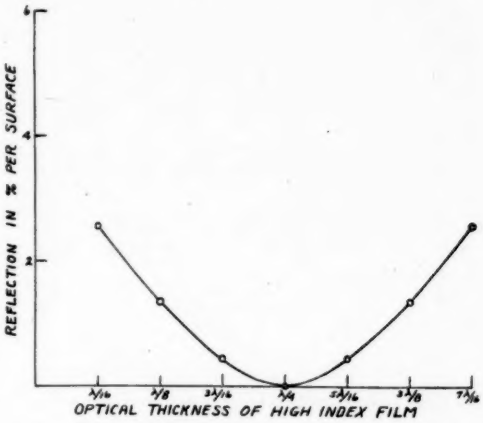

FIG. 3. Variation of the reflection minima of a two-layer system with changes in thickness of the high index film under a quarter-wave film of low index material. Index of top film, 1.47; index of inner film, 1.80; index of glass, 1.525. (Theoretical)

When one considers the point of minimum reflection and the effect of variation in the index of the glass on this minimum, the two-layer system is quite effective compared with the one layer. It is not necessary to change the index of the lower layer for each different glass to obtain very effective coatings. Figure 4 shows the change in the minimum of the reflection curve for the one and two-layer cases. Given two materials having indices of 1.47 and 1.80, glass from 1.50 to 1.70 can be coated and the minimum reflection still be less than 0.5 percent.

The simplest case to consider in applying two layers of material to a glass object is the one in which each is a quarter-wave-length thick. The theoretical reflection curve for this is shown in Fig. 5 by the dotted line. The solid line is the experimental curve; the agreement is good and the differences between the two can be explained by very slight errors in the thicknesses of the coatings and by the fact that the indices were assumed to be constant over the entire range. At the minimum point, where the indices were

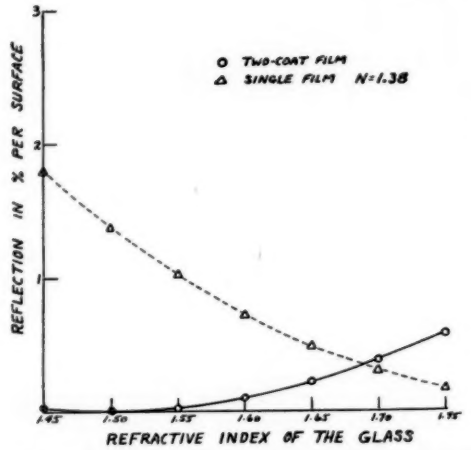

FIG. 4. Comparison of the reflection minima obtainable with a magnesium fluoride film (index 1.38) and a coating composed of two quarter-wave films on glasses of different indices. (Index of top film, 1.47; index of bottom film, 1.80.) (Theoretical)

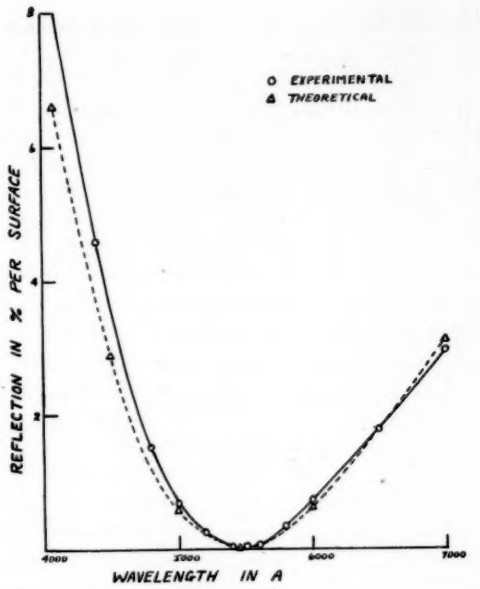

FIG. 5. Spectral reflection of a coating composed of two quarter-wave films. Index of top film, 1.47; index of inner film, 1.80; index of glass, 1.525.

correct, the experimental and calculated points coincide. When a three-quarter wave-length film of low index material is placed over a quarter of high index, the type of result obtained is shown in Fig. 6. The agreement between theory and experiment is good.

Although quarter-wave films do give a minimum, other combinations can also result in zero reflection as has been shown. The shape of the reflection curve obtained may be changed considerably from that of quarter wave films but the effectiveness is maintained. Figure 7 shows a combination which results in zero reflection when other than quarter-wave films are used. In this case a 0.190 wave-length film of low index was used over a 0.385 wave-length film of high index material. The values were $n_1=1.53$, $n_2=2.0$, and $n_3=1.47$.

A coating was produced using a film of high index (1.87) approximately $\frac{3}{8}$ wave thick and a sufficient thickness of a film of low index (1.47) to give a low over-all reflection to white light. The spectral curve of this coating is shown in Fig. 8 and is compared with the calculated spectral curve for a coating composed of a 0.350 wave film of 1.87 index under a 0.20 wave film of 1.47 index. Such a combination does not result in zero reflection for any particular wave-length, but its minimum is about 0.04 percent

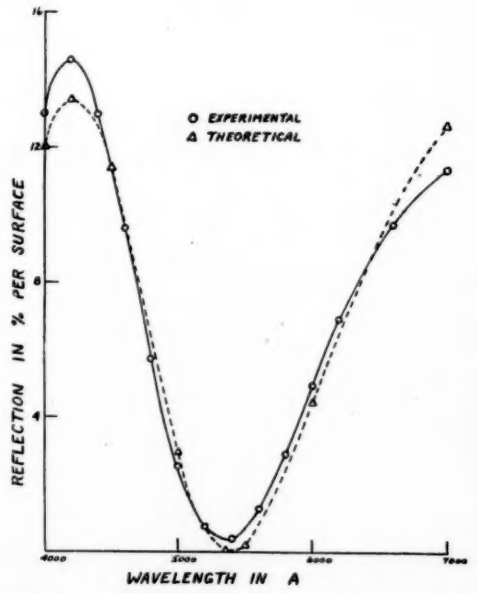

FIG. 6. Spectral reflection of a coating composed of a three-quarter wave film of low index over a quarter-wave film of high index. Index of top film 1.47; index of inner film 1.87; index of glass, 1.53.

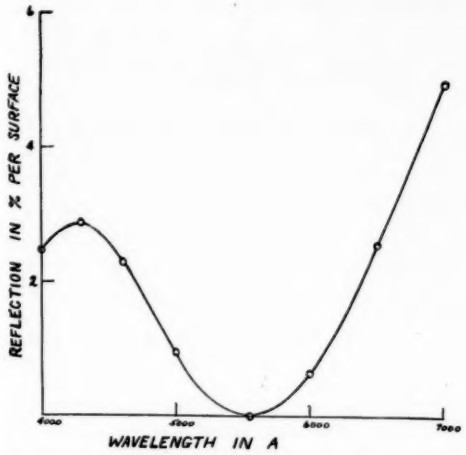

FIG. 7. Spectral reflection of a coating composed of a 0.190 wave film of low index over a 0.385 wave film of high index. Index of top film, 1.47; index of inner film, 2.00; index of glass, 1.53. (Theoretical)

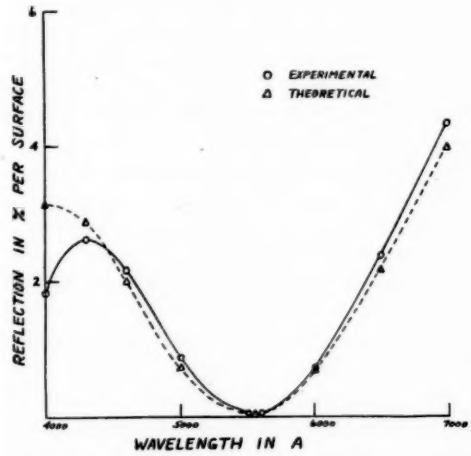

FIG. 8. Spectral reflection of a coating having a low over-all reflection toward visible light but not having zero reflection at the minimum. Index of top film, 1.47; index of inner film, 1.87; index of glass, 1.53.

per surface and its over-all reflection is low. Experimentally, the reflection amounts to 0.53 percent per surface when measured with a cell whose response is similar to that of the eye.

Considering Fig. 2 where it is shown that 1.81 index material is needed next to the glass to

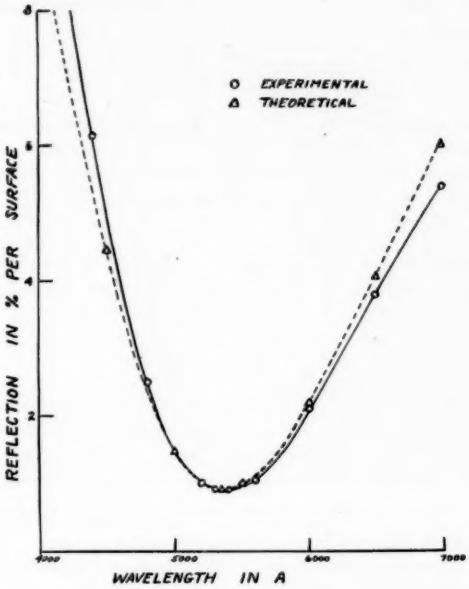

FIG. 9. Spectral reflection of a coating composed of two quarter-wave films whose indices are not properly matched. Index of top film, 1.47; index of inner film, 2.00; index of glass, 1.53.

give zero reflection, an index of 2.0 gives a minimum reflection of a little less than 1 percent. What happens to the over-all reflection of such a system is shown in Fig. 9. The minimum reflection is as expected and the experimental points agree with the theoretical. The over-all reflection to white light is not high; when measured with a cell whose response is similar to that of the eye, it is about 1.6 percent.

Similar curves can be obtained for an infinite number of combinations of thicknesses and indices. The point of minimum reflection can be changed at will and also the amount of light reflected at the minimum. The best combination which results in zero reflection for a particular frequency is not yet known. For low reflecting coatings that system which gives the greatest "band width" at the minimum would be the most satisfactory.

We wish to thank Dr. D. C. Packer of the Naval Gun Factory for obtaining the experimental spectral reflection curves.

JOURNAL OF THE OPTICAL SOCIETY OF AMERICA VOLUME 36, NUMBER 9 SEPTEMBER, 1946

A Fast Superconducting Bolometer*

DONALD H. ANDREWS, ROBERT M. MILTON, AND WARREN DESORBO
Chemistry Department, The Johns Hopkins University, Baltimore, Maryland

A superconducting bolometer has been developed for the fast detection of infra-red signals. It has a compound response in which the primary response time is about 5×10^{-4} sec. and the secondary response time about 5×10^{-2} sec. In the primary range a signal of $5\times10^{-4}\,\mu$ watt is equivalent to the noise of the apparatus. The frequency at which the response is down 6 db from the primary maximum value is 3000 c.p.s. and from the secondary maximum value about 140 c.p.s. The bolometer consists of a ribbon of CbN, $200\times10\times0.25$ mils, attached to the surface of a copper base-plate by means of a coating of Bakelite cement which covers the lower face of the ribbon and is about 0.1 mil thick. This unit is placed beneath a rocksalt window in the vacuum chamber of a cylindrical cryostat, 12″ long×6″ diameter, which maintains operating temperature for about twelve hours when filled with 1000 cm³ each of liquid nitrogen, and liquid hydrogen kept at the triple point. For best operation this temperature must lie within a certain region of the superconducting transition zone at about 15°K where $dR/dT=10$ ohm deg.$^{-1}$ and $R=0.2$ ohm. The noise level varies with temperature in the transition zone and passes through several maxima and minima with variations in level of more than tenfold. Even at the minima it is at least ten times higher than in either the normal or superconducting states immediately above or below. For most sensitive operation, the temperature is kept constant at one of these minima by means of a precisely adjusted current which passes through a heating coil wound on the copper rod supporting the base plate. Radiation signals produce variations in resistance of the ribbon, observed by means of a bridge circuit, transformer, and amplifier.

IN the construction of receivers for the measurement of infra-red radiation, there have always been two objectives: sensitivity and speed. The nature of the measurement sometimes emphasizes sensitivity, sometimes speed, but both are always desirable. During the last few years a number of measuring devices have been built which have pushed sensitivity to the limit imposed by Brownian movement, that is, by inherent fluctuation in the instrument itself. If the sensitivity were to be increased beyond this limit, it would be necessary to lower the temperature of the essential parts of the receiving elements. Generally, such a lowering turns out to be a mixed blessing, because the reduction in thermal fluctuation is accompanied by even greater reduction in the response coefficient of the instrument, leaving one with a net decrease in sensitivity. For example, a single constantan-copper thermocouple has a response coefficient of about 40 microvolts per degree at room temperature, and this drops to about 3.7 microvolts per degree at 15°K. Over the same range the thermal fluctuation in terms of microvolts is reduced only by a factor of $4\frac{1}{2}$.

There are, however, certain phenomena for which the associated response coefficients increase markedly at low temperatures. Of these, superconductivity is particularly suited for bolometric purposes. Thus, one finds that a coil of tantalum, with 0.7-ohm total resistance, has a response coefficient of 260 ohms per degree in the transition interval between the normal and the superconducting state.

This suggested to us the possibility of making bolometers of superior sensitivity by operating in the temperature range where superconducting transitions could be found. There were, of course, two disadvantages in such a procedure: first, the complexity of the apparatus necessary to produce and maintain a temperature near absolute zero, and, second, the difficulty in thermostating the superconducting bolometer so as to maintain it in its sensitive region within the superconducting transition zone. Nevertheless, the need for faster and more sensitive bolometers justified an investigation, and research[1] along these lines was started at The Johns Hopkins University in 1938. Before the first results[2] were published, the idea of the superconducting bolometer was suggested independently by A. Goetz.[3] The response characteristics of the first superconducting bolometer made of tantalum were so encouraging with regard to high sensitivity that a second

* Paper presented at the Winter Meeting of the Optical Society of America, Cleveland, Ohio, March 7–9, 1946.

[1] D. H. Andrews, *American Philosophical Yearbook* (1938), p. 132.
[2] D. H. Andrews, W. F. Brucksch, Jr., W. T. Ziegler, and E. R. Blanchard, Rev. Sci. Inst. **13**, 281 (1942).
[3] A. Goetz, Phys. Rev. **65**, 1270 (1939).

investigation was started in the fall of 1942 in order to see whether this high sensitivity could be coupled with high speed of response. Such bolometers are peculiarly suitable for high speed work because of the reduction in the heat capacity of all substances which takes place at low temperatures.

In planning this work we decided to try to overcome, insofar as possible, the two primary disadvantages of the superconducting bolometer, namely, the difficulty of producing low temperatures and of maintaining precisely thermostated surroundings. The discovery of the superconductivity of CbN by F. H. Horn, and subsequent studies by a group at Johns Hopkins,[4] pointed to the possibility of operating a superconducting bolometer in the region obtainable with liquid hydrogen alone, thus reducing the expense of maintaining the low temperature to perhaps $\frac{1}{10}$ that necessary to operate in the helium range. Horn and his co-workers had found that samples of powdered CbN, through changes in their magnetic properties, gave evidence of becoming superconducting in the region between 14–16°A. Horn nitrided his powdered columbium by heating in nitrogen and because of the difficulties associated with the high temperature of the process, had not prepared CbN in wire form. Following a suggestion by P.H. Emmett, we heated columbium wire in an atmosphere of ammonia and found that we were able to prepare samples which exhibited superconductivity in the range between 14–17°K. The temperature of the mid-point of the transition and the sharpness of the transition depended on the conditions of heating.

PREPARATION OF CbN

Nitriding both by ammonia and by nitrogen has been extensively studied in our laboratory during the last four years and will be reported in detail in subsequent publications, but it may be of interest to cite briefly a typical method of preparation here. A ten-inch piece of columbium wire (0.12 mm diameter) or of the ribbon rolled from it (25μ thick and 0.4 mm wide), is cut, and washed with carbon tetrachloride to remove any grease. This length is carefully folded in the middle to form a "V" and the two ends are attached by friction joints to electrical leads which come through the removable top of the Pyrex nitriding tube which is vertically suspended. A small weight is hung from the fold at the bottom of the V in order to keep the wire or ribbon taut. However, care must be taken not to put too much mechanical strain on the metal, as it may cause uneven heating, and as a consequence, inhomogeneous nitriding, thus affecting the shape and position of the superconducting transition.

The top of the nitriding tube with its suspended columbium wire is now fitted into the rest of the tube. A stream of ammonia, after passing through a mercury bubbler and a calcium chloride dryer, enters through the top of the nitriding tube. It passes out of the bottom and goes through a calcium chloride dryer, a safety trap, and is finally bubbled into water. When the air has been completely flushed away, a current is passed through the wire or ribbon, sufficient to raise the temperature to the desired level, 1200°–1400°C, which is maintained for 45 minutes. This gives a sample with the desired properties.

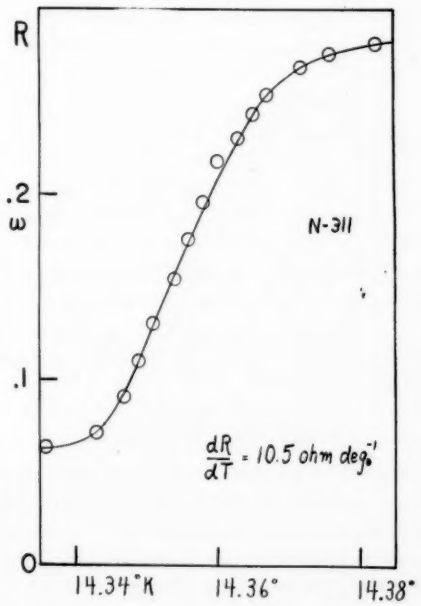

FIG. 1.

[4] F. H. Horn, W. F. Brucksch, Jr., W. T. Ziegler, and D. H. Andrews, Phys. Rev. 61, 738 (1942).

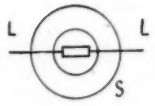

FIG. 2.

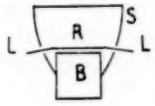

The change of resistance with temperature in the superconducting transition is shown in Fig. 1 for such a sample. The original columbium wire was obtained from Fansteel Metallurgical Corporation, Chicago, Illinois, and had specifications of impurity less than 1 percent.

MOUNTING OF CbN

The next problem was the mounting of this wire or ribbon in such a way that the radiation signal could be received and then withdrawn rapidly by thermal conduction so as to provide both a fast response and a fast restoration of initial temperature. A response time of the order of 1 millisecond was set as the objective.

The design of bolometer finally adopted is shown in Fig. 2. A piece (*R*) of CbN ribbon $0.5 \times 0.025 \times 0.0006$ cm is attached by Bakelite lacquer to the upper surface of a copper post (*B*) approximately 1 cm in diameter and 1 cm high. It is estimated that the thickness of the Bakelite lacquer between the ribbon and the post is about 0.001 cm thick. Since CbN is not wetted by solder directly, the ends of the ribbon are copper plated and tinned, and wires (*LL*) of No. 40 copper are soldered to them to provide electrical connections. A small half-sphere (*S*) spun from copper is soldered to the post and serves as a protection against mechanical shock. This is necessary because the ribbon, after nitriding, is exceedingly brittle.

BOLOMETER RESPONSE

Figure 3 shows a plot of signal response against frequency obtained with the bolometer for which the transition curve was given in Fig. 1. The form of signal used was a square-wave impulse of radiation obtained with a chopping wheel. The source of radiation was an iron plate with dulled surface, at a temperature of 128°C, the temperature being measured with a calibrated thermocouple attached to the plate. The chopping wheel, which was placed about a centimeter in front of the radiation source, was made of heavy cardboard and was about 30 cm in diameter. It contained two holes located 1 cm in from the rim, diametrically opposite and 1.4 cm in diameter. The source was placed behind a hole in a plate back of the chopping wheel. Radiation from this source fell directly on the ribbon of CbN, without passing through any lens or mirror system, the only attenuation being caused by the rocksalt window. The ends of the ribbon were heavily tinned and thus not sensitive. It is estimated that the remaining area sensitive to radiation was approximately 0.01 cm². Thus, the energy falling on the bolometer was 0.08 erg per second.

The response is plotted in terms of the inches peak to peak, observed on the oscilloscope screen. In this particular observation, a current of 30 milliamperes was passed through the bolometer, which was connected to a bridge circuit and thence through a two-stage amplifier to an oscillograph, as shown in Fig. 4. The following items are included in the circuit: (*R*) bolometer, (*D*) dummy matching resistance, (*BB*) opposite bridge resistances, (*T*) transformer, (*SS*) secondary circuit to amplifier. A calibration indicated that a peak-to-peak voltage of 1 inch on the scope corresponded to a peak-to-peak voltage of 0.192 microvolt at the bolometer terminals. The corresponding noise level was 0.1 inch on the scope.

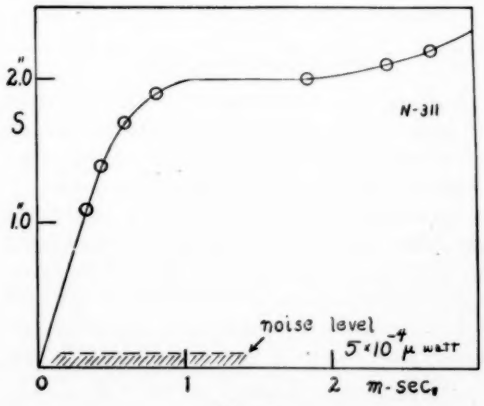

FIG. 3.

The signal rose lineally as the speed of chopping was decreased and leveled off for flashes in the range 1–2 milliseconds long. It then started to rise again. This behavior is explainable in terms of the construction of the bolometer which gives it a compound time constant. The shorter value corresponds to pulses of energy which are absorbed primarily in the CbN, but do not have time to penetrate through the layer of Bakelite into the copper. The longer time constant corresponds to a heating and cooling of parts of the upper surface layer of the copper rod. Because of the limitations of the amplifier with which we were working, we did not follow the response curve to the lower speeds of chopping.

Defining the time constant as that length of flash at which the response is equal to 0.632 of the response for a longer period sufficient to level off the curve, we see that this bolometer has a time constant of 5×10^{-4} sec. For a flash of this duration, the signal is about 15 times above the noise level. The limit of detection of the bolometer is thus about 2×10^{-6} erg. The noise level corresponds to a flux of 5×10^{-4} microwatt. This is in approximate agreement with the value of 6×10^{-4} microwatt reported by Bell, Buhl, Nielsen, and Nielsen,[5] in a study of bolometers of this type made by us.

Approximately 500 bolometers of various types were made during the course of our investigation, and detailed results will be reported in later publications. Some general comments may be of interest, however, on the effect of various factors on the behavior. For example, the thermal fluctuations were somewhat higher than might have been expected. The theoretical fluctuation level may be calculated[6] from the approximate formula $E^2=4kTR(f_1-f_2)$, where k is the Boltzmann constant, T is absolute temperature, R is resistance in ohms, and (f_1-f_2) is the band width of frequency considered. Taking $R=5$ and $(f_1-f_2)=1000$ we find for 300°K a value of E of 10^{-2} microvolt. At 15°K, $E=2\times10^{-3}$ microvolt. The average noise level at the time of the observations shown in Fig. 3 was, however, about 10 times this value, or 2×10^{-2} microvolt.

[5] E. E. Bell, R. F. Buhl, A. H. Nielsen, and H. H. Nielsen, Abstract of Paper presented to The Optical Society of America, Cleveland Meeting, March 6–9, 1946.

[6] J. Strong, *Procedures in Experimental Physics* (Prentice Hall, Inc., New York, 1939), p. 436.

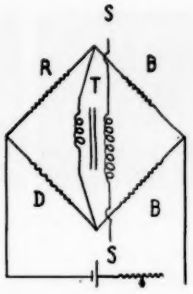

FIG. 4.

It appears that there is a special kind of fluctuation associated with superconductivity. This is illustrated in the photographs of the oscilloscope screen in Fig. 5. Figure 5A shows the noise when the element was completely normal. It is probable that this is amplifier noise. Figure 5B shows the noise at the point in the transition which yielded the best signal to noise ratio, a point lying approximately half way between the normal and the superconducting state. As may be seen, this noise is about 5 times the noise in the normal state. The noise when the columbium nitride is completely superconducting shrinks to a value lower than that observed in this part of the transition. However, over a region usually including about the upper 15 percent of the transition zone, the noise goes to much larger values, as shown in Figs. 5C, 5D, and 5E.

For values of the current through the bolometer between 5 and 50 milliamperes, the noise increases roughly proportionally to the current. Usually, in the region of around 50 milliamperes of current an instability develops in the bolometer with signs of violent fluctuation, ultimately resulting in a jump to the normal state where the bolometer remains until the current is cut off for a minute or two. This appears to be caused by the relation between resistance, current, and heat generated as discussed in the paper[2] on the tantalum superconducting bolometer. Unfortunately, at this stage of the development, there has not been sufficient time to work out in detail the relation between these factors and the shape and composition of the CbN ribbon, so that only a qualitative report can be given. The practical result is that usually a current of about 30 milliamperes gives best signal to noise ratio.

In various applications, it may be desirable

FIG. 5.

either to have a bolometer with as small a receiving area as possible in order to get sharp definition, or with a relatively large receiving area. For applications of the latter sort, we experimented with bolometers made with 2 to 10 ribbons laid parallel and connected in series. As a rule, the noise increases in proportion to the number of joints necessary in making such multiple ribbon bolometers. It thus appeared that some of the noise may be associated with the junction between the CbN and the lead wires. In fact, the greatest care was necessary in getting a well-adhering copper plate in order to avoid excessive noise.

With a very small current passing through the bolometer, it was found that the noise still persisted. In fact, superconductivity could be detected, even though no current were passing through the bolometer, merely by watching the changing characteristics of noise on the screen. Thus Figs. 5C, 5D, and 5E show the type of noise pattern in the upper 15 percent of the transition when no current was being passed through the bolometer at all. When these photographs were taken, the bolometer was merely coupled in series with the primary of the transformer in the amplifier, so that any fluctuating currents originating in the bolometer itself were transmitted to the amplifier, although all external sources of power were completely cut off. Under these conditions the bolometer exhibited a noise such as shown in Fig. 5A when either completely normal or completely superconducting as shown by reading of the resistance thermometer attached to the bolometer posts, and showed the fluctuation exhibited in Figs. 5C, 5D, and 5E in the upper part of the transition range. The base width of these peaks corresponded to a time interval of less than 10^{-4} second; it was impossible with the apparatus on hand to make any accurate measurements. The height of the peaks corresponded to about 0.15 microvolt, and it appeared that an input of something like 10^{-5} erg would be required to produce such a signal. It does not appear that the cause of these fluctuations can be ascertained until further investigations are made. It is, perhaps, worth noting that bolometers of this sensitivity should respond to individual radioactive pulses.

In closing, we wish to make some brief comments on the apparatus with which the low temperature was maintained. It may be seen from Fig. 1 that in order to keep the bolometer in its sensitive range, it is necessary to maintain temperature constant to 2×10^{-2} degree and that within this range the rate of change in temperature must be relatively slow. By comparison with similar substances, we estimate that the heat capacity of CbN is 10^{6} ergs degree^{-1} cm^{-3}, and that the bolometer ribbon has a heat capacity of 25 ergs degree^{-1}. Thus the minimum detectable radiation pulse of 2×10^{-6} erg yields a change in temperature of 10^{-7} degree. The bolometer is thus changing temperature at the rate of 10^{-4} degree per second when receiving this signal and fluctuation must be at a lower rate in order to avoid confusion.

This constancy of temperature was obtained with the help of a small metal cryostat made of cans of spun copper. The cryostat is shown schematically in Fig. 6. The main part of the cryostat is about 25 cm long and 12 cm in diameter. It consists of a series of nested copper cans with wall thickness 0.1 millimeter; the outer can serves as the vacuum jacket. The inner chamber, N, or "pot," contains the liquid hydrogen; this has a volume of approximately 1050 cc. A copper post, M ($\frac{3}{8}$" O.D., $\frac{1}{4}$" I.D., $\frac{1}{16}$" wall tubing) soldered to the "hydrogen" pot, extends through

it from one end to the other and supports the superconducting bolometer base, *S*. Wound around the rod at *M* is a bolometer sensitizing coil (No. 40 constantan, approximately 500 ohms resistance). The purpose of this is to aid in controlling temperature as explained in a later section. The refrigerant is transferred into the pot through the tube, *D*, which is a supernickel tube ($\frac{3}{16}$″ O.D., 0.010″ wall). The outer end of the tube has a screw cap, fitted with a rubber washer which holds the glass transfer tube through which the refrigerant is admitted. A supernickel tube ($\frac{1}{4}$″ O.D., 0.010″ wall parallel to *D* but not shown) acts as a vent tube while the pot is being filled; through it one evacuates the space above the surface of the liquid hydrogen to obtain temperature below the normal boiling point of hydrogen. "*O*" designates the "nitrogen" pot having a volume of approximately 900 cm³. The purpose of this chamber is to provide a thermal dam to cut down the heat leak both by radiation and conduction into the hydrogen pot. While in operation, this contains liquid nitrogen whose normal boiling point is 77.4°K. The inlet and outlet tubes (both tubes $\frac{3}{16}$″ O.D., 0.010″ wall) for transferring the nitrogen refrigerant into this pot are similar to those on the hydrogen pot. In both cases the ends of the tubes come up to the top of the pot facing each other. Therefore, when the cryostat is almost full of refrigerant, i.e., liquid hydrogen in the hydrogen pot and liquid nitrogen in the nitrogen pot, it may be held either horizontally or vertically without spilling. *A* is the outer copper case which encloses the vacuum compartment surrounding both the hydrogen and nitrogen pot. Masonite spacers ($\frac{3}{16}$″ thick), *L* and *W*, are used as insulator rings between the hotter part which is at room temperature, and the colder inner pots, which in turn are similarly thermally insulated from one another. *Q* and *R* are radiation shields. These shields are made of copper sheet, and are each soldered to one of the refrigerant pots. The holes through the shields for the radiation beam are $\frac{15}{32}$″ and $\frac{13}{32}$″ in diameter, respectively. *I* is the window frame (having a $\frac{3}{4}$″ hole) which supports a rocksalt blank, *G*, which is about $\frac{3}{16}$″ thick and 1.0″ in diameter. A vacuum-tight connector is attached to the base of the cryostat. It consists of the metal base of an ordinary 8-prong radio tube with the top cut off, and plate, grid, etc., removed. It is soldered into a hole in the cryostat. Eight copper leads (No. 32) in the cryostat are soldered to it. Four of the leads are connected to the bolometer (i.e., two potential and two power leads) and four corresponding ones are connected to the temperature regulator, *M*. Tube *V* (supernickel tube $\frac{1}{2}$″ O.D.) is used to evacuate the cryostat.

Two cylindrical charcoal containers (not shown) are attached to the nitrogen pot to neutralize any small vacuum leaks. A vacuum sufficient to provide good thermal insulation may be maintained for several days without the aid of any external pumping, even though the vacuum compartment is cut off from the atmosphere only by an ordinary rubber tube and pinch clamp.

The weight of the cryostat and its dimensions are as follows:

Weight of copper cryostat, empty	10.7 lb.
Maximum diameter	5.2 in.

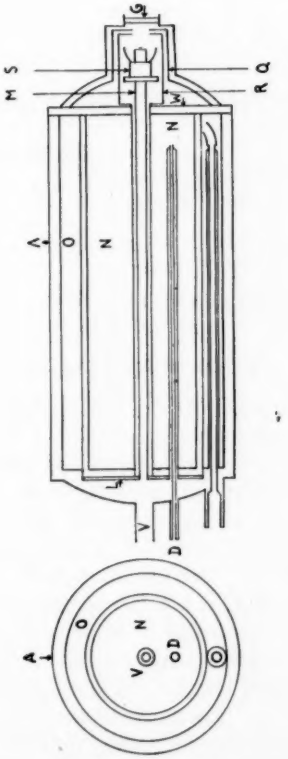

FIG. 6.

Over-all length tip of window frame to end of electrical plug	15 in.
Longest external tube projection (nitrogen inlet and exhaust tube)	1.0 in.
Length of electrical plug	1⅛ in.
Weight of liquid nitrogen, 900 cc (density 0.80 g/cc)	1.6 lb.
Weight of liquid hydrogen, 1050 cc (density 0.07 g/cc)	0.16 lb.
Total weight of cryostat when completely filled	12.5 lb.

When the hydrogen is kept at the triple point, at 14.0°K and a current approximately 10 milliamperes is passed through the resistance coil of 500 ohms wound on a post; the bolometer is maintained in the middle of the transition zone with no need for adjustment for a period of 4 or more hours, depending on the type of operation being performed.

In order that the use of the bolometer might not be limited to the few laboratories in the country where large scale plants were available for making liquid hydrogen, we have developed a small portable liquid hydrogen unit. It consists of a liquefier of the Ahlberg Type, with a purifying unit which can be employed if the commercial hydrogen available contains impurities which may clog the liquefier. Operating from commercial tank hydrogen and blowing down the tank from 2500 to 1500 lb., it is possible to produce the liquid hydrogen necessary to charge the cryostat in about two hours. The liquefier stands about 1 meter high and is about 30×50 cm cross section, and weighs about 50 lb. Thus it can be transported readily.

Liquefier units of this type have been used at a dozen places in various parts of the country completely removed from any laboratory facilities, and have demonstrated their ruggedness and dependability over three years of operation.

Work is now under way to investigate the usefulness of superconducting bolometers in infra-red spectroscopy. Later publications will present further detail on various phases of construction and operation of the bolometer, the cryostat, and the refrigerating unit.

JOURNAL OF THE OPTICAL SOCEITY OF AMERICA VOLUME 36, NUMBER 9 SEPTEMBER, 194

Radiation in a Diffusing Medium

FRANK BENFORD
Research Laboratory, General Electric Company, Schenectady, New York
(Received July 9, 1946)

PART I. INTEGRAL AND FRACTIONAL THICKNESS OF MEDIA

Nature of Investigation

THE manner in which radiation progresses through a diffusing medium will be treated as a statistical phenomenon; no inquiry will be made about the part played by the individual diffusing particle and attention will be confined solely to the mass action of the particles. To simplify matters the radiation falling upon the diffusing medium will be considered as completely diffused before it is incident, and therefore, the medium can transmit, reflect, and absorb without making any fundamental change in the spatial distribution of the radiation. The transmitted radiation and the reflected radiation are diffused as before, but there has been a quantitative change or, in the case of reflection, a change in direction of mass action, but the degree of diffusion remains constant.

Definitions of Terms

By radiation is meant any of the wave-lengths that are usually spoken of as ultraviolet, light, or infra-red, and certain wave-lengths may be implied by the context, but this is not a limitation to the generality of the equations. If a medium, such as a piece of opal glass is said to absorb radiation, it is clear that true absorption is not meant. The energy that disappears is temporarily absorbed and raises the temperature of the glass, which then re-radiates the energy at longer and invisible wave-lengths. If all wave-lengths are taken into consideration, there is

transmission and reflection, but no absorption. But if we are concerned solely with light, then there is a loss of visible radiation and we have transmission, reflection, and absorption.

The linear unit of measurement of the diffusing medium is the perpendicular distance between the two parallel infinite planes that are considered to represent the bounds of the medium. It is also considered that there is no surface action and that all optical action takes place between surfaces. In contradiction to what has just been said it should be pointed out that many of the equations to be given later apply rigidly to the case of linear radiation on reflecting surfaces, such as when projected light passes through pieces of clear glass. The condition that will be avoided is the case of mixed surface and body action, and this can be treated by variations in the method that will often be fairly obvious.

The reflectance R of a unit layer is simply the ratio of the ergs per second (or watts or lumens) leaving the medium in the backward direction divided by the ergs per second (or watts or lumens) incident upon the medium. The transmittance T is the fraction found by dividing the ergs per second leaving a unit thick medium in the forward direction divided by the incident ergs per second. Any energy unaccounted for after measuring T and R is the absorptance A. These terms are connected by the fundamental equation

$$R+T+A=1. \tag{1}$$

When R, T, and A are used without subscript it is understood that the subscript $_1$ is omitted and unit thickness is being considered. If the thickness is n units, then we have

$$R_n+T_n+A_n=1. \tag{2}$$

Ray Diagrams

In the development of expressions for transmission and reflection as in Fig. 1, it is not necessary to assume that the two thicknesses i and j are integral, or that the two media are identical in optical properties. Thus, i might represent a piece of paper and j a piece of diffusing plastic, and there is no necessity for any optical similarity between the two.

Let us here adopt the convention of referring to a medium by its reflectance, transmittance, and absorptance, always given in this order, and represented symbolically by (R_i, T_i, A_i) for the i medium and (R_j, T_j, A_j) for the j medium. Since if R and T are known, A is also known from (1) we can shorten the symbols to (R_i, T_i) and (R_j, T_j) without loss of definiteness. The subscripts will be used either as identifying marks or as indications of the thickness of the media. The context will usually make clear which is meant, and in many cases the distinction is meaningless. Thus, in Fig. 1 the symbols i and j may indicate different materials or they may represent i and j units of the same material.

The ray lines in the diagram indicate directions only in a general sense. The incident energy comes from every downward direction to every point on the upper boundary of i and a fraction of it is reflected in every upward direction and not merely along the ray R_i. Also, every part of the layer i takes part in the reflection and the point where the two rays separate has no significance except to indicate that part of the energy is reflected backward at all points within i to form the reflected portion R_i. The radiation T_i that completely penetrates i is incident upon layer j. The separation of i and j in the diagram is made to allow space for the writing of symbols and is without optical meaning. The radiation that leaves i arrives without change in quantity or direction at the upper boundary of j. Part

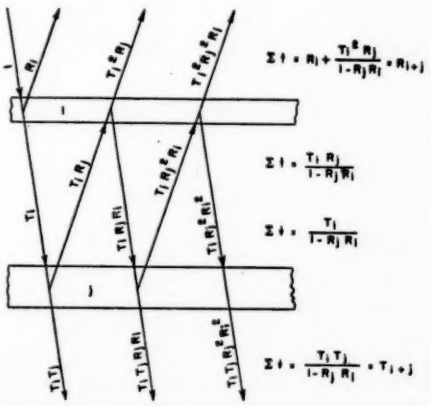

FIG. 1. The mass action of a diffuser receiving fully diffused radiation is here schematically represented by single rays. The strength of each ray is given by symbols and at the right the corresponding rays are summed. No optical action takes place between layers i and j and these two letters may represent either similar or dissimilar media.

of the energy T_j penetrates j and emerges with a strength T_iT_j, while part is reflected backward as represented by the ray T_iR_j. This first reflection sets up an infinite series of reflections from i and j alternately and from these, when summed, we get for the backward direction the energy $T_iR_j/(1-R_jR_i)$ incident upon i and the total energy $T_i/(1-R_jR_i)$ incident upon j. At each reflection some of the energy penetrates the layer and emerges as part of the total reflected energy

$$R_{i+j}=R_i+T_i^2R_j/(1-R_jR_i), \tag{3}$$

or as part of the total transmitted energy

$$T_{i+j}=T_iT_j/(1-R_jR_i). \tag{4}$$

Enough rays are indicated on the diagram to give the necessary data for the summations, and this part of the work will not be gone into. The arrows after the sigma indicate the direction of the rays being summed.

In general the terms R and T and their subscripts will be written in the order in which they are encountered in deriving the equations. Later we shall take up cases where this order has numerical effect and therefore must be taken into consideration.

Absorption of Energy by Incidence Method

The absorption of energy in a unit layer is equal to the energy incident times the absorptance. Thus, in Fig. 1 the loss of energy A_i' in i is

$$A_i'=\left(1+\frac{T_iR_j}{1-R_jR_i}\right)A_i \tag{5}$$

and in j

$$A_j'=T_iA_j/(1-R_jR_i), \tag{6}$$

or combined

$$A_{i+j}=\left(1+\frac{T_iR_j}{1-R_jR_i}\right)A_i+\frac{T_iA_j}{1-R_jR_i}. \tag{7}$$

If now (3), (4), and (7) are added, the sum is equal to unity, and this indicates that all the incident energy has been accounted for.

If the layer i stood alone, a measuring instrument such as a photometer would indicate a transmission T_i, but upon restoring j to its position back of the photometer the apparent transmission becomes

$$T_i'=T_i/(1-R_jR_i)$$

due to the internal reflections between i and j. This dependence upon both i and j is important to note since it is sometimes assumed in the literature that the conditions within a diffuser depend only on the distance of penetration; actually both the distance of penetration and the remaining distance to the plane of exit enter into the computation and, therefore, both i and j must be known.

Ascending Series in i

One of the theorems of integral numbers says that any of the natural numbers 1, 2, 3, 4, $\cdots i$ can be represented by the sum of terms from the series 1, 2, 4, 8, $\cdots 2^{i-1}$, none of the terms being used twice. For example, 13 is the sum of $8+4+1$ and 19 is the sum of $16+2+1$. This theorem is of interest here because there is a series of transmission and reflection equations that depends on the doubling of the thickness of the media at each step. In (4) put both i and j (which here represent thickness) equal to unity, then

$$T_2=T^2/(1-R^2), \tag{8}$$

and (3) becomes

$$\begin{aligned}R_2&=R[1+(T^2/(1-R^2))]\\&=R(1+T_2).\end{aligned} \tag{9}$$

Making both i and j equal to 2, we get the expression for four unit layers of the same medium

$$T_4=\frac{T_2^2}{1-R_2^2} \tag{10}$$

$$R_4=R_2(1+T_4) \tag{11}$$

and the same process repeated leads to T_8, R_8, etc. The general expression is

$$T_{2i}=T_i^2/(1-R_i^2) \tag{12}$$

$$R_{2i}=R_i(1+T_{2i}). \tag{13}$$

These results may now be combined for multiple layers, using (3) and (4) and substituting proper numerical values for i and j. It is neces-

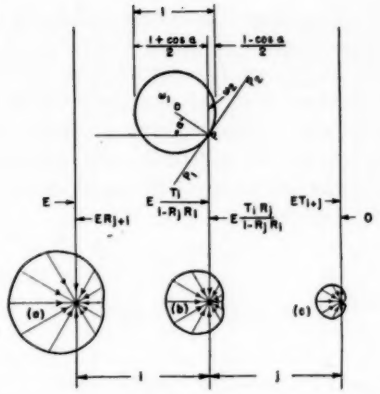

FIG. 2. Angular distribution of radiation within a diffusing medium when $T=0.6$, $R=0.3$, $i=1$, $j=1$. The irradiation, or illumination, that a plane would receive at various points in a diffusing medium of thickness $i+j$ is given by the distribution curves (a), (b), and (c). The intensity on a plane normal to any radius is given by the length of the radius, and the radiation is in each case toward the center of the curve.

sary to compute all intermediate terms in T_i and R_i up to the highest value of i that is needed, and then the combination of integers is made to get the desired value of total thickness. It is also obvious that T_i and R_i are parts of an interlacing series since both T_{2i} and R_{2i} depend on the terms T_i and R_i that immediately precede them.

An alternate method is to add successive unit layers of the diffuser, getting the series

$$T_2=T^2/(1-R^2), \tag{14}$$

$$R_2=R(1+T_2), \tag{15}$$

$$T_3=T_2T/(1-R_2R), \tag{16}$$

$$R_3=R_2+T_2^2R/(1-R_2R), \tag{17}$$

$$T_4=T_3T/(1-R_3R), \tag{18}$$

$$R_4=R_3+[T_3^2R/(1-R_3R)] \text{ etc.} \tag{19}$$

The choice of methods depends largely upon the total thickness. If this is small (14) to (19) may be shorter, while if the thickness is great, say 10 or more, (12) and (13) may entail less work.

Later when equations for the direct determination of R_n (where n is not limited to integral values) and T_n are investigated, there are occasions when there are residual errors in the computation and when reference is then made to exact values, the use of some of the foregoing equations is indicated.

Descending Series in f

There is a second pair of series in T_f and R_f where f is less than unity that proceeds by the steps 1, 1/2, 1/4, $1/8\cdots(1/2)^{n-1}$. Putting both i and j equal to 1/2 in (13) we have

$$R=R_{\frac{1}{2}}(1+T)$$

$$R_{\frac{1}{2}}=R/(1+T) \tag{20}$$

and from (12)

$$T=T_{\frac{1}{2}}^2/(1-R_{\frac{1}{2}}^2),$$

$$T_{\frac{1}{2}}=[T(1-R_{\frac{1}{2}}^2)]^{\frac{1}{2}}. \tag{21}$$

Similarly, for any thickness n, where n need not be a whole number

$$R_{n/2}=R_n/(1+T_n), \tag{22}$$

$$T_{n/2}=[T_n(1-R_{n/2}^2)]^{\frac{1}{2}}. \tag{23}$$

Here matters are reversed, that is, the computation of R_f precedes that of T_f, and both the interlacing series must be completed up to the smallest desired term. The series in i was limited to integral values and likewise here in this fractional series it is impossible to get $T_{1/3}$, $R_{1/3}$, for example, because 1/3 cannot be obtained exactly by any combination of 1, 1/2, 1/4, $1/8\cdots$ but it, of course, may be approximated closely by $1/4+1/16+1/64+1/256+\cdots$ to as many terms as is necessary for the desired accuracy.

The first two steps would be

$$T_{1/4+1/16}=T_{1/4}T_{1/16}/(1-R_{1/4}R_{1/16}),$$

$$R_{1/4+1/16}=R_{1/4}+T_{1/4}^2R_{1/16}/(1-R_{1/4}R_{1/16}).$$

Fractions between 1/2 and 1 are obtained by suitable additions starting with 1/2. Thus, $T_{15/16}$ requires the computation of $R_{1/2}$, $T_{1/2}$, $R_{1/4}$, $T_{1/4}$, $R_{1/8}$, $T_{1/8}$ and finally $R_{1/16}$ and $T_{1/16}$. We then have $R_{1/2}$, $T_{1/2}$ combined with $R_{1/4}$, $T_{1/4}$ to get $R_{3/4}$, $T_{3/4}$. Then $R_{3/4}$, $T_{3/4}$ are combined with $R_{1/8}$, $T_{1/8}$ to get $R_{7/8}$, $T_{7/8}$. Finally these latter are combined with $R_{1/16}$, $T_{1/16}$ to get $R_{15/16}$ and $T_{15/16}$. The fractions close to unity are thus seen to be as difficult to compute as those close to zero.

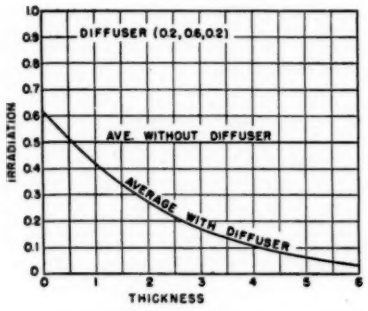

FIG. 3. Irradiation from all directions at points within a diffuser (0.2, 0.6, 0.2) six units thick. For a depth of about 0.5 unit the presence of the diffuser increases the total irradiation, but beyond this depth the diffuser causes a decrease in irradiation.

Combination of Ascending and Descending Series

The descending series can be used to interpolate values between the natural numbers. For example

$$T_{3\frac{1}{2}}=T_3T_{\frac{1}{2}}/(1-R_{\frac{1}{2}}R_3), \tag{24}$$

$$R_{3\frac{1}{2}}=R_3+T_3^2R_{\frac{1}{2}}/(1-R_{\frac{1}{2}}R_3). \tag{25}$$

There is an alternate way of writing (25)

$$R_{3\frac{1}{2}}=R_{\frac{1}{2}}+T_{\frac{1}{2}}^2R_3/(1-R_3R_{\frac{1}{2}}), \tag{26}$$

and in fact any combination of thicknesses that add up to $3\frac{1}{2}$ may be used. The two forms for $R_{3\frac{1}{2}}$ were derived by simply reversing the order of the layers of the diffusing material and if the layers are of identical nature, the two equations yield the same numerical values. In the first case it was a 3-unit layer plus a $\frac{1}{2}$-unit layer, while in the second the $\frac{1}{2}$-unit layer was first and the thicker layer was added. Since the order can have no physical effect on a homogeneous medium we conclude that (25) and (26) give identical results.

Angular Distribution of Radiation Within a Diffusing Medium

In studying the angular distribution of radiation within a diffusing medium we may assume that we are interested in visible radiation and that the measuring device is a photometer. In Fig. 2 the photometer plate lies in the plane P_1PP_2 and faces toward the left. The original direction of propagation is from left to right and there is an angle α between the light axis and the photometer axis PO. Let us place a spherical shell in contact with the photometer plate at P and then pass a plane through P parallel to the boundaries of the medium. We know from geometry that this plane will cut the sphere into the solid angles

$$\omega_1=4\pi(1+\cos\alpha)/2$$

and

$$\omega_2=4\pi(1-\cos\alpha)/2,$$

but since we are interested only in relative solid angles we may use the relative areas of sphere $(1+\cos\alpha)/2$ and $(1-\cos\alpha)/2$ instead of the full expressions.

In Fig. 1 the two layers were shown separated with an open space between in which no optical action took place. Again assuming such an open space and that P is within it, the photometer plate will face in the general direction of layer i but will receive some illumination from layer j. As a first approximation we assume that both layers will exhibit uniform brightness as viewed from all directions in the open space. If the original illumination at the entrance plane to i is E, then the brightness of the layer i as seen from the photometer will be

$$B_i=ET_i/(1-R_jR_i). \tag{27}$$

In the other direction the brightness of layer j will be

$$B_j=ET_iR_j/(1-R_jR_i). \tag{28}$$

Since the illumination at P is proportional to the brightness of the illuminator times its solid angle, we have

$$E_\alpha=E\left[\frac{T_i}{1-R_jR_i}\left(\frac{1+\cos\alpha}{2}\right)+\frac{T_iR_j}{1-R_jR_i}\left(\frac{1-\cos\alpha}{2}\right)\right]. \tag{29}$$

This shows that the illumination curve as the photometer plate rotates through the angle α is the sum of two cardioids, one for each source, and that these cardioids have their maxima pointed in opposite directions. At the bottom of Fig. 2 the three angular distribution curves are for positions of the photometer at the entrance

plane, in the center of the diffuser, and at the exit plane. The diffuser has the characteristic $R=0.3$, $T=0.6$, $A=0.1$ and i and j are each taken as unity. When the photometer plate is at the entrance plane and facing directly to the left, the illumination is simply E, the brightness of the illuminant, which is assumed to be infinite in extent and uniform in intensity. As the plate is rotated the diffuser comes into effect and when the rotation is 180 deg., the entire illumination is from the diffuser. The length of the radius to the left curve (a) represents the illumination at the entrance plane, and the radius to the right represents the reflected radiation. A comparison of the three distribution curves (a) at entrance, (b) at the center, and (c) at the exit plane shows the first position to have the greatest uniformity. At (c) no radiation is received from the right and this curve is a single cardioid with a zero value to the right.

It should be noted that this analysis is only an approximation in the case where the source of radiation is not infinite in extent or uniform in intensity in all directions. The nature of the diffusing particle will also have an influence, but regardless of these factors the application of these formulas in the following sections will lead to results that are useful, and when the results are averaged for all possible angles, exact as well.

Average Irradiation or Illumination

The average density of radiation within a diffusing medium may be found by placing a cube within the customary open space used in Fig. 1 and finding the irradiation on each face. The cube is placed with two of its faces parallel to the bounding planes. Let E be the density of irradiation (or of illumination) incident on the entrance plane; then from Fig. 1 we can again write

$$E_i=ET_i/(1-R_jR_i) \tag{30}$$

and

$$E_j=ET_iR_j/(1-R_jR_i) \tag{31}$$

for the faces parallel to the bounds of i and j, and for the other four sides the irradiation E_s is the average density of the two irradiating sections i and j, since each fills half of the surrounding solid angle.

$$E_s=ET_i(1+R_j)/2(1-R_jR_i). \tag{32}$$

The average on all six sides is

$$E_{Av}=\tfrac{1}{6}[E_i+E_j+4E_s] \tag{33}$$
$$=\frac{E}{2}(1+R_j)\frac{T_i}{1-R_jR_i}.$$

Any errors made in dividing radiation between the six faces will cancel out since the average is not influenced by shifting radiation from one face to another.

In the complete absence of a diffusing medium the irradiation on the two parallel faces would be E and 0, and on the other four faces $E/2$ since the source would fill half of the surrounding solid angle. The average E_0 is then

$$E_0=\tfrac{1}{6}E[1+0+4(1/2)]$$
$$=\tfrac{1}{2}E. \tag{34}$$

A comparison of (33) and (34) shows the former to contain the factors $(1+R_j)\ T_i/(1-R_jR_i)$ in addition to the common term $E/2$. An object in a surrounding diffusing medium can receive more irradiation than if it faced the source directly providing the additional factors are greater in numerical value than 1. It therefore can happen that a diffuser, even if it absorbs, can increase the irradiation of a contained body.

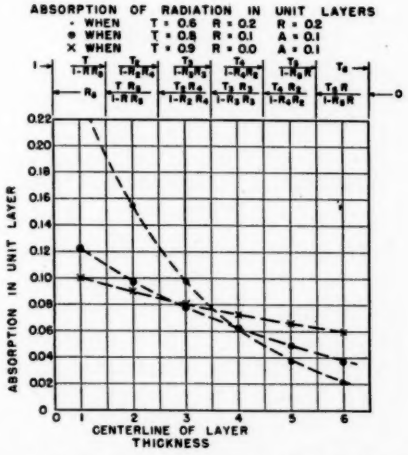

FIG. 4. The points on the curves show the fraction of radiation absorbed in unit layers of three different media. The equations show the amount of radiation falling on the plane at the point of the arrows. The absorption is found by noting the difference of radiation entering and leaving any unit layers.

TABLE I. Figurate numbers.

Column line	1	2	3	4	5	6	7 ···	i
1	1	1	1	1	1	1	1···	$\frac{(i-1)!}{0!(i-1)!}$
2	1	2	3	4	5	6	7···	$\frac{(i+0)!}{1!(i-1)!}$
3	1	3	6	10	15	21	28···	$\frac{(i+1)!}{2!(i-1)!}$
4	1	4	10	20	35	56	84···	$\frac{(i+2)!}{3!(i-1)!}$
n	—	—	—	—	—	—	—···	$\frac{(i+n-2)!}{(n-1)!(i-1)!}$

Figure 3 shows some results for a body in various parts of a diffuser 6 units thick and having an (R, T, A) characteristic of (0.2, 0.6, 0.2). With a source of unity intensity per unit area at the left the average irradiation (all directions included) at any point in space would be 0.5 in the complete absence of any diffusing body. Adding a diffuser (0.2, 0.6, 0.2) of total thickness of 6 back of the cube increases the average irradiation to 0.62. When the cube is at a depth of 0.6 unit the irradiation is again the original average and then drops to 0.03 at the exit plane. Additions to the thickness will add to the peak irradiation and give lower values at the new exit plane, and in addition will change the irradiation at all intermediate points.

Absorption of Radiation by Method of Differences

The absorption of radiation in any particular case can be determined when the sum of the transmission and reflection is known. The radiation that is unaccounted for in these two measurements is the radiation that has been absorbed. In Fig. 4 a diffuser of 6-units thickness has been explored at all the separating planes. The division line in each equation given above the curves has an arrow head indicating the direction and plane of incidence of the energy denoted by the equation. This plane is at the point of the arrow. Thus, the third layer receives energy from two sides

$$E_r=\frac{T_2}{1-R_2R_4}+\frac{T_3R_3}{1-R_3R_3} \tag{35}$$

and emits energy from the same two sides

$$E_e=\frac{T_3}{1-R_3R_3}+\frac{T_2R_4}{1-R_2R_4} \tag{36}$$

as indicated by the arrow heads. The absorbed energy is

$$E_a=E_r-E_e. \tag{37}$$

The top line of equations, Fig. 4, gives the energy arriving at each plane from the left. The form of equation shows it to be the transmission from the entrance plane to the plane in question divided by a factor $1-R_jR_i$ that arises from the internal reflections at that plane. The customary open spaces between layers is here omitted, but the familiar interreflections can be visualized without them. The second row of equations gives energy returning from the right, as indicated by the R_j in each numerator.

In a preceding paragraph the absorption was computed by multiplying the incident energy by the absorptance, and we now have an alternate method that depends on the difference between entering and leaving energy. The two methods yield identical results.

PART II. INDEPENDENT EQUATIONS FOR INTEGRAL THICKNESSES

In the preceding section the solutions for i units thickness depended upon a series of equations that led by steps to the desired thickness. This method therefore requires the solution of a number of intermediate equations between T and T_i and between R and R_i. In this section it will be shown that there are general expressions for T_i and R_i that permit their direct determination.

Figurate Numbers

As a preliminary let us set down a short table (Table I) of figurate numbers because these historic numbers occur in the equations to be given; and once a series of figurate numbers is recognized, we can then extend it as far as we

please; and in fact we can write directly an expression for any desired term and thus arrive at a general expression, but one that is limited to integral thicknesses.

The factorial expressions at the right edge of the table permit a direct determination of any figurate number in the table, or in an extension of the table for any column i and for any line n. The final expression in the lower right corner is for the general case of any i and any n. The use of this table will be explained later.

Direct Equations for T_i

The equations that follow were determined by solving for T_i and R_i when the total thickness increases by unity at each step, thus 1, 2, 3, $\cdots i$. These equations, if left in the form as first derived would have several hundred terms for T_{10}, but it was found by trial that they could be grouped in various ways and this led to much shorter equations.

One combination that is of frequent occurrence in the original expansion is the difference between T^2 and R^2. Let us use Q to denote this difference, then

$$Q = T^2 - R^2. \tag{38}$$

We have the following solutions for transmissions of 0, 1, 2, $\cdots 7$ thicknesses,

$$\begin{aligned}
T_0 &= 1 \\
T_1 &= T \\
T_2 &= T^2/\{1 - R^2(1)\} \\
T_3 &= T^3/\{1 - R^2(2 + Q)\} \\
T_4 &= T^4/\{1 - R^2(3 + 2Q + Q^2) + R^4(1)\} \\
T_5 &= T^5/\{1 - R^2(4 + 3Q + 2Q^2 + Q^3) + R^4(3 + 2Q)\} \\
T_6 &= T^6/\{1 - R^2(5 + 4Q + 3Q^2 + 2Q^3 + Q^4) + R^4(6 + 6Q + 3Q^2) - R^6(1)\} \\
T_7 &= T^7/\{1 - R^2(6 + 5Q + 4Q^2 + 3Q^3 + 2Q^4 + Q^5) + R^4(10 + 12Q + 9Q^2 + 4Q^3) - R^6(4 + 3Q)\}.
\end{aligned} \tag{39}$$

If these equations are inspected for coefficients in the various columns, it will be found in every case that each column is identical with or a multiple of a column in Table I. Thus, the coefficients in the R^2 parentheses are the natural numbers 1, 2, 3, $\cdots$, Q, $2Q$, $3Q$, $4Q$, etc., as in the second column of the table. In the R^4 parentheses the first coefficients are 1, 3, 6, 10$\cdots$ as in the third column of Table I. The second coefficients, associated with Q are 2, 6, 12, or in each case twice the figurate number of column 3. The third set of coefficients, with Q^2, is 3, 9$\cdots$ or 3 times the third column of figurate numbers. All of the coefficients in the R^4 parentheses are thus taken from the third column of Table I, and the multipliers 1, 2, 3 noted above are from the second column of the table. In the R^6 parentheses the columns (extended) are 1, 4, 10, 20, etc.; 3, 12, 30, 60, etc.; 6, 24, 60, 120, etc. These will be recognized as the fourth column of Table I, multiplied in turn by the figures of column 3.

The signs in front of R^2, R^4, R^6, etc. are $-$, $+$, $-$ alternately and a new R parenthesis is added for each increment of 2 in thickness i. The Q columns, Q^1, Q^2, etc., increase by 1 for each increment of i, and all Q terms have a $+$ sign. Q itself may be either positive or negative, depending on whether T or R is the larger, and when $R > T$ the numerical values of the Q terms are alternately $-$ and $+$. The factorial expressions of Table 1 were used in the general equation that is to follow, but numerical changes must be made to compensate for the fact that the coefficients associated with R^4 for example start with 1 when i equals 3, and the R^6 exponents start with 1 when i is 6. We can now apply these rules of coefficients

and signs to get the general expression

$$T_i = T^i \Big/ \left\{ 1 - \frac{R^2}{1!}\left[1\frac{(i-1)!}{(i-2)!} + 1\frac{(i-2)!}{(i-3)!}Q + 1\frac{(i-3)!}{(i-4)!}Q^2 \cdots \right] \right.$$
$$+ \frac{R^4}{2!}\left[1\frac{(i-2)!}{(i-4)!} + 2\frac{(i-3)!}{(i-5)!}Q + 3\frac{(i-4)!}{(i-6)!}Q^2 \cdots \right] \qquad (40)$$
$$- \frac{R^6}{3!}\left[1\frac{(i-3)!}{(i-6)!} + 3\frac{(i-4)!}{(i-7)!}Q + 6\frac{(i-5)!}{(i-8)!}Q^2 \cdots \right]$$
$$\left. \cdots\cdots\cdots\cdots\cdots \right\}.$$

This equation, which is of course limited to integral values of thickness, may be extended by observation to the necessary limits for any value of i. The coefficients R^2, $R^4 \cdots$ have a ratio $-R^2$ between them, and they are divided by 1!, 2!, 3!, 4!, $\cdots$ where the factorial number is half the exponent of R. The factorial fractions within the brackets are preceded by the coefficients 1, 1, $1 \cdots$; 1, 2, 3, $\cdots$; 1, 3, $6 \cdots$ which are the figurate numbers of Table I. Each coefficient is the sum of the coefficient to the left on the same line and the coefficient above it in the same column. Since the first series is always present in a computation of T_i and the others are used up to some limiting values, there are no unused terms in the determination of the complete expression.

Each factorial series in Q is self-limiting. The final term in each series is identified by the appearance of 0! in the denominator. Since $0! = 1$, this is a real number, but if it is carried one step further, there would be a $(-1)!$ in the denominator and since $(-1)!$ equals infinity, the fraction vanishes. For example, if $i = 4$, the final terms in $(R^2/2!)\,[\ ]$ is

$$1\frac{(4-3)!}{(4-4)!}Q^2 = 1\frac{1!}{0!}Q^2 = Q^2.$$

In $(R^4/2!)\,[\ ]$ the final terms are

$$1\frac{(4-2)!}{(4-4)!} = \frac{2!}{0!} = 2!,$$

and this yields

$$\frac{R^4}{2!}2! = R^4(1)$$

as previously given in the group of T_i equations.

The factorial fractions are given in full detail so that the progression of the factors can be observed. The numbers in both the numerator and the denominator increase by unity in the successive terms of each series. The numbers in the denominator are greater than the corresponding numbers in the numerator by the factorial number under the R. All signs within the brackets are +, but Q may be either + or −, and in the latter case the complete computation gives alternate plus and minus terms.

Direct Equations for R_i

The denominators in Eq. (39) will be used for determining reflections R_i in Eq. (41) and it will be convenient to designate them by $D_1, D_2, \cdots D_i$ for thickness of 1, 2, $\cdots i$; thus,

$$R_4 = R + \frac{RT^2}{D_4}[(1+Q+Q^2) - R^2],$$

where

$$D_4 = \{1 - R^2(3+2Q+Q^2) + R^4\}$$

from the preceding Eq. (39) for T_4. The expressions for R_i, where i varies from 0 to 7 by integral steps are

$$R_0=0$$

$$R_1=R$$

$$R_2=R+\frac{RT^2}{D_2}[(1)]$$

$$R_3=R+\frac{RT^2}{D_3}[(1+Q)]$$

$$R_4=R+\frac{RT^2}{D_4}[(1+Q+Q^2)\qquad -R^2(1)] \tag{41}$$

$$R_5=R+\frac{RT^2}{D_5}[(1+Q+Q^2+Q^3)\qquad -R^2(2+2Q)]$$

$$R_6=R+\frac{RT^2}{D_6}[(1+Q+Q^2+Q^3+Q^4)\qquad -R^2(3+4Q+3Q^2)\qquad +R^4(1)]$$

$$R_7=R+\frac{RT^2}{D_7}[(1+Q+Q^2+Q^3+Q^4+Q^5)-R^2(4+6Q+6Q^2+4Q^3)+R^4(3+3Q)].$$

The formation of the coefficients follows rules that differ from those found for the transmissions. In the R^2 parentheses the coefficients are those of the second column of Table I and the multipliers are from the same second column. We have 1, 2, 3, 4, $\cdots$; 2, 4, 6, 8, $\cdots$; 3, 6, 9, 12, $\cdots$; for the Q^0, Q^1, and Q^2 columns. It will be recalled that the figurate numbers for the denominators of T_i were multiplied by numbers from the preceding columns, and not as here from the same column.

The general expression is

$$\begin{aligned}R_i=R+\frac{RT^2}{D_i}\Big\{&Q^0+Q^1+Q^2+\cdots Q^{i-2}\\
&-\frac{R^2}{1!}\left[1\frac{(i-3)!}{(i-4)!}+2\frac{(i-4)!}{(i-5)!}Q+3\frac{(i-5)!}{(i-6)!}Q^2+\cdots\right]\\
&+\frac{R^4}{2!}\left[1\frac{(i-4)!}{(i-6)!}+3\frac{(i-5)!}{(i-7)!}Q+6\frac{(i-6)!}{(i-8)!}Q^2+\cdots\right]\\
&-\frac{R^6}{3!}\left[1\frac{(i-5)!}{(i-8)!}+4\frac{(i-6)!}{(i-9)!}Q+10\frac{(i-7)!}{(i-10)!}Q^2+\cdots\right]\\
&\cdots\cdots\cdots\cdots\cdots\Big\}.\end{aligned} \tag{42}$$

It should be noted that the series Q^0, Q^1, $Q^2\cdots$ starts with Q^0 which is equal to 1. The rules for the factorial terms are similar (but not identical) to those for the T_i terms, and they can be found by inspection and the terms extended to the limit without too much study.

Limiting Value of R_i

If the values of R_i are computed for increasing values of i, there will come a time when R_i seemingly reaches a maximum, and this pseudo-maximum occurs for all values of T and R. This maximum can be visualized by considering a

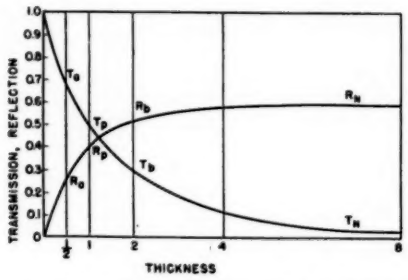

FIG. 5. A typical transmission curve looks like an exponential curve starting at one for zero thickness and dropping asymetrically to zero for great thicknesses. The reflection curve starts at zero and rises to a saturation value indicated by R_N. There is always a crossing point where R and T are equal.

piece of thin typewriter paper laid on top of a piece of carbon paper. The reflectance of the paper will seem to be rather low for a single sheet of the white paper since the black background will have an effect. Let us then add another layer of white paper, and the two together will be noticeably whiter. If successive sheets are added, the stack will soon remain unchanged in appearance as new sheets are added, and this is the condition represented by the level section of the R curve of Fig. 5. Let the number of sheets that satisfies this condition be N. Then since $N+1$ sheets will give sensibly the same reflection as N sheets, we can write, replacing R_{N+1} by R_N

$$R_N = R + T^2 R_N/(1 - R_N R). \tag{43}$$

Solving for R_N we get

$$R_N = \frac{(1 - T^2 + R^2) - [(1 - T^2 + R^2)^2 - 4R^2]^{\frac{1}{2}}}{2R} \tag{44}$$

for the maximum reflectance for the given values of T and R.

This equation has proven to be a useful analytic tool, since if we know any pair of values T_a and R_a for a given material, this pair will yield the same value of R_N as any other pair T_b and R_b as illustrated in Fig. 5. Since Eq. (44) relates the general terms T_n, R_n, and R_N, it follows that if any two of these terms are known, the third may be determined with one limiting condition to be noted shortly.

Assume that T_a and R_a, Fig. 5, are known and that R_N has been computed. If now T_b is measured (or assumed), then R_b may be determined by solving (44) for R_b after T_b has been substituted in the quadratic solution

$$R_b = \frac{R_N^2 + 1 - [(R_N^2+1)^2 - 4R_N^2(1 - T_b^2)]^{\frac{1}{2}}}{2R_N}. \tag{45}$$

Similarly, given R_b we can find T_b

$$T_b = \left[\frac{(R_N - R_b)(1 - R_N R_b)}{R_N}\right]^{\frac{1}{2}}. \tag{46}$$

It sometimes happens that considerable work goes into computing R_b and T_b and in place of checking the computation an independent determination of R_b or T_b by (45) and (46) will serve to detect the presence of an error.

Equation (43) can be written

$$R_N = R_N + T_N^2 R/(1 - RR_N), \tag{47}$$

and this equation can be true only if T_N^2 is zero. In the range where R_b approaches R_N the numerical value of T_b must therefore be small and of course T_b^2, as it appears in (45) is still smaller. Equation (45) thus becomes more and more difficult to use with accuracy, and the same condition applies to (46) when $R_N - R_b$ approaches zero.

To avoid these purely numerical difficulties we can first determine a pair R_b and T_b, Fig. 5, that are near the plateau range of R_N but not in it. Then we can double the thickness and get R_{2b} and T_{2b} with accuracy, and R_{2b} must be a close approximation to the limiting value of R_N. It will be shown later that if x is any increment added to $2b$, then T_{2b+x} is a continuous function of x that can be written

$$T_{2b+x} = T_{2b}\left(\frac{T}{1 - RR_N}\right)^x; \tag{48}$$

and since all terms in the parenthesis are constants, we have a pure exponential equation in x. This useful expression will be gone into in some detail in the section on continuous functions.

The Characteristic Curve of a Material

The three defining properties R, T, and A of a material are effectively reduced to two because the sum of the three is always unity. This unity value suggests that some triangular form of plotting web be used, as in Fig. 6, to represent R, T, and A for a given medium. The abscissae are reflections; the ordinates are transmissions; and the absorptions, although not specifically

shown in the figure, can always be read from the web. Thus, point v, where R equals 0.27 and T equals 0.55, is at horizontal distance

$$A=w-v=0.18$$

from the sloping upper boundary of the web and these three numerical values satisfy (1). The three variable R, T, and A now define a single point v on the diagram, and any two define it equally well. The path pursued by v as the thickness changes is therefore a line that may be computed from R and T, from R and A, or from T and A.

The standard condition (R, T, A) may occur in any part of the diagram, and the point v for a given material might be taken at any point on the curve on which it occurs and it would definitely define that particular material. The curve is therefore a characteristic curve, and all such curves have two features in common. They converge to the upper point where $T=1$ and $R=0$, and these two limits are common to all materials as they approach zero thickness. Also all the curves are perpendicular to the base of the diagram where $T=0$. Here R remains sensibly unchanged for small changes in T and this corresponds to the R_N region that has been previously explored.

While any given material has but one characteristic curve, this same curve may represent any number of different materials, and these materials might, by a casual inspection, seem quite dissimilar. As an example we might compare a piece of thin paper with a characteristic (0.45, 0.45, 0.10) with a denser sample (0.615, 0.095, 0.29) and finally with a blotter (0.63, 0.00, 0.37). These three points all lie on the same characteristic line of Fig. 6 and the three materials differ only in requiring different thicknesses to give the same point on the characteristic curve.

In Fig. 6 a line from (0, 0) to the middle of the upper boundary of the web has been arbitrarily selected as representing unit thickness at the points where it crosses the characteristic curves. Starting here values for $R_{\frac{1}{2}}$, $T_{\frac{1}{2}}$ were computed and plotted as the curve marked 1/2 on the thickness scale. Other curves for 1/4 and 1/8 thickness are shown, as well as the ascending thicknesses 2, 4, 8, 16, and 32. Visual interpolation is here difficult and these various curves are good only for rough approximations.

PART III. CONTINUOUS FUNCTIONS OF THICKNESS

Thickness Range from 1 to 2

The work so far presented has been limited to integral thicknesses, or to the fractional values $1/2$, $1/4\cdots(1/2)^s$, where s is an integer. It will be shown in this section that a continuous solution, between $n=1$ and $n=2$ is possible, and this removes a rather serious limitation. A number of solutions have been attempted and the one here presented is at once the simplest and the most accurate that has been found. Certain factors in the equation are empirical and hence it is not a physical equation.

The equation was derived by considering the equations for transmission in the region from T_1 and T_2 with particular regard to the exact equation for $T_{1\frac{1}{2}}$. We have

$$T_{1\frac{1}{2}}=\frac{TT_{\frac{1}{2}}}{1-RR_{\frac{1}{2}}}=\frac{T\left\{T\left[1-\left(\frac{R}{1+T}\right)^2\right]\right\}^{\frac{1}{2}}}{1-\frac{R^2}{1+T}}$$

$$=\frac{T^{\frac{1}{2}}[(1+T)^2-R^2]^{\frac{1}{2}}}{(1+T)-R^2}. \tag{49}$$

If now we can make the various exponents func-

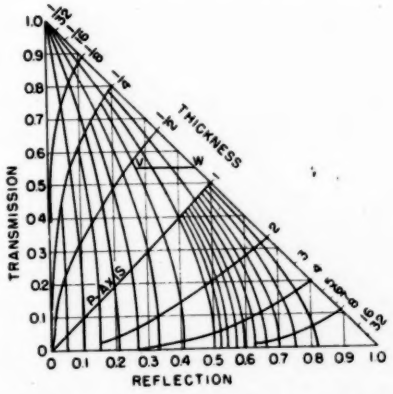

FIG. 6. The curves radiating from the top of the diagram are characteristic curves that show the relation between R and T for varying thickness of media. The curves radiating from the lower left corner form a thickness scale, as marked on the sloping upper boundary. In addition, any distance V–W from a curve to this boundary is a measure of the absorption corresponding to the given R and T.

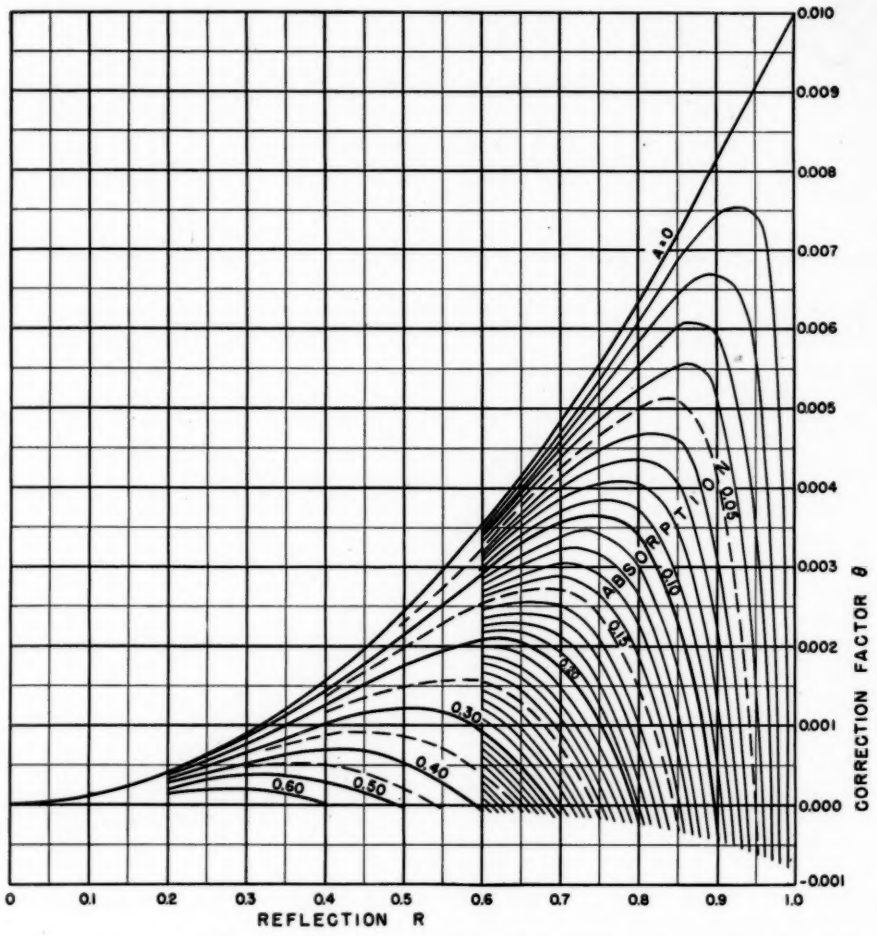

FIG. 7. This correction factor θ is used in connection with Eq. (51) when computing transmission of thicknesses between 1 and 2. The errors to be corrected are greatest when f is $\frac{1}{4}$ and $\frac{3}{4}$, and zero when f is 0, $\frac{1}{2}$, and 1. The corrected results will be accurate to one part in ten thousand.

tions of f (the fractional part of the thickness), we will have an expression that is physically correct for $n=1$, $n=1.5$, and $n=2$, and is an approximation between these points. Let us express the thickness as $1+f$ where f is any fraction between 0 and 1, and $1+f$ therefore covers the desired range between 1 and 2.

By trial it will be found that an expression such as

$$T_{1+f}=\frac{T^{1+f}[(1+T)^2-R^2]^{1-f}}{(1+T)^{2(1-f)}-R^2} \qquad (50)$$

reduces to the exact values

$$T_1=T$$

$$T_{1.5}=\frac{T^{\frac{3}{2}}[(1+T)^2-R^2]^{\frac{1}{2}}}{(1+T)^2-R^2}$$

$$T_2=T^2/(1-R^2)$$

when 0, 0.5, and 1 are substituted for f, but for all other values of f the expression is inexact. Any correction terms added to the equation should vanish for f equal to 0, 0.5, and 1 and this

suggests that the added factor should contain the expression $f(f-0.5)(f-1)$ which has roots at 0, 0.5, and 1, and therefore vanishes at the proper points.

For the interval between 1 and 2 we have the continuous function

$$T_{1+f}=\frac{T^{1+f}[(1+T)^2-R^2]^{1-f}}{[(1+T)^{2(1-f)}-R^2]\left[1+\frac{64}{3}f(f-0.5)(f-1)\theta\right]} \tag{51}$$

where θ may be regarded as a correction factor. In Fig. 7 values of θ are given for R and A. An algebraic expression has been found for θ, but since this expression is somewhat involved, and not wholly accurate, it seems simpler to use θ from the chart. It will be noted from the chart that the maximum error in (51) if θ is omitted is exactly 1 percent when f is either 0.25 or 0.75 and less for other values of f. This maximum occurs when the absorptance A is zero, and the equation seems to yield numerically exact data when A approaches 1.

It now remains to find a way to extend this information about T_{1+f} to all values of T between $n=0$ and $n=\infty$, and to determine corresponding values of R between the same limits.

A layer of material of thickness $1+f$ can be considered as made up of a unit layer plus a fractional layer or a fractional layer plus a unit layer. The two ways of assembling lead to two different equations that are numerically equal.

Using this equality we can express the reflection for $2+f$ layers as follows

$$R_{1+f}+\frac{T_{1+f}^2R}{1-RR_{1+f}}=R+\frac{T^2R_{1+f}}{1-R_{1+f}R} \tag{52}$$

and since T_{1+f}, R, and T are known we have the solution

$$R_{1+f}=\frac{1+R^2-T^2-[(1+R^2-T^2)^2-4R^2(1-T_{1+f}^2)]^{\frac{1}{2}}}{2R}. \tag{53}$$

These values of T_{1+f} and R_{1+f} can now be combined with (39) or (40) to get any transmission for any thickness greater than 1, and likewise with (41) or (42) for the reflection for any thickness greater than 1.

Thickness Range from 1 to ∞

The words "continuous function" in the heading of this section should, for the sake of accuracy of expression, be qualified to mean continuous from 1 to 2. We can however write the general expressions for thicknesses greater than 1,

$$T_{i+f}=T_{i-1}T_{1+f}/(1-R_{1+f}R_{i-1}) \tag{54}$$

and

$$R_{i+f}=R_{i-1}+T_{i-1}^2R_{1+f}/(1-R_{1+f}R_{i-1}) \tag{55}$$

which are solvable by direct substitution from equations already given. We here have a solution that is continuous over the range 1 to ∞ but it is not simple and direct since several separate equations, (51) and (53), must first be set up and solved, and these solutions substituted in (54) and (55).

As a numerical example let us find the characteristics of a diffusing material in terms of inches when they are already known in terms of centimeters. Since there are 2.54 cm in an inch we have (putting $i=2$ in (54) and (55))

$$T_{2.54}=TT_{1.54}/(1-R_{1.54}R)$$

and

$$R_{2.54}=R+T^2R_{1.54}/(1-R_{1.54}R).$$

Thickness Range from 0 to 1

The region $f=1$ to $f=0$ remains to be explored and there is no direct method for deriving R_f from R_{1+f} or T_f from T_{1+f}. We must start anew with

$$R+\frac{T^2R_f}{1-R_fR}=R_f+\frac{T_f^2R}{1-RR_f},$$

containing both T_f and R_f as unknowns and the equation

$$T_{1+f}=TT_f/(1-R_fR) \tag{56}$$

containing the same two unknowns. Since T_{1+f} is known, we can express T_f in terms of T_{1+f} and R_f and thus eliminate it. The solutions are

$$R_f=\frac{R^2T^2+T^2-T^4-2T_{1+f}^2R^2-[(R^2T^2+T^2-T^4-2T_{1+f}^2R^2)^2-4R^2(T^2-R^2T_{1+f}^2)(T^2-T_{1+f}^2)]^{\frac{1}{2}}}{2R(T^2-R^2T_{1+f}^2)} \tag{57}$$

and

$$T_f=\frac{T_{1+f}}{T}(1-RR_f) \tag{58}$$

and these complete the work of finding continuous equations.

Some Special Physical Conditions

T_N Region

In the region where the reflection is saturated and $R_{N+x}=R_N$, the transmission equation

$$T_{N+1}=T_NT/(1-RR_N) \tag{59}$$

can be written

$$T_{N+1}=T_N\left(\frac{T}{1-RR_N}\right) \tag{60}$$

and the terms in the parenthesis are all constants. Next we have

$$\begin{aligned}T_{N+2}&=T_{N+1}T/(1-RR_N),\\&=T_{N+1}\left(\frac{T}{1-RR_N}\right),\\&=T_N\left(\frac{T}{1-RR_N}\right)^2.\end{aligned} \tag{61}$$

If now the process is continued by adding unit layers, it will be found that the exponent on the parenthesis always agrees with the total added thickness, hence

$$T_{N+x}=T_N\left(\frac{T}{1-RR_N}\right)^x \tag{62}$$

which is a continuous exponential function in x, and x may be either positive or negative, but care must be taken to see that $-x$ is not great enough to get out of the legitimate R_N region.

T_0 Region

Another exponential region exists for T_f when R_f is small enough to be neglected in the equations

$$T_{2f}=T_f^2/(1-R_f^2),$$

$$T_{3f}=T_f^3/[1-R_f^2(2+Q)].$$

These become simply

$$T_{2f}=T_f^2 \tag{63}$$

$$T_{3f}=T_f^3 \tag{64}$$

and in general

$$T_{nf}=T_f^n \tag{65}$$

where n may be any number that is not large enough to go out of the region where R_f is sufficiently small to be dropped. This equation also holds for n between 1 and 0, and hence (65) is an approximation down to zero where $T_0=1$.

R_N Region

The third condition is the extremal of R_N which has been covered in some detail in Section II.

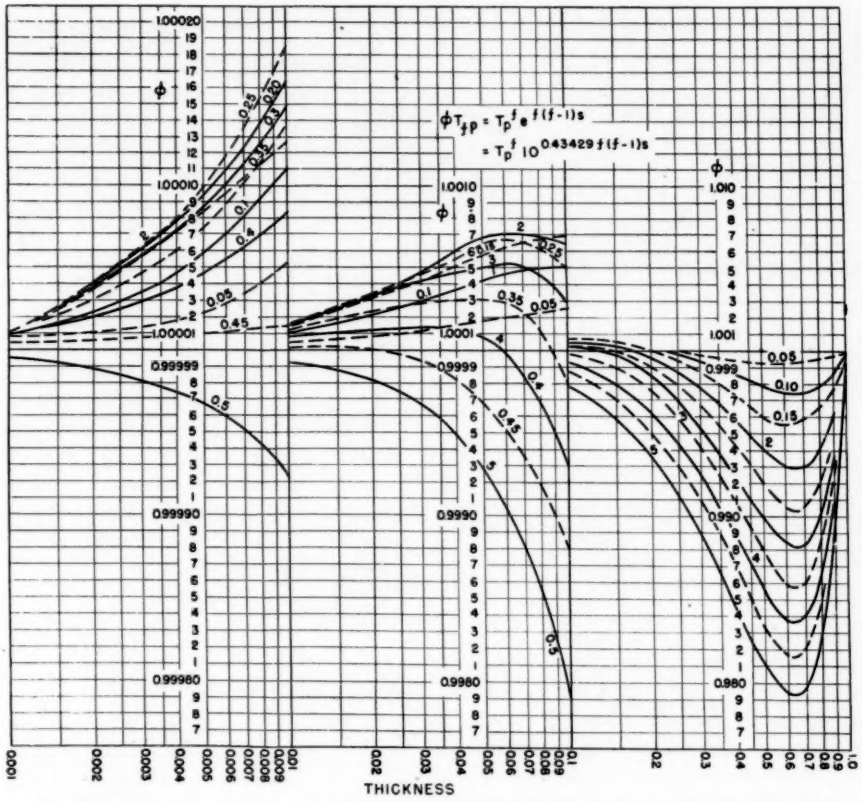

FIG. 8. The correction factor φ applies to transmission Eq. (70) for fractional thickness of media having transmittance and reflectance equal. Each of the vertical scales of this figure applies over the range covered by the curves in that section.

R_0 Region

The last condition is that of small thicknesses where R_f is small and T_f approaches 1 in value. We here have for small changes x in thickness

$$R_{f+x}=R_f+T_f^2R_x/(1-R_fR_x).$$

R_x is also small and R_fR_x can be neglected.

$$R_{f+x}=R_f+R_x, \text{ approximately.} \qquad (66)$$

Here the reflections add arithmetically, and making the layer three times as thick multiplies the reflection by 3. A more general expression is

$$R_{nf}=nR_f, \qquad (67)$$

and here n may have any value from 0 up to a value that makes the discarded denominator and the discarded T_f^2 of numerical importance again.

PART IV. UNIT LAYERS HAVING TRANSMITTANCE EQUAL TO REFLECTANCE

Reducing Q to Zero

When the thickness of the diffusing medium reaches about 10 units the equations for R_i and T_i become unduly long. Also, because of the presence of both plus and minus signs in the denominator the computation loses accuracy since the difference between the positive and negative terms may be several significant figures shorter than the original terms.

An inspection of the group of transmission equations, (39), and the general expression (40) shows that the factor Q occurs far more frequently than the factor R, and the reflection equations (41) and (42) also have identical proportions of Q and R. When i is an odd number the

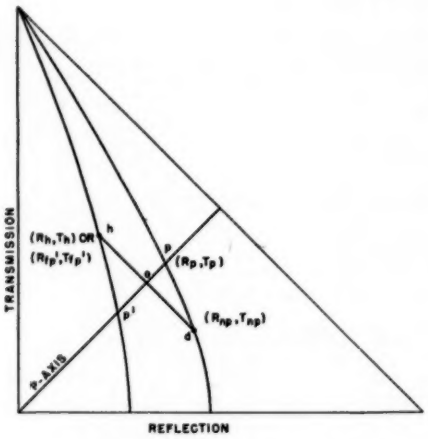

FIG. 9. In this figure the points d and h are at equal linear distance from the p-axis and these correspond to thicknesses n and f on the thickness scale. It is demonstrated in the text that $nf=1$. A solution for f is always possible and from this n may be determined. Given the coordinates of point d, the coordinates of h are found by writing those of d in the reverse order.

factor Q occurs $[(i-1)/2]^2$ times, and the factor R only $[(i-1)/2]$ times. Thus, the equation for T_{15} would contain 49 terms Q, Q^2, Q^3, etc., and 7 terms R^2, R^4, $\cdots$. The elimination of Q would therefore materially shorten the equations and make them much easier to work with. Selecting a thickness p of the medium so that the transmittance and the reflectance of the new unit layer are equal will bring about the desired elimination of Q since Q is the difference T^2-R^2. Let us call the new unit of reflectance R_p and the new unit of transmittance T_p and write R_{ip} for any multiple i of the unit thicknesses p, and R_{fp} for any fractional thickness. It is necessary to retain the subscript p in all cases since many of the equations in this section hold only when T_p equals R_p.

The determination of a thickness p so that T_p equals R_p in any particular case depends upon a preliminary computation of the saturation value R_N from (44). If T_p and R_p are substituted in (44), one gets the simplified form

$$R_N=[1-(1-4R_p^2)^{\frac{1}{2}}]/2R_p; \tag{68}$$

and this gives

$$R_p=R_N/(R_N^2+1) \tag{69}$$

for the crossing point of the R and T curves of Fig. 5 in the preceding section.

Solution for p and f

The numerical value of the thickness p remains to be found, and none of the equations so far given can be solved for thickness. There are two cases to be investigated, one where the known values of R and T are for a thinner layer of medium than that for R_p. This corresponds to some point R_a, Fig. 5, and the thickness here can be expressed as some fraction f of the new standard of thickness. The second case is where the thickness is greater than p, as point (R_b, T_b), Fig. 5, and the solution of this case will be shown to depend on the solution of the first case.

The preliminary steps in determining f are a little complicated and it has been found helpful to make a rough sketch similar to Fig. 9 to keep track of the various moves. The sketch shows points np and p on one characteristic curve and fp and p' on the other curve that is used only for the determination of f.

The empirical equation

$$\varphi T_{fp}=T_p{}^{f(f-1)s}, \tag{70}$$

where φ is a correction factor and

$$s=\frac{R_p{}^2}{R_p+0.3}, \tag{71}$$

may be solved for f when T_{fp} (the original value of T) and T_p are known. Taking natural logarithms of both sides of (70) we have

$$\ln\varphi+\ln T_{fp}=f(f-1)s+\ln T_p, \tag{72}$$

and this quadratic in f yields

$$f=\frac{s-\ln T_p-[(s-\ln T_p)^2+4s(\ln\varphi+\ln T_{fp})]^{\frac{1}{2}}}{2s} \tag{73}$$

or, if common logarithms are used,

$$s'=0.43429R_p{}^2/(R_p+0.3). \tag{74}$$

This value of s' substituted in (73) with common logarithms of T_p, T_{fp}, and φ gives a solution for f.

There is a mathematical inconsistency in the given solution of (70), since φ is assumed as known before f has been determined. This seeming impossibility is accomplished by making a graphical determination of f from either Fig. 6,

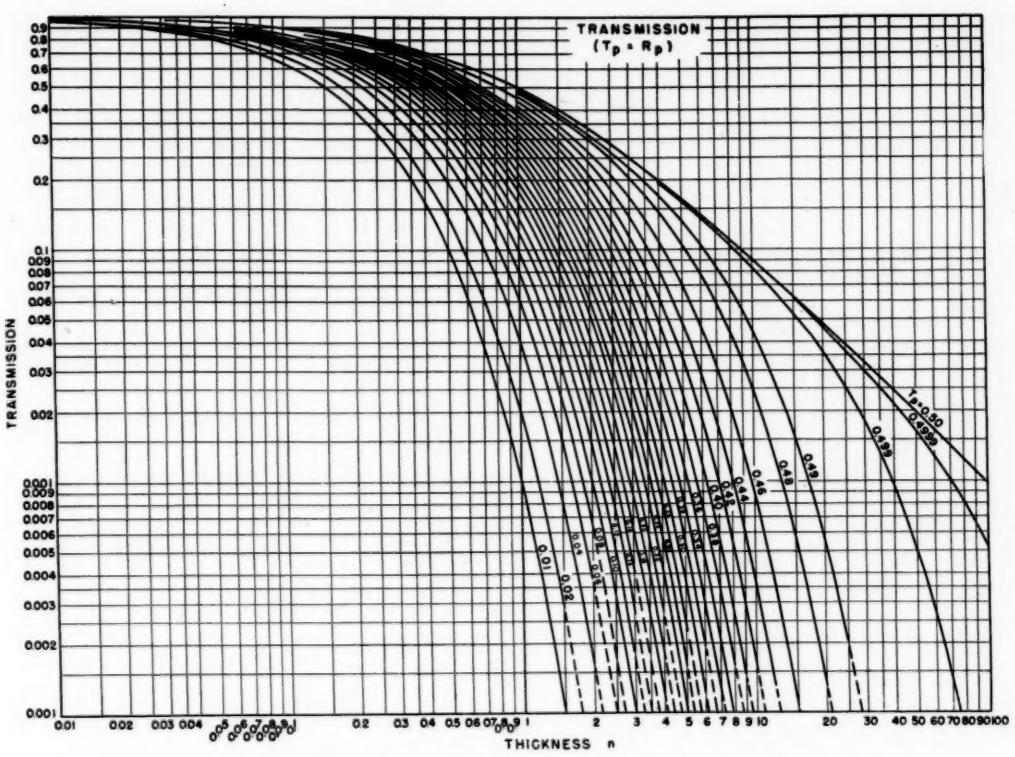

FIG. 10. These transmission curves are for the par conditions $T_p = R_p$ at thickness 1. The curves may be extended below $T_{0.001}$ by an exponential factor given in the text.

or better still, from Fig. 19 or Fig. 20 to be given later.

Values of φ are given in Fig. 8 where the curves are plotted for R_p from 0.05 up to the maximum 0.50. The value of φ is the same for either system of logarithms and the choice is solely a matter of convenience. Since tables of common logarithms are more often available, the second form may find more use.

In Fig. 6 the locus of points where R_p and T_p are equal is the axis of symmetry; this line is called the p-axis. The point where the characteristic curve cuts this axis is taken as the standard of reflectance and transmittance and the thickness of p of this standard is taken as the unit of thickness.

Demonstration of a Reciprocal Relation

In Fig. 9 a point d has coordinates $R=0.450$ and $T=0.175$. By the symmetry of the figure there is a point $T=0.450$ and $R=0.175$ that can be found by drawing the line $d\ o\ h$ perpendicular to the p-axis and making $o\ h$ equal to $o\ d$. It can be shown that, starting at some point (R_p, T_p) on the p-axis a point (R_{np}, T_{np}) at a distance n on the characteristic line passing through these two points has a complementary point $(R_{fp'}, T_{fp'})$ where R_{np} and $T_{fp'}$ are numerically equal, and T_{np} and $R_{fp'}$ are also equal. If the distance (in thickness of medium) of the first point from the p-axis is n and the distance of the second point is f, then, as has been observed in a number of numerical examples

$$nf=1 \tag{75}$$

and this reciprocal relation will be demonstrated for the simplest possible case, that of n equal to 2 and f equal to 0.5.

The transmittance at point p is T_p and the reflectance is R_p. For double thickness we have

$$\begin{aligned} T_{2p} &= T_p^2/(1-R_p^2) \\ R_{2p} &= R_p[1+T_p^2/(1-R_p^2)] \end{aligned} \tag{76}$$

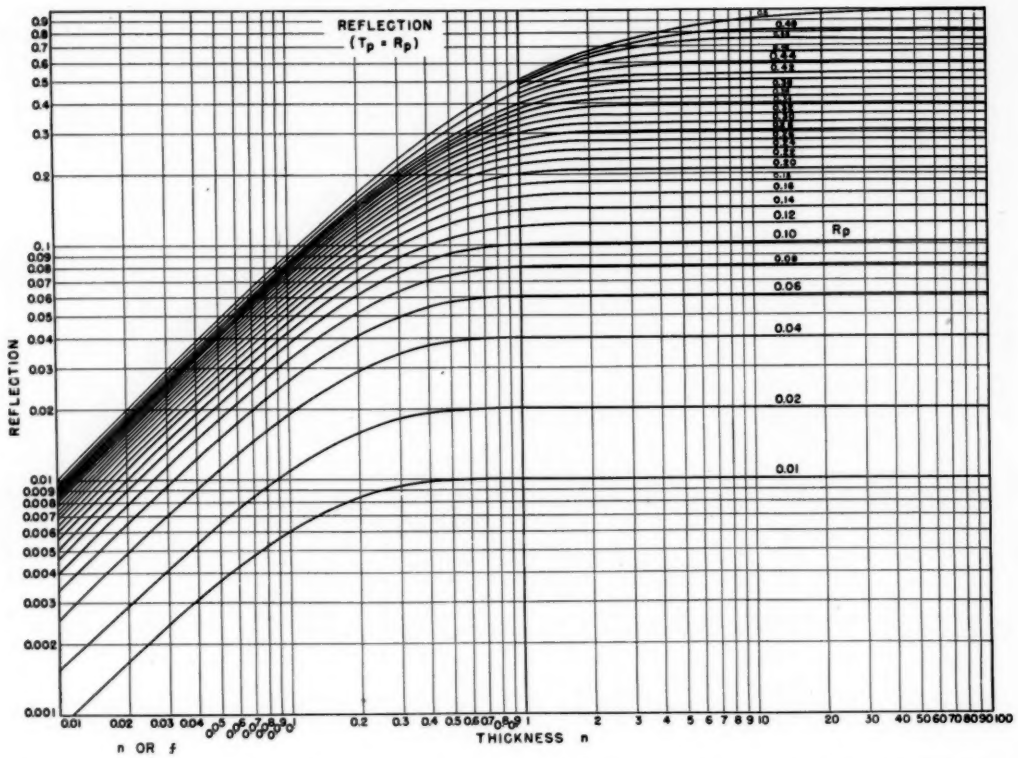

FIG. 11. These reflection curves are for the par condition $T_p = R_p$ at thickness 1. The curves may be extended to thickness less than 0.01 by assuming that the reflection is directly proportional to the thickness, using $f = 0.01$ as a base.

and since T_p^2 equals R_p^2 we have the simplified expression

$$R_{2p} = R_p/(1-R_p^2). \tag{77}$$

Let us now take the point (R_h, T_h) symmetrically placed on the opposite side of the p-axis. This gives us

$$T_h = R_{2p} \text{ numerically}, \tag{78}$$

$$R_h = T_{2p} \text{ numerically}. \tag{79}$$

Doubling the thickness from (R_h, T_h) one gets

$$T_{2h} = T_h^2/(1-R_h^2) = R_{2p}^2/(1-T_{2p}^2) \tag{80}$$

by (78) and (79) and from (76) and (77) this reduces to

$$T_{2h} = R_p^2/(1-2R_p^2). \tag{81}$$

Next solving for R_{2h} and substituting by means of (78) and (79)

$$R_{2h} = R_h\left(1+\frac{T_h^2}{1-R_h^2}\right) = T_{2p}\left(1+\frac{R_{2p}^2}{1-T_{2p}^2}\right) \tag{82}$$

and from (76) and (77), (with several steps omitted)

$$R_{2h} = T_p^2/(1-2R_p^2), \tag{83}$$

but T_p^2 equals R_p^2 and (81) and (83) are identical. Since doubling the thickness h gave a point on the p-axis it follows that

$$h = \tfrac{1}{2}p'.$$

This shows that a point at $2p$ has a complementary point at $\frac{1}{2}p'$, Fig. 9, or in more general terms, a point at any np has a complementary

point at fp' where

$$nf=1. \tag{75}$$

Since point d and point h are on different characteristic curves of Fig. 9 the value of p' that will give par values of reflectance and transmittance is of no importance except in deriving information about the original point d, as will be taken up in the following paragraphs.

Having a material (R, T) and wishing to determine the thickness that will give the (R_p, T_p) point we have two cases—

(1) $T>T_p$, that is, T is to the left and above the p-axis, as point h in Fig. 9.
(2) $T<T_p$, or T is to the right and below the p-axis as point d in the same figure.

In the first case the reduction to the (R_p, T_p) standard requires a solution of (44) for R_N, a solution of (69) for R_p, then (71) for s, and finally a solution of (73) or (74) for f and the new unit thickness p.

There are two alternatives in Case (2). The thickness of the medium may be doubled (repeatedly if necessary) until a point on the characteristic curve is reached that brings it under Case (1), or the reciprocal properties of (75) may be employed. Here the transfer equation (78) and (79) are used, then (49), (69), (71), (73), and finally (75).

Transmission T_{ip}

When R_p equals T_p the value of the Q that appears in (39) is zero, and these equations take on the simpler forms

$$\begin{aligned}
T_{0}&=1\\
T_{1p}&=T_p\\
T_{2p}&=T_p^2/\{1-R_p^2\}\\
T_{3p}&=T_p^3/\{1-2R_p^2\}\\
T_{4p}&=T_p^4/\{1-3R_p^2+R_p^4\}\\
T_{5p}&=T_p^5/\{1-4R_p^2+3R_p^4\}\\
T_{6p}&=T_p^6/\{1-5R_p^2+6R_p^4-R_p^6\}\\
T_{7p}&=T_p^7/\{1-6R_p^2+10R_p^4-4R_p^6\}.
\end{aligned} \tag{84}$$

Equation (40) becomes

$$T_{ip}=T_p^i\Big/\left\{1-\frac{(i-1)!}{1!(i-2)!}R_p^2+\frac{(i-2)!}{2!(i-4)!}R_p^4-\frac{(i-3)!}{3!(i-6)!}R_p^6+\cdots\right\}. \tag{85}$$

Since these equations reduce all transmission data to a single family, it is possible to summarize matters by a group of curves as in Fig. 10. The range of T_p is from 0.01 to 0.50, and the thickness is from $0.01p$ to $10p$. The transmission varies from 0.001 to nearly 1, but on account of the logarithmic scale, both the zero thickness and T_0 (perfect transmission) are out of the bounds of the figure. One remarkable feature is the high sensitivity of a medium that is almost without absorption. The wide spacing between (0.49, 0.49, 0.02) and (0.50, 0.50, 0) shows how critical this condition is where a change of 0.01 in absorptance may make a tenfold change in the transmission of a thick sample.

Reflection R_{ip}

The reflection equations of Eq. (41) are shortened to

$$\begin{aligned}
R_0&=0\\
R_{1p}&=R_p\\
R_{2p}&=R_p+\frac{T_p^2R_p}{D_{2p}}\{1\}\\
R_{3p}&=R_p+\frac{T_p^2R_p}{D_{3p}}\{1\}\\
R_{4p}&=R_p+\frac{T_p^2R_p}{D_{4p}}\{1-R_p^2\}\\
R_{5p}&=R_p+\frac{T_p^2R_p}{D_{5p}}\{1-2R_p^2\}\\
R_{6p}&=R_p+\frac{T_p^2R_p}{D_{6p}}\{1-3R_p^2+R_p^4\}\\
R_{7p}&=R_p+\frac{T_p^2R_p}{D_{7p}}\{1-4R_p^2+3R_p^4\}.
\end{aligned} \tag{86}$$

The general expression (42) is now

$$R_{ip}=R_p+\frac{T_p^2R_p}{D_{ip}}\left\{1-\frac{(i-3)!}{1!(i-4)!}R_p^2+\frac{(i-4)!}{2!(i-6)!}R_p^4-\frac{(i-5)!}{3!(i-8)!}R_p^6+\cdots\right\}. \tag{87}$$

The family of R_p curves are given in Fig. 11. Two features of these curves are quite pronounced. The plateau for $R_p=0.5$ is just starting at thickness 100, while for $R_p=0.1$ it begins at unit thickness. The entire group of curves are nearly straight lines at thickness 0.01, and in this region the reflection is nearly proportional to thickness, and a simple linear relation exists between fp and R_{fp}, as has already been noted.

The equation for T_{1+f} that was used in connection with the θ corrections of Fig. 7 now becomes

$$T_{(1+f)p}=\frac{T_p^{1+f}[1+2T_p]^{1-f}}{[(1+T_p)^{2(1-f)}-R_p^2]\left[1+\frac{64}{3}f(f-0.5)(f-1)\theta\right]} \tag{88}$$

and θ is used as before.

Instead of (53) we have

$$R_{(1+f)p}=\frac{1-[1-4R_p^2(1-T^2_{(1+f)p})]^{\frac{1}{2}}}{2R_p} \tag{89}$$

and (54) and (55) remain the same except for changes in the subscripts.

The new expression for R_{fp} is

$$R_{fp}=\frac{1-2T^2_{(1+f)p}-[(1-2T^2_{(1+f)p})^2-4(1-T^2_{(1+f)p})(T_p^2-T^2_{(1+f)p})]^{\frac{1}{2}}}{2T_p(1-T^2_{(1+f)p})} \tag{90}$$

and for T_{fp} we get

$$T_{fp}=\frac{T_{(1+f)p}}{T_p}(1-R_pR_{fp}). \tag{91}$$

Equations (70) and (71) furnish a complete solution for T_{fp} and with the aid of the correction factor φ of Fig. 8 a high degree of accuracy can be attained. When f is less than 0.01 the error of the uncorrected equation is much less than 2 parts in a thousand, and for smaller values of f the error decreases until at $f=0.001$ the results are accurate to the fifth significant figure. The corresponding value of R_{fp} can be found by using this T_{fp} in

$$R_{fp}=\frac{1+R^2_N-[(1+R^2_N)^2-4R^2_N(1-T_{fp}^2)]^{\frac{1}{2}}}{2R_N}. \tag{92}$$

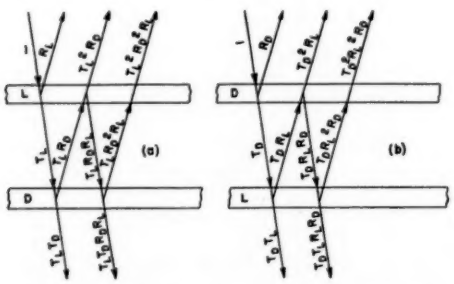

FIG. 12. The rays in these two diagrams lead to equations that show that the transmission through two dissimilar media is independent of the direction of transmission. By numerical trial the reflection, however, is always influenced by the direction of passage of the radiation.

In the section on continuous functions four special physical conditions were treated. That discussion need not be here repeated since the equations remain unchanged except for the additions of subscripts denoting the new unit p of thickness.

PART V. MIXTURES OF DISSIMILAR MEDIA

Rules of Transmission by Laminae

The diffusing materials so far considered have always been uniform in composition in each case, but it is now proposed to see what happens

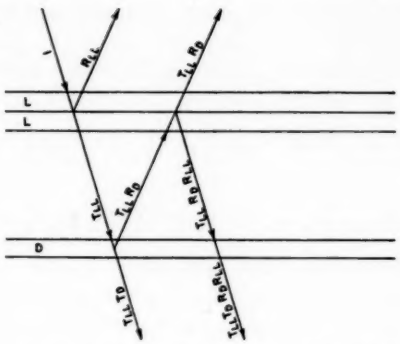

FIG. 13. The addition of one L layer to Fig. 12 does not change the general relations there noted, and by further additions one arrives at the generalization that the transmission through any assembly of laminated media is independent of the direction of passage.

when two dissimilar media are used either in physical contact or as an actual physical mixture. In order to visualize matters better let us consider what happens when two grades of paper are combined. Let us select a light colored paper L having the characteristic (R_L, T_L, A_L) for a single sheet, and a dark colored paper D having the characteristic (R_D, T_D, A_D). In writing equations for this and similar combinations strict attention will be paid to the order of events. Thus when the passage of radiation is from L to D the transmission and reflection symbols are written T_{LD} and R_{LD} and if in the opposite direction, the subscripts are T_{DL} and R_{DL} to indicate that the passage is now from D to L.

In Fig. 12 (a) a ray is traced through the LD arrangement and then in 12 (b) through the DL arrangement. The first rays completely through are T_LT_D and T_DT_L in intensity. These must be identical since they differ only in order of setting down and this can have no effect on the product. The second rays are $T_LR_DR_LT_D$ and $T_DR_LR_DT_L$ and again we have numerical identity. When all the transmitted rays are summed we have

$$T_{LD}=T_LT_D/(1-R_DR_L) \tag{93}$$

$$T_{DL}=T_DT_L/(1-R_LR_D) \tag{94}$$

which are numerically the same, and we have the identity for two layers of dissimilar media—

$$T_{LD}\equiv T_{DL}. \tag{95}$$

This result may be generalized by noting that if one of the layers is doubled, say the L layer, then, with D as the third layer (see Fig. 13)

$$T_{LLD}=T_{LL}T_D/(1-R_DR_{LL}), \tag{96}$$

while in the reverse direction

$$T_{DLL}=T_DT_{LL}/(1-R_{LL}R_D) \tag{97}$$

and again we have an identity.

The process of analysis can be extended by adding one layer at a time, and it will be found that in every case the transmission will be independent of the direction of transmission, or

$$T_{AB\cdots YZ}\equiv T_{ZY\cdots BA}. \tag{98}$$

Rules of Reflection by Laminae

Again letting the arrangement of subscripts indicate the direction of transmission, we have from Fig. 12

$$R_{LD}=R_L+T_L^2R_D/(1-R_DR_L), \tag{99}$$

$$R_{DL}=R_D+T_D^2R_L/(1-R_LR_D). \tag{100}$$

These equations give no indication of equality or of inequality, but we can fall back on numerical trial, or better still on everyday experience which tells us that a combination of a light sheet of paper and a dark sheet of paper looks light on one side and dark on the other. Since we see by

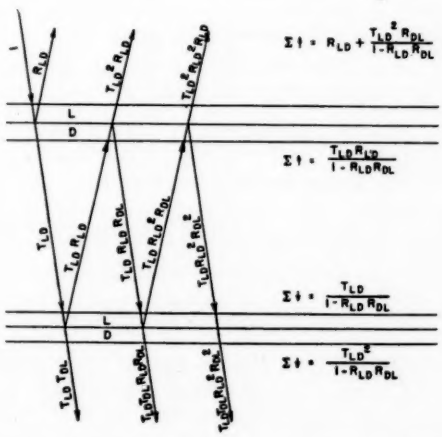

FIG. 14. An assembly of dissimilar media L and D in the order $LDLD$ gives equal transmissions in the two directions, but unequal reflections. The internal radiation is also influenced by the direction of passage.

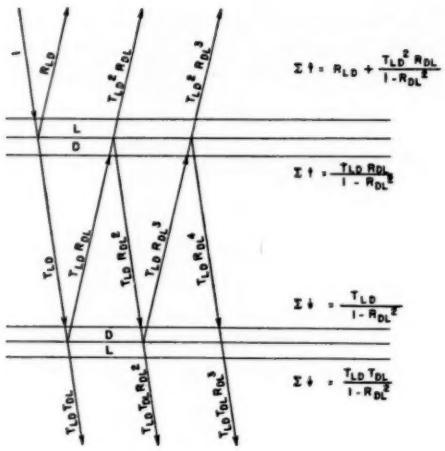

FIG. 15. The arrangement *LDDL* leads to symmetry in both T_{LDDL} and R_{LDDL} and the internal reflections are also the same for both directions of passage.

reflected light, we can write without formal proof the reflection relations

$$R_{LD} \neq R_{DL} \tag{101}$$

where L differs from D.

Multiple Layers of L and D

If the various permutations of two light sheets and two dark sheets are tabulated, it will be found that there are eight cases, and a fewer number of combinations when the optical duplicates are canceled out.

Since the transmission has been found to be independent of direction, we have

$$T_{DDLL}=T_{LLDD}=T_{DD}T_{LL}/(1-R_{LL}R_{DD}) \tag{102}$$

and the symmetrical pair (see Fig. 14).

$$T_{LDDL}=T_{LDDL}=T_{LD}^2/(1-R_{DL}^2). \tag{103}$$

There is another symmetrical arrangement

$$T_{DLLD}=T_{DLLD}=T_{DL}^2/(1-R_{LD}^2) \tag{104}$$

which has a numerically identical numerator but its denominator differs from (103). The final combinations are, as in Fig. 15,

$$T_{DLDL}=T_{LDLD}=T_{DL}^2/(1-R_{DL}R_{LD}) \tag{105}$$

and this gives four different equations for the transmissions of the eight arrangements of the four sheets.

The reflections, taken in the same order of arrangement, are

$$R_{DDLL}=R_{DD}+T_{DD}^2R_{LL}/(1-R_{LL}R_{DD}), \tag{106}$$

and

$$R_{LL}R_{DD}=R_{LL}+T_{LL}^2R_{DD}/(1-R_{DD}R_{LL}), \tag{107}$$

which are numerically different.

The arrangement *LDDL* reads the same from left to right as from right to left, hence, from Fig. 14,

$$R_{LDDL}=R_{LDDL}=R_{LD}+T_{LD}^2R_{DL}/(1-R_{DL}^2), \tag{108}$$

and the same conditions hold for *DLLD*

$$R_{DLLD}=R_{DLLD}=R_{DL}+T_{DL}^2R_{LD}/(1-R_{LD}^2) \tag{109}$$

and this differs from (108).

The final arrangements give the two different equations

$$R_{DLDL}=R_{DL}+T_{DL}^2R_{DL}/(1-R_{DL}R_{LD}) \tag{110}$$

and

$$R_{LDLD}=R_{LD}+T_{LD}^2R_{LD}/(1-R_{LD}R_{DL}). \tag{111}$$

There are thus four possible transmission values for the permutations of two pairs of media, and six reflection values. In general there will be fewer transmission values for multiple arrangement than there will be reflection values because transmission is independent of the direction of passage and reflection is not.

In place of equal numbers of L and D sheets let us examine the case of one D associated with four L's, with the D placed in succession in the first, second, $\cdots$ fifth place. In Fig. 16 D has the characteristic (0.2, 0.7, 0.1) and L is defined as (0.8, 0.1, 0.1). The various arrangements are indicated at the bottom of the web by *DLLLL*, etc. showing where the D sheet is located.

The transmission curve is symmetrical right and left, which was to be anticipated from the independence of T from influence by direction of transmission. If in this example T_{DLLLL} differed from T_{LLLLD}, then there would be a

difference in T for the two directions, since changing D from first place to last place is physically the same as leaving D in first position and changing the direction of the incident radiation.

The lowest transmission was found when the dark sheet was in the central position. This checks with previous experience[1,2] with colored filters used in temperature determination. The central positions in groups of three or more filters were found best for producing color changes, and here the dark element has the greatest effect when in the center of the group.

The reflection curve shows its lowest value where D is on the side of the incident light, and it rises to a maximum when D is last in the series.

The absorption is greatest when D is first since here the flux density is greatest (see Fig. 4 for a comparable case). The unit absorptance is the same for both L and D and the difference in results arises from the relative amounts of energy available for absorption.

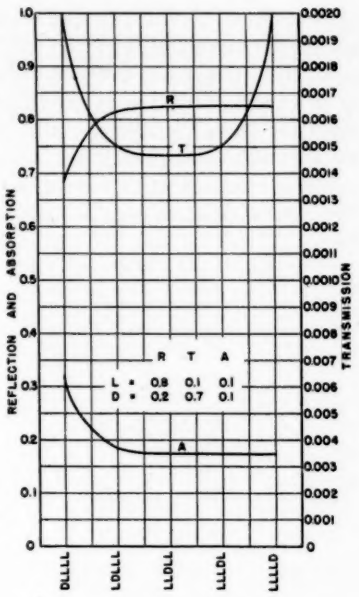

FIG. 16. In this diagram a single D layer is associated with four L layers in various positions. All three characteristics R, T, and A are influenced by the position of L. The T curve is symmetrical while the R and A curves show a dependence on direction of propagation.

General Rules of Transmission and Reflection by Laminae

With the data thus far available we can now put down some generalities.

1. Both transmittance and reflectance of a single medium are independent of the direction of incident radiation.

2. When two different media are associated the transmission is independent of and the reflection is dependent on the direction of incident radiation.

3. When three or more different media are associated the transmission is dependent on the arrangement of the media, except for the right and left symmetry, and is independent of the direction of passage of the radiation. The reflection varies with both arrangement and with direction of the incident radiation.

4. A given medium has the greatest influence when in the center of a group of other media, and the least effect when in an outside position.

TABLE II.

Trial	Laminae	R_M	T_M	A_M
1	0.5	0.18889	0.58794	0.22317
2	0.25	0.18754	0.58728	0.22518
3	0.125	0.18719	0.58705	0.22576
4	0.0625	0.18710	0.58698	0.22592
Extrap.	0.0	0.1871	0.5869	0.2260

[1] F. Benford, J. Opt. Soc. Am. **25**, 136–141 (1935).
[2] F. Benford, Gen. Elec. Rev., pp. 277–281 (June, 1935).

Mixtures of Dissimilar Media

The preceding discussion of dissimilar media was for cases of media placed in contact without admixture. It will be realized that such an arrangement will be different from a true mixture where each medium permeates all parts of the other. We can approximate this condition as closely as we please by dealing with thinner and thinner laminae of media, for while true mixture does not occur the average distance between adjacent diffusing element approaches that of an actual mixture.

The procedure is to compute the R, T, and A value of two adjacent $\frac{1}{2}$-unit layers of different media. The assumption is then made that these data represent a homogeneous mixture (R'_M, T'_M, A'_M) of unit thickness. By taking $\frac{1}{4}$-unit layers next we get data for a $\frac{1}{2}$-unit mix-

ture, and this when doubled in thickness gives a second trial value (R''_M, T''_M, A''_M). The laminae are then reduced to 1/8 or 1/16 if necessary and third and fourth approximations found. These data for (R_M, T_M, A_M) are then plotted and extrapolated to zero thickness of laminae.

In Table II various trial values are given along with the results of a graphic extrapolation to zero thickness of laminae of (0.1, 0.5, 0.4) and (0.3, 0.7, 0.0).

It has been found that two trial values are not sufficient for extrapolation since the lines are curves and they may have changing curvature near the lower limit.

The mixing equations for half-thickness laminae are

$$R_M=\tfrac{1}{2}[R_{(D/2)(L/2)}+R_{(L/2)(D/2)}]$$

$$=\tfrac{1}{2}\left[R_{D/2}+\frac{T_{D/2}{}^2R_{L/2}}{1-R_{L/2}R_{D/2}}+R_{L/2}+\frac{T_{L/2}{}^2R_{D/2}}{1-R_{D/2}R_{L/2}}\right] \tag{112}$$

$$T_M=\frac{T_{L/2}T_{D/2}}{1-R_{D/2}R_{L/2}} \tag{113}$$

$$A_M=\tfrac{1}{2}\left[A_{L/2}+A_{D/2}+\frac{T_{D/2}R_{L/2}A_{D/2}+T_{D/2}A_{L/2}+T_{L/2}R_{D/2}A_{L/2}+T_{L/2}A_{D/2}}{1-R_{L/2}R_{D/2}}\right], \tag{114}$$

and by changing subscripts the same equations apply to the thinner laminae.

In Fig. 17 the results of some special cases are plotted to illustrate several rules that apply with various degrees of approximation. The black dots on the ends of the plotted lines define the two media in a mixture, and the central dot is at the arithmetical mean of the two. This is given merely as a reference point for the computed mixture as represented by an open circle.

When two materials have the same reflectance, (a) in Fig. 17, the mixture has a slightly greater reflectance than the original media. This seems anomalous, but it will be recalled that the elements R_M, T_M, and A_M are rigidly connected by (1) and any change in one inevitably leads to change in at least one of the other two. Here R_M is not the constant that might be expected, and it will later appear that this is the normal behavior for all three elements, R, T, and A.

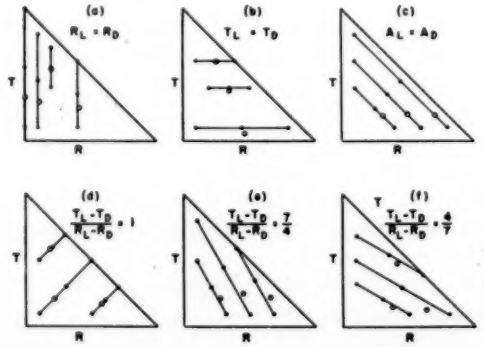

FIG. 17. In these diagrams are illustrated the results of computing a physical mixture of two widely dissimilar media. In general, even if the two R's (or T's or A's) are the same, the R_M (or T_M or A_M) will have a different numerical value. The dot at the center of each line is the arithmetic average of the two end dots which define the two media while the open circle is the computed mixture.

The values of T_M in the case where the reflectances are equal is approximately

$$T_M=(T_LT_D)^{\frac{1}{2}}. \tag{115}$$

As an example, when the mixture of (0.1, 0.8, 0.1) and (0.1, 0.1, 0.8) is computed we have

$$R_L=0.1$$
$$R_D=0.1$$
$$R_M=0.1\dot{0}5$$
$$T_M=0.2840$$
$$(T_LT_D)^{\frac{1}{2}}=0.2828.$$

An exception to the observed rule for reflectance occurs when the reflectances in both samples are zero, and here one could hardly expect a mixture of the two to create reflectance and hence it remains zero. Also under these conditions we can write

$$T_L=T^x$$
$$T_D=T^y$$
$$(T_LT_D)^{\frac{1}{2}}=T^{(x+y)/2}, \tag{116}$$

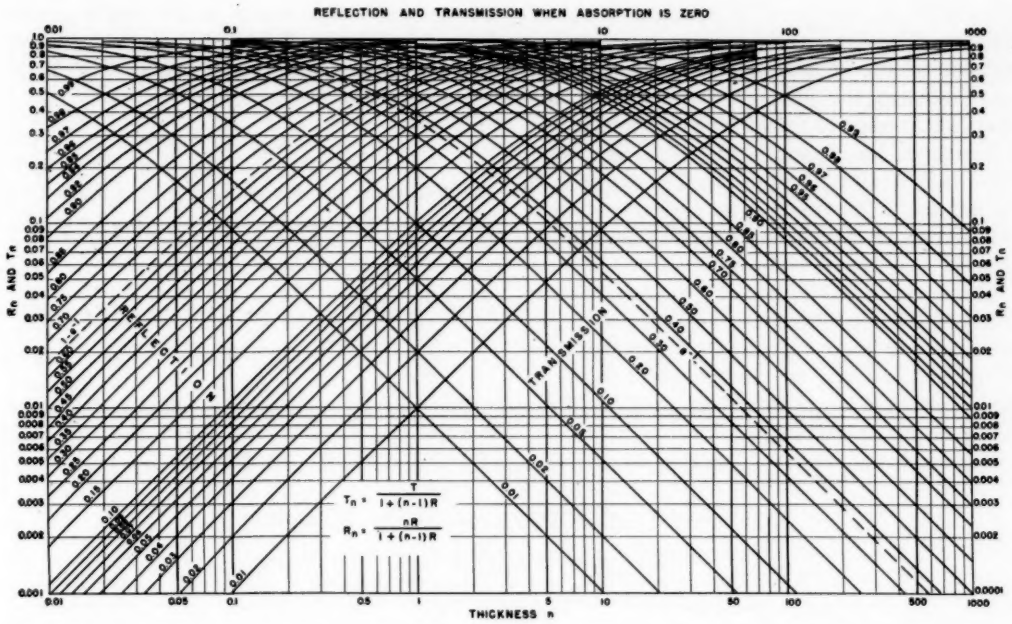

FIG. 18. When a medium does not absorb transmitted radiation, the equations become continuous first degree functions of the thickness n. There is a right-and-left symmetry about the $n=1$ ordinate, and when T' equals R', any T'_n equals $R'_{1/n}$ and any $T'_{1/n}$ equals any R'_n.

and here (116) is in the customary exponential form of non-reflectors and is exact.

In the case where one material is perfectly transparent, that is, it has the characteristic (0, 1, 0), a mixture with another material will simply dilute the latter, and when the volumes are one to one the mixture will be simply a half layer of the active material.

If either component of a mixture has zero transmittance, then the mixture also has zero transmittance in all proportions of admixture, that is, the opaque component has absolute dominance.

Figure 17(b) illustrates what happens when two media of identical transmittances are mixed. The resultant transmittance is lower than the original; in the case of (0.1, 0.1, 0.8) and (0.8, 0.1, 0.1) the result is a transmittance of 0.05, that is, just half the starting values. The reflectance of the mixture is, however, not far from the arithmetic average, and this is the best agreement found for these two original points.

In the case of equal absorptances, the result is in excellent agreement with the original values, as illustrated in Fig. 17(c). Here the computed points lie on the drawn lines, as closely as can be seen. The following data give a more exact idea of the relative stability of absorptance in a mixture.

Absorptance of elements	Absorptance A_M of mixture
0.1000	0.1002
0.3000	0.3019
0.5000	0.5030

One rather surprising feature of 17(c) is the small effect the more transparent of the two elements has on the average T_M. The three circles are within the range 0.18 to 0.20 although the high transmittances are 0.40, 0.60, and 0.80. This brings into prominence the dominant part the component of lower transmittance plays in the mixture and illustrates how the general trend of T_M is downward, even as in the case 17(b) already noted, producing a mixture transmittance lower than that of either of the components.

Diagrams 17 (d), (e), and (f) illustrate three other relations between components and mix-

tures that do not have any constant characteristic. When the components are on a line parallel to the p axis the mixture circle lies practically on the joining line, and the transmittance is roughly found by (115) which here is somewhat less accurate than when applied to the conditions of 17(a). Since T_M and R_M lie on the line, it follows that an approximation of T_M allows an approximation of R_M and A_M as well.

Conditions in 17(e) and 17(f) are obviously not favorable for formulating any approximation since some of the computed circles are far from the parent line, and the direction and degree of departure could hardly have been predicted from the preceding special cases.

Nearly all the mixtures considered have been extreme cases of materials as different as possible in certain characteristics. When the distance D between points in the diagrams of Fig. 17 are not in excess of 0.15 as found by

$$D=[(R_L-R_D)^2+(T_L-T_D)^2]^{\frac{1}{2}}, \quad (117)$$

the following approximation may be used regardless of the orientation of the connecting line

$$R_M=\tfrac{1}{2}(R_L+R_D), \quad (118)$$

$$T_M=(T_LT_D)^{\frac{1}{2}}, \quad (119)$$

$$A_M=1-\tfrac{1}{2}(R_L+R_D)-(T_LT_D)^{\frac{1}{2}}. \quad (120)$$

One case that has been worked out by both laminae and by these equations is the mixture of (0.5, 0.3, 0.2) and (0.4, 0.3, 0.3)

(114) gives $R_M=0.45000$ against 0.45005 by laminae

(115) gives $T_M=0.30000$ against 0.29852 by laminae

(116) gives $A_M=0.25000$ against 0.25143 by laminae.

The mixtures thus far considered have all been in one-to-one proportion by volume, but the equations can be applied to any two volumes, or what is the same thing, to any two thicknesses. Suppose one diffuser of volume 3 is to be combined with another of volume 5. A direct mixture would have a volume 8 and by solving for 1/8 thickness the approximate characteristics of unit volume would be found. The reduction of both components to unit thickness before mixing would not be permissible since this would lead to a 1 to 1 proportion instead of the desired 3 to 5 proportion. If one or both of the components are fractional in volume the combination must be made in fractional form and the resultant mixture then reduced to the desired unit volume.

PART VI. THREE SPECIAL CONDITIONS AND SUMMARY

Media with No Absorption

In the rare (and perhaps impossible) case of diffusion without absorption the basic equation becomes

$$T+R=1, \quad (121)$$

since A equals zero. Starting with the general equation for double thickness, we can reduce it as follows

$$T_2=T^2/(1-R^2)$$

$$=\frac{(1-R)T}{(1-R)(1+R)}$$

$$=T/(1+R). \quad (122)$$

Similarly, it can be demonstrated that

$$T_3=T/(1+2R) \quad (123)$$

$$T_4=T/(1+3R) \quad (124)$$

and from the evident relation between the subscripts and the coefficients we get

$$T_n=T/[1+(n-1)R] \quad (125)$$

as a general expression that is no longer limited to integral values and is continuous between $n=0$ and $n=\infty$.

The corresponding values for R are

$$R_2=1-[T/(1+R)]$$

$$=2R/(1+R) \quad (126)$$

$$R_3=3R/(1+2R) \quad (127)$$

$$R_4=4R/(1+3R) \quad (128)$$

$$R_n=nR/[1+(n-1)R]. \quad (129)$$

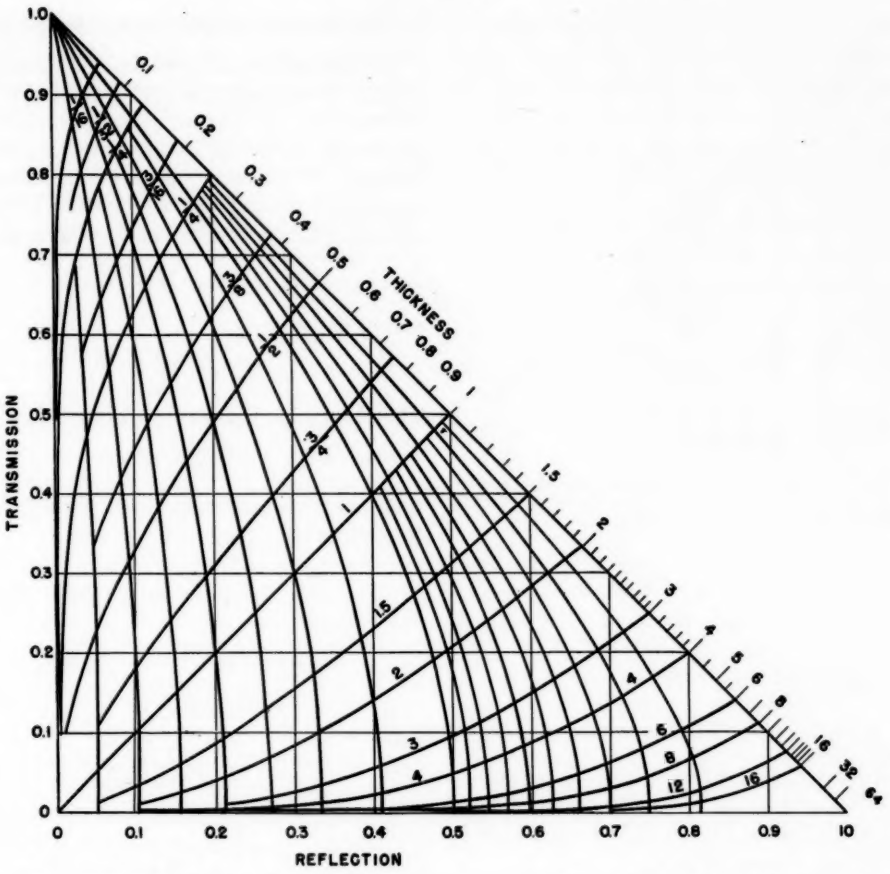

FIG. 19. This diagram may be used in many cases for a rough determination of either R, T, n, or f, but interpolation is difficult in some parts, particularly near the extreme right and left limits.

In spite of any question that may be raised about the physical possibility of diffusion without absorption, these general expressions are of great service in an investigation such as the present one, since they furnish a quick numerical check on equations that are discontinuous, but which may be reduced to a comparative basis by making A equal to zero.

The slope of the transmittance curve is

$$dT_n/dn = -T_n/[n-(n-1)T]^2 \qquad (130)$$

and the slope of the reflectance curve is

$$dR_n/dn = R_n/[1+(n-1)R]^2. \qquad (131)$$

If $1-T$ is substituted for R in this denominator, the two slopes will be found to be equal but opposite in sign. This is a necessary condition since with no loss by absorption the gain in reflection must be just equal to the loss in transmission. In Fig. 18 a double logarithmic scale is used and both T_n and R_n are plotted for values of T and R from 0.01 to 0.99 over a range of n from 0.01 to 1000. The curves are mirror images T_n against R_n, the mirror being vertical along the $n=1$ ordinate.

Media with No Reflection

The second special case occurs when R is zero and it is properly only a limit for the general case of reflection by diffusion. By substituting zero for R in the general equations we get

$$T_2 = T^2 \qquad (132)$$

$$T_3 = T^3 \qquad (133)$$

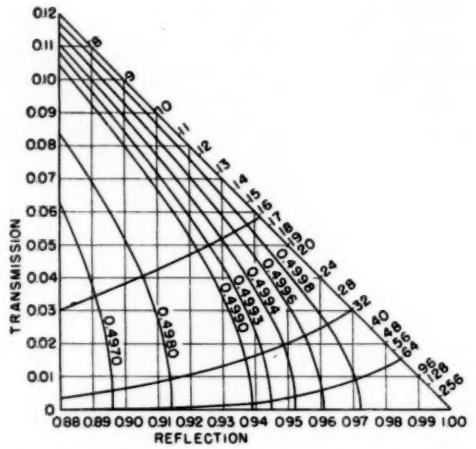

FIG. 20. This is an enlargement of the lower right corner of Fig. 19. The values marked on the characteristic are the par values where the curves cross the p axis.

and in general

$$T_n = T^n. \tag{134}$$

This expression is often seen as

$$T_n = e^{-kn}. \tag{135}$$

Since, if e is to be used as a base, it is necessary to use e^{-1} in order to get a number less than 1, as T always is. Then e^{-1} is raised to some power k to get the unit transmittance

$$T = e^{-k}. \tag{136}$$

Finally e^{-k} is raised to the nth power to get the desired value for n thicknesses

$$T_n = (e^{-k})^n. \tag{137}$$

This matter is gone into in some detail because of the use of the term "extinction coefficient" to describe k. The equation expresses transmittance, not extinction, and k is an exponent not a coefficient. The resultant confusion of thought particularly among people who deal with radiation only occasionally is a real detriment to the use of a very real and very simple equation. It originated in the early days of photography among people who were interested in an isolated phenomenon and it seems to have been unfortunate in its genealogy.

Maximum Absorption in a Selected Layer

In engineering and sometimes in therapy there is need for an equation giving the physical conditions that will lead to a maximum absorption of energy at some selected depth below the surface. If we may assume the absence of scattering, we get the energy W_n arriving at depth n when W units of energy fall on unit area

$$W_n = We^{-kn} \tag{138}$$

and at depth $n+1$

$$W_{n+1} = We^{-k(n+1)}. \tag{139}$$

The absorption between n and $n+1$ is

$$W_\Delta = W_n + W_{n+1} = W(e^{-kn} - e^{-k(n+1)}). \tag{140}$$

This will be a maximum when the derivative of W_Δ is zero or

$$\frac{dW_\Delta}{dk} = W[ne^{-kn} - (n+1)e^{-k(n-1)}] \tag{141}$$

$$We^{-kn}[n - (n-1)e^{-kn}] = 0 \tag{142}$$

$$e^{-kn} = n/(n-1) \tag{143}$$

$$\ln e^{-k} = \frac{1}{n} \ln [n/(n-1)]$$

$$\ln T = \frac{1}{n} \ln [n/(n+1)]. \tag{144}$$

In therapy the transmittance T of the flesh cannot be changed, but since there is often some control over the radiation used it may be possible to find a wave-length λ whose T_λ is in agreement with the above equation. If the radiator is a blackbody, the temperature is selected so that the product of absolute temperature and the selected wave-length equals 3669 micron-degrees.

The Searchlight Beam

In searchlight practice it is commonly assumed that the transmittance is a simple exponential and this is justified by results in spite of the fact that the loss by scattering is a strong, if not a predominating, factor. The searchlight beam is of small angular width, from one to two degrees, and light reflected out of this pencil is almost completely lost so far as the target is concerned.

The internal reflections that play a dominant role in the case of a diffusing medium infinite in lateral dimensions are here almost non-existent. Each reflection scatters over a complete sphere and a second scattering is necessary to turn the light into the forward direction again, and only about one part in 50,000 of this light will fall upon the target. Here, in final results, scattering is the same as absorption and R is effectively zero, while A has an enhanced value, being in effect the sum of the true A and R.

The Triangle Chart

The curves of Fig. 19 are useful for preliminary exploration and for rough determinations of R, T, and A but their accuracy is limited by the nature of the thickness scale. This scale is uneven in spacing and visual interpolation is difficult. The p axis is arbitrarily taken as the unit thickness, and the other thickness curves are computed on this basis. For increasing thickness there are curves for 2, 4, 8, 16 and the interpolated curves for 1.5, 3, 6, 12. For fractional thicknesses the curves are for 1/2, 1/4, 1/8, 1/16 and the additional curves for 3/4, 3/8, 3/16, and 3/32. The curve for 4 units thickness is symmetrical with the curve for 1/4 unit thickness, but this relation does not hold for the interpolated curves for 1.5 and 3/4 since these are not reciprocals. If this figure is used to make visual estimates of numerical values, there are certain areas where the accuracy leaves much to be desired. This is particularly true for values of R greater than 0.90 and to aid in this region Fig. 20 has been computed. The seven characteristic curves given are marked with their R_p values for identification, and the manner in which they spread out along the R_N limit explains why this region has been so difficult to explore by means of equations, and why empirical equations have usually failed when R was large. A variation of 0.003 in R_p between 0.497 and the limit 0.500 produces a variation of 0.104 in R_N, or 34 times as much. The importance of this high ratio will become apparent if we consider the possibility of testing a reflecting material of such thickness as to obtain par values T_p and R_p, and then from the test data attempt a computation of R_N.

A known magnification of test errors by a factor of 30 would cause doubt as to the probable accuracy of the final results, and obviously the conditions of the test should be altered to get better dependability. This might be done by having the thickness greater than p so that the range between p and N is at least reduced. The best accuracy conditions will of course be realized when the test thickness is near the right-hand corner of Fig. 20, that is, near the R_N region, but not actually in it, for this would make the test for R insensitive to changes in thickness. The selection of test conditions therefore calls for a preliminary study of conditions, and perhaps a second test once the characteristic curve has been approximated.

Summary of Methods

When only integral thicknesses are considered, as in Part I, the characteristics of any thick layer may be computed by first computing the thickness series 1, 2, 4, 8, $\cdots$ and then combining the needed terms of this series. The same method applies for the thicknesses less than 1 where the series 1, 1/2, 1/4, 1/8, $\cdots$ is used. An alternate method is to build up the integral series 1, 2, 3, 4, $\cdots$, or, after finding some of the first terms of this series they may then be combined to get the desired thickness.

The integral solution may be combined with the fractional solution to get a restricted number of solutions between any two integers.

A direct solution for integral thickness is given by the factorial equations, Part II, for T_i and R_i, and here there are no theoretical limits to the magnitude of i, but there is a practical limit imposed by the number of terms in the equations where i is much greater than 10.

A continuous function in Part III from T to T_2 permits any fractional value of n greater than 1 to be obtained by combining T_{i-1} with T_{1+f} to get the desired T_{i+f}. A correction factor θ is used with the equation for T_{1+f} and the final error is of the order of 1 part in 10,000. Having found T_{1+f} the value of R_{1+f} can be computed from R, T, and T_{1+f}, and this extends the range of continuous values from $n=1$ to $n=\infty$.

A set of separate solutions for fractional thicknesses also depends on a prelimingry solution for T_{1+f} and these extend R_f and T_f down to zero thickness.

Since values for any T_n and R_n may be used to

solve for the limiting reflectance R_N the equation may be put into a form that will give a solution for the condition of transmittance equal to reflectance as in Part IV. This eliminates Q from the equations and naturally lessens the work of solving thick layers. An empirical equation is given for T_f and a correcting factor φ, in chart form, takes care of the errors in the equation. In this case there is a solution for f from a known T_f and this is the only case where a solution for thickness is given.

When n is greater than 1, the above equation cannot be used directly, but by simply exchanging the numerical values of R and T a value f is obtained that is the reciprocal of n and indirectly any value of thickness between zero and infinity may thus be obtained. The solutions are in several steps as before and the procedure is the same as previously given for T_{i+f} and R_{i+f}.

When dissimilar media are associated, Part V, the transmission of radiation is the same for the two directions, but the reflectances differ with direction. Also, if three or more dissimilar media are associated, both the transmission and reflection depend on the arrangement of the media, except that symmetrical changes from right to left do not influence the transmissions. An approximate solution for a physical mixture of two media is found by solving for successive thin laminae and then building up these combined laminae to the original unit of thickness. By extrapolation the constants for a physical mixture are approximated.

When a diffusing medium transmits without loss, the equations in Part VI reduce to a continuous linear form and R_n and T_n may be computed directly for any n. In the case of no diffusion the equations are exponential and continuous.

At the extremes near zero thickness (see Part III) and for great optical thickness many of the equations for R_f, T_f, and R_N, T_N take on simplified forms that are either linear or exponential, and they are continuous over the limited range permitted by the approximations introduced into the equations as the limits are approached.

The absorption in any particular case, Part I, can be found by computing the radiation incident on both sides of the selected laminae, or by taking the difference between the sum of the entering radiation and the sum of the emitted radiation.

Book Review

Collected Abstracts Published during 1945 on Spectrochemical Analysis

Compiled by Edwin S. Hodge; Ohio Valley Spectrographic Society, Engineers Club Building, Dayton, Ohio, 1946. Paper covers. $1.25 postpaid, or $1.00 cash with order.

This 64-page booklet, arranged according to topics and well indexed, contains verbatim copy of all abstracts published during 1945 by Chemical Abstracts on articles dealing with spectrochemical analysis. More than 80 references are cited covering all the latest developments in the field. The booklet is lithoprinted.